Universität Potsdam
Institut für Geowissenschaften

Neon, Helium and Argon Isotope Systematics of the Hawaiian Hotspot

Dissertation
zur Erlangung des akademischen Grades
"doctor rerum naturalium"
(Dr. rer. nat.)
in der Wissenschaftsdisziplin Geowissenschaften

eingereicht an der
Mathematisch-Naturwissenschaftlichen Fakultät
der Universität Potsdam

von
Tina Mailer, geb. Krüsmann

Potsdam, Juni 2009

Published online at the
Institutional Repository of the University of Potsdam:
URL http://opus.kobv.de/ubp/volltexte/2009/3963/
URN urn:nbn:de:kobv:517-opus-39633
http://nbn-resolving.org/urn:nbn:de:kobv:517-opus-39633

Fire and Ice

Some say the world will end in fire,
Some say in ice.
From what I've tasted of desire
I hold with those who favor fire.
But if it had to perish twice,
I think I know enough of hate
To say that for destruction ice
Is also great
And would suffice.

Robert Frost, 1923

Table of Contents

Abstract

This study presents noble gas compositions (He, Ne, Ar, Kr, and Xe) of lavas from several Hawaiian volcanoes. Lavas from the Hawaii Scientific Drilling Project (HSDP) core, surface samples from Mauna Kea, Mauna Loa, Kilauea, Hualalai, Kohala and Haleakala as well as lavas from a deep well on the summit of Kilauea were investigated.

Noble gases, especially helium, are used as tracers for mantle reservoirs, based on the assumption that high $^{3}He/^{4}He$ ratios (>8 R_A) represent material from the deep and supposedly less degassed mantle, whereas lower ratios (~ 8 R_A) are thought to represent the upper mantle. Shield stage Mauna Kea, Kohala and Kilauea lavas yielded MORB-like to moderately high $^{3}He/^{4}He$ ratios, while $^{3}He/^{4}He$ ratios in post-shield stage Haleakala lavas are MORB-like.

Few samples show $^{20}Ne/^{22}Ne$ and $^{21}Ne/^{22}Ne$ ratios different from the atmospheric values, however, Mauna Kea and Kilauea lavas with excess in mantle Ne agree well with the Loihi-Kilauea line in a neon three-isotope plot, whereas one Kohala sample plots on the MORB correlation line.

The values in the $^{4}He/^{40}Ar^{*}$ ($^{40}Ar^{*}$ denotes radiogenic Ar) versus ^{4}He diagram imply open system fractionation of He from Ar, with a deficiency in ^{4}He. Calculated $^{4}He/^{40}Ar^{*}$, $^{3}He/^{22}Ne_S$ ($^{22}Ne_S$ denotes solar Ne) and $^{4}He/^{21}Ne$ ratios for the sample suite are lower than the respective production and primordial ratios, supporting the observation of a fractionation of He from the heavier noble gases, with a depletion of He with respect to Ne and Ar. The depletion of He is interpreted to be partly due to solubility controlled gas loss during magma ascent. However, the preferential He loss suggests that He is more incompatible than Ne and Ar during magmatic processes. In a binary mixing model, the isotopic He and Ne pattern are best explained by a mixture of a MORB-like end-member with a plume like or primordial end-member with a fractionation in $^{3}He/^{22}Ne$, represented by a curve parameter r of 15 ($r=(^{3}He/^{22}Ne)_{MORB}/(^{3}He/^{22}Ne)_{PLUME\ or\ PRIMORDIAL}$).

Whether the high $^{3}He/^{4}He$ ratios in Hawaiian lavas are indicative of a primitive component within the Hawaiian plume or are rather a product of the crystal-melt- partitioning behavior during partial melting remains to be resolved.

Zusammmenfassung

Im Rahmen dieser Arbeit wurden Edelgaszusammensetzungen (He, Ne, Ar, Kr, Xe) verschiedener hawaiianischer Vulkane ermittelt. Bohrkernproben vom Hawaii Scientific Drilling Project (HSDP), Oberflächenproben von den Vulkanen Mauna Kea, Mauna Loa, Kilauea, Hualalai, Kohala und Haleakala, sowie Proben aus einer Bohrung am Gipfel des Kilauea wurden untersucht.

Edelgase, insbesondere Helium, dienen als geochemische Tracer. Dies ist auf der Annahme begründet, dass hohe $^{3}He/^{4}He$ Verhältnisse ($> 8\ R_A$) Material aus dem tiefen Erdmantel repräsentieren, während niedrigere $^{3}He/^{4}He$ Verhältnisse ($\sim 8\ R_A$) dem oberen Erdmantel entsprechen.

Mauna Kea, Kohala und Kilauea Laven erreichten MORB-ähnliche bis mäßig hohe $^{3}He/^{4}He$ Verhältnisse, während Haleakala Laven MORB-ähnliche $^{3}He/^{4}He$ Verhältnisse ergaben. Nur wenige Proben zeigten $^{20}Ne/^{22}Ne$ und $^{21}Ne/^{22}Ne$ Verhältnisse unterschiedlich vom Luftwert. Proben vom Mauna Kea und Kilauea, die einen Exzess im Bezug auf Mantel-Ne aufweisen, korrelieren mit der Loihi-Kilauea Linie im Neon-Drei-Isotopendiagramm, während eine Kohala Probe auf der MORB Korrelationslinie liegt.

Die Werte im $^{4}He/^{40}Ar^{*}$ ($^{40}Ar^{*}$ ist radiogenes Ar) versus ^{4}He Diagramm implizieren eine Fraktionierung von He und Ar im offenen System, mit einem Defizit an He. Berechnete $^{4}He/^{40}Ar^{*}$, $^{3}He/^{22}Ne_s$ ($^{22}Ne_S$ ist solares Ne) and $^{4}He/^{21}Ne$ Verhältnisse für die Proben sind niedriger als die entsprechenden Produktions- und primordialen Verhältnisse. Dies unterstützt die Beobachtung einer Fraktionierung von He gegenüber den schwereren Edelgasen, mit einer Verarmung von He gegenüber Ne und Ar. Ein beitragender Faktor bei der He Verarmung ist der löslichkeitskontrollierte Gasverlust während des Magmenaufstiegs. Der bevorzugte Verlust von He lässt jedoch auch darauf schließen, dass He sich bei magmatischen Prozessen inkompatibler verhält als Ne und Ar. In einem binären Mischungsmodell kann die Isotopenzusammensetzung von He und Ne am besten durch eine Mischung von einem MORB-ähnlichen mit einem Plume-ähnlichen oder primordialem Endglied mir einer Fraktionierung von $^{3}He/^{22}Ne$ erklärt werden, dargestellt durch den Kurvenparameter r von 15 ($r=(^{3}He/^{22}Ne)_{MORB}/(^{3}He/^{22}Ne)_{PLUME\ or\ PRIMORDAL}$).

Inwiefern die hohen $^{3}He/^{4}He$ Verhältnisse in hawaiianischen Laven ihren Ursprung in primitiven Komponenten innerhalb des hawaiianischen Plumes haben oder vielmehr in dem Verteilungsverhalten zwischen Mineralphase und Schmelze begründet sind, bleibt zu klären.

Motivation and goals of this study

The understanding of the evolution of the Earth has often been revolutionized by great findings or theories. Of major importance for the determination of the age of the Earth was the development of radiometric age dating, a method that was established in the early 20th century. Groundbreaking was the development of the plate tectonic theory, which is based on Alfred Wegener's theory of continental drift, proposed in 1912. The theory of plate tectonics became more and more accepted between 1940 and 1950, and lead to a new understanding of the Earth. The theory basically states that the Earth's surface is covered by crustal plates that are moved by convection currents beneath these plates, which are driven by heat that is generated deep in the Earth by radioactivity.

J. Tuzo Wilson (1963), who greatly contributed to the plate tectonic theory, postulated a theory for the evolution of the Hawaiian Islands, which is widely accepted, but not beyond dispute. This theory proposes that a fixed "hotspot" beneath the tectonic plate lead to the formation of the Hawaiian Island chain. Wilson describes a hotspot as an upper-mantle-fixed lava source. W. Jason Morgan (1971) further developed Wilson's theory of the evolution of the Hawaiian Islands and postulated the theory of mantle plumes. Since then, the concept of mantle plumes has further been developed, and according to a widely held view intraplate volcanic island chains such as the Hawaiian Islands are formed from upwelling plumes that originate at thermal boundary layers in the Earth's mantle, some possibly as deep as the core-mantle boundary. This theory is however controversial, and the study of hotspot volcanoes is vital to ascertain the validity of the mantle plume theory. Gathering information about the composition, structure, and processes within the mantle is essential for achieving this.

This study investigates the noble gas geochemistry of several Hawaiian volcanoes, with the aim of extending the knowledge on the chemical and isotopic composition of the Hawaiian plume in order to draw conclusions on the structure and evolution of the mantle plume beneath the Hawaiian Islands. Noble gases are particularly useful in this context because due to their chemical attributes they are ideal geochemical tracers. Noble gases, especially helium, are used as tracers for reservoirs in the Earth's mantle based on the assumption that high $^{3}He/^{4}He$ ratios (> 8 R_A, R_A refers to the atmospheric $^{3}He/^{4}He$ ratio) represent material from the deep, supposedly less degassed mantle, whereas lower $^{3}He/^{4}He$ ratios (~ 8 R_A) are thought to represent the upper mantle. Recent Hawaiian volcanoes have been subdivided into two trends, the "Loa" and "Kea" trends, based on their systematic isotopic differences. Investigating the noble gas systematics of samples from the older "Kea trend" volcanoes is

essential for a deeper insight into the evolution of the Hawaiian plume, especially since noble gas data, other than helium, from these sites are scarce.

For the noble gas measurements, drill core samples from Mauna Kea and Kilauea, as well as surface samples from Kohala, all located on the Island of Hawaii, and Haleakala, located on Maui, have been analysed. The advantage of drill core samples is not only that the long-term history of lavas from one volcano can be revealed, but also that the overprinting by cosmogenic nuclides like ^{3}He and ^{21}Ne is insignificant because the samples have not been exposed to cosmic radiation for an extensive amount of time, but have been buried by overlying lava flows. Where drill core samples were unavailable, surface samples have been analysed. Mauna Kea drill core samples were derived from the Hawaii Scientific Drilling Project (HSDP). Kilauea samples from the NSF well were kindly provided by Shaul Hurwitz (U.S. Geological Survey). Surface samples were collected during field campaigns in 2005 and 2006.

The data presented here have been obtained at the GFZ German Research Centre for Geosciences.

1 Noble Gas Geochemistry

1.1 Noble Gases as Geochemical Tracers

Noble gases (He, Ne, Ar, Kr, and Xe) have been studied in geosciences for decades, and are nowadays particularly useful as inert tracers of geochemical processes. In the field of mantle geochemistry they provide a powerful tool for distinguishing between different sources for mantle-derived rocks like Mid Ocean Ridge Basalts (MORB) and Ocean Island Basalts (OIB).

The following attributes make the noble gases especially sensitive as tracers of geochemical processes, the origin, evolution and structure of the Earth's mantle.

As a result of their maximum number of valence electrons in their outer shell, noble gases are chemically inert, only exhibiting weak van der Waals type interactions; hence their element and isotope ratios are alterable only by physical processes such as vapour/liquid/solid partitioning, transport processes like diffusion, solubility, and nuclear interactions. Element and isotope ratios of noble gases bear information about igneous processes like partial melting, crystal fractionation, and magmatic degassing that result in systematic elemental fractionation. The solubility of noble gases in basaltic melts decreases with increasing atomic mass and is directly related to the atomic radius. Hence degassing of basaltic melts leads to a fractionation of the relative abundance of noble gases within the residual melt showing a preferential depletion in the heavier noble gases (e.g. GRAHAM, 2002). Furthermore the noble gas solubility is dependent on pressure and temperature, on melt composition and on the H_2O as well as CO_2 content of silicate melts which affects the relative degassing behavior (GRAHAM, 2002). In general, noble gas solubilities are higher in more silica-rich melts (CARROLL and DRAPER, 1994). During mantle melting, the noble gases likely partition into the melt (FARLEY and NERODA, 1998), which is indicated by their distribution coefficients (D). Although the behavior of noble gases between minerals and melt is still poorly understood, results of various studies indicate that they have D values below 1 (GRAHAM, 2002), hence they behave as incompatible elements during melting events, resulting in a depletion of noble gases in the solid Earth. This in combination with their exclusion from solid materials during planetary formation causes their low abundance in the terrestrial environment. Furthermore, except for helium, the rather large radii make the accommodation in mineral lattices difficult (WHITE, 2005). This low background inventory in the terrestrial environment, the different distributions between the various terrestrial

reservoirs and the therefore diagnostic isotope ratios in them help to make the noble gases an excellent tracer for mantle reservoirs (GRAHAM, 2002). The different distribution between the terrestrial reservoirs (atmosphere, crust, mantle) is however still partly puzzling. Especially the noble gas state of the mantle is a matter of debate. Critical points in this discussion are e.g. if the mantle contains a reservoir which is undegassed, or less degassed than other mantle regions.

Radiogenic and nucleogenic noble gases are produced within the Earth as a result of spontaneous decay of parent radionuclides or by subsequent nuclear reactions. The distribution of radiogenic and nucleogenic noble gases due to radioactive decay of the nuclides K, U and Th causes modifications of the (primordial) isotope composition of noble gases (Table 1). For instance, the He composition is controlled by the α-particle production by U and Th decay, the isotope composition of Ne is modified by nuclear processes in which α-particles and neutrons collide with O, F and Mg, respectively, while the radioactive decay of ^{40}K controls the Ar isotopic composition (GRAHAM, 2002).

The least reactive member of the noble gas family, helium, has two naturally occurring isotopes, ^{3}He and ^{4}He, the latter being the more abundant one. The terrestrial inventory of ^{4}He has its origin in the radioactive decay of U and Th, whereas almost all of the ^{3}He is of primordial origin, which means it has existed since the formation of the Earth. The atmospheric $^{3}He/^{4}He$ ratio (R_A) is $1.39*10^{-6}$ ($^{3}He/^{4}He$ ratios are commonly quoted as multiples of R_A, and by convention often expressed as $^{3}He/^{4}He$, i.e. as the non-radiogenic to radiogenic isotope) (GRAHAM, 2002). Unlike the other noble gases, helium undergoes gravitational escape from the Earth's atmosphere and is probably not recycled by plate tectonics, which makes it a unique isotopic tracer since the source signal is not altered by atmosphere derived helium. The $^{3}He/^{4}He$ ratio in terrestrial reservoirs varies by several orders of magnitude due to processes like radiogenic ingrowth. While mantle-derived materials are characterized by high values ($> 10^{-5}$), the continental crust shows rather low values ($\sim 10^{-8}$) (GRAHAM, 2002). Hence, helium isotopes provide useful possibilities to distinguish between mantle and crustal contaminants as well as the potential to indicate different mantle source signatures.

Neon has three stable isotopes: ^{20}Ne, ^{21}Ne and ^{22}Ne. While ^{20}Ne and ^{22}Ne in the Earth's mantle are mainly of primordial origin (although there may be a small but probably negligible nucleogenic production of ^{22}Ne by $^{19}F(\alpha, n)^{22}Na(\beta^{+})\ ^{22}Ne$), ^{21}Ne is produced by nuclear

processes [$^{18}O(\alpha, n)^{21}Ne$;$^{24}Mg(n,\alpha)^{21}Ne$]. Besides the nucleogenic production, ^{21}Ne is also produced by interactions of high-energy cosmic ray particles with rock surfaces. Atmospheric contamination of mantle neon is a ubiquitous problem.

Argon is composed of the two primordial isotopes ^{36}Ar and ^{38}Ar, and of ^{40}Ar produced by the decay of ^{40}K ($t_{1/2}$= $1.25*10^9$ yr). The primordial $^{40}Ar/^{36}Ar$ ratio of the solar system, measured in graphite-diamond aggregates from a rare class of stony meteorites, is in the range of 10^{-3} and lies therefore close to the estimated value of 10^{-4} (BEGEMANN et al., 1976). The Earth's atmosphere exhibits a $^{40}Ar/^{36}Ar$ ratio of 296, the highest values measured in MORBs reach up to 40,000 (BURNARD et al., 1997), whereas OIBs have, due to their primitive source, ratios closer to the atmospheric value.

Krypton has five naturally occurring stable isotopes: ^{80}Kr, ^{82}Kr, ^{83}Kr, ^{84}Kr and ^{86}Kr. ^{83}Kr, ^{84}Kr and ^{86}Kr are additionally produced in minor amounts by spontaneous fission of ^{238}U ($t_{1/2}$= 4.47 Ga).

Xenon has nine stable isotopes. All Xenon isotopes are primordial, with ^{129}Xe additionally produced by β decay of the extinct nuclide ^{129}I ($t_{1/2}$= 17 Ma) and the four heaviest Xe isotopes being fission products of ^{238}U ($t_{1/2}$= 4.47 Ga) and the extinct ^{244}Pu ($t_{1/2}$= 82 Ma).

The main features of the different noble gas reservoirs will be compiled in the following sections.

Table 1: Some production pathways for noble gas isotopes (GRAHAM, 2002).

Isotope	***Process***	***Half Live (Ma)***
	Long-Lived Radioactivity	
^{4}He	$^{238}U \rightarrow {}^{206}Pb+8\ {}^{4}He^{++}+6\beta^{-}$	4,468
	$^{235}U \rightarrow {}^{207}Pb+7\ {}^{4}He^{++}+4\beta^{-}$	704
	$^{232}Th \rightarrow {}^{208}Pb+6\ {}^{4}He^{++}+4\beta^{-}$	14,010
^{40}Ar	^{40}K -^{ec}-> $0.105^{1}\ {}^{40}Ar$	1,250
$^{136,134,132,131}Xe$	^{238}U Fission	4,468
	Extinct Radioactivity	
^{129}Xe	$^{129}I \rightarrow {}^{129}Xe+\beta^{-}$	16
$^{136,134,132,131}Xe$	^{244}Pu Fission	82
	Nuclear reactions subsequent to U and Th decay	
^{21}Ne	$^{18}O(\alpha,n)\ {}^{21}Ne$	
	$^{24}Mg(n,\alpha)\ {}^{21}Ne$	

[1] 0.105 is the branching ratio of ^{40}K to ^{40}Ar by electron capture (ec)

1.2 Noble Gas Reservoirs

1.2.1 Noble Gases in the Solar System

The solar system formed 4.6 Ga ago from the well-mixed solar nebula. The isotopic abundances in studied materials from the solar system are rather similar to each other except for the noble gases which are strongly depleted in solid matter due to their inertness and volatility (WIELER, 2002). Several noble gas components have been identified in the solar system. The noble gas components “solar” and “planetary” (also referred to as “Q” or “P1”), found in solar wind and primitive meteorites respectively, show isotopically contrasting patterns. The planetary noble gases show a much stronger elemental fractionation compared to the solar component, with lighter noble gases being depleted relative to heavier gases. The origin of the planetary noble gas component in meteorites is not well understood (OZIMA et al., 1998; OZIMA and PODOSEK, 2002; PATZER and SCHULTZ, 2002; VERCHOVSKY et al., 2002). Knowing the noble gas composition of the early solar nebula and revealing to what extent planetary bodies reflect the early nebula noble gas composition is of great

interest. Since it is not possible to sample the sun, which is believed to represent materials from which the solar system has formed, the noble gas pattern of solar wind is a present-day proxy for the early solar nebula composition (OZIMA and PODOSEK, 2002; WIELER, 2002).

The origin of the primordial terrestrial noble gases is still a matter of debate. The noble gases in the Earth's atmosphere are distinctly different from the solar pattern. It was proposed that the terrestrial noble gases as well as the component found in meteorites (planetary, "Q", or P1), could have been fractionated from the solar composition by Rayleigh distillation processes (OZIMA and PODOSEK, 1999). TRIELOFF et al. (2000) challenged this hypothesis and claimed the initial solar component in the Earth to be a component called Ne-B (BLACK, 1972), which is a mixture of solar wind and solar energetic particles found in gas-rich meteorites. Other models assert that solar-type noble gases, which have been incorporated into the mantle, were partially lost and fractionated into the atmosphere to form the atmospheric composition (PEPIN, 1991).

Table 2: Solar and planetary isotopic abundances of neon and argon.

Component	$^{20}Ne/^{22}Ne$	$^{21}Ne/^{22}Ne$	$^{38}Ar/^{36}Ar$
Solar[1] (solar wind composition)	13.6±0.4	0.0326±0.0010	0.1818±0.0007
Q Phase[2] (planetary component)	10.70±0.15	-	0.188±0.007
Ne-B[3]	12.52±0.18	0.0335±0.0015	0.186±0.004

[1] WIELER, 2002

[2] WIELER et al., 1991

[3] BLACK, 1972

1.2.2 Noble Gas State of the Earth's mantle

The noble gas state of the Earth's mantle can be determined in mantle-derived materials that have trapped mantle noble gases. These materials are mainly oceanic basalts, which can be divided into two basic types, MORBs (Mid Ocean Ridge Basalts) and OIBs (Ocean Island Basalts). MORBs originate at oceanic ridges, whereas OIBs are generated from intra-plate volcanoes. OIBs are compositionally more varied than MORBs, richer in incompatible elements (such as K, Rb, Ba) and Rare Earth Elements (REE), and they tend to have more radiogenic isotope ratios (such as Sr and Nd) (e.g. MCBIRNEY, 1993). Both, MORBs and OIBs, are presumably derived from different mantle sources and can therefore be used to asses the noble gas state in different zones of the mantle (e.g. OZIMA and PODOSEK, 2002).

There is an evident dissimilarity in the $^3He/^4He$ ratios between these two mantle-derived materials that is widely accepted as a strong evidence for two distinct mantle source regions of MORBs and OIBs (GRAHAM, 2002). The global variability along mid-ocean ridges is important to understand in the context of convective mixing and melt generation in the upper mantle (GRAHAM, 2002). GRAHAM (2002) evaluated a compilation of $^3He/^4He$ analyses of submarine glasses sampled along mid-ocean-ridges and determined the mean $^3He/^4He$ ratio to be 8.75 ± 2.12 R_A. According to GRAHAM (2002) this small range implies several processes that could be involved: Relatively rapid mixing rates in the MORB source accompanied by input of high $^3He/^4He$ material from deep in the mantle, radiogenic ingrowth in the upper mantle, input of subducted crust and lithosphere that is enriched in U and Th as well as partial melting of heterogeneous upper mantle. MORB samples with higher $^3He/^4He$ ratios are from ridge sections that show anomalous geochemical features, like the sub-ridge mantle being influenced by nearby ocean islands (GRAHAM, 2002).

When investigating ocean islands associated with a mantle plume, the parameters of interest include the depth of plume origin, the plume mass flux, the extent and depth of partial melting, and the proximity of a hotspot to a plate boundary. The general pattern of $^3He/^4He$ ratios in OIBs is characterized by a much higher variability from MORB-like values to much higher ratios. This variability may be related to the distance from the centre of the mantle upwelling beneath an island, to the stage of a volcano's evolution, to a variability in mixing between plume-derived material and material derived from the upper mantle, and in addition isotopic heterogeneity within the plume can also account for the observed variabilities (GRAHAM, 2002). The high $^3He/^4He$ ratios of OIBs ("high-^{3}He" hotspots like Iceland, Hawaii, Samoa, Réunion, or Easter Island, where Iceland and Hawaii provide the highest magmatic $^3He/^4He$ ratios) are accredited to a lower mantle source with a higher time-integrated $^3He/(U+Th)$ ratio compared to a shallow mantle source for MORBs. A small group of "low-^{3}He" hotspot islands (5-8 R_A) is thought to result from addition of radiogenic helium from recycled ancient crustal material (HILTON and PORCELLI, 2003). It is however difficult to generalize about global relationships between $^3He/^4He$ and other geochemical parameters of OIBs, like for instance their large variability in major or trace element composition (GRAHAM, 2002). Ocean islands that have been studied for their $^3He/^4He$ ratios include Iceland, Hawaii, Samoa, Canary Islands, Réunion or Galápagos, which are all quite unique in their settings and show a wide range in their $^3He/^4He$ ratios. The Iceland hotspot is ridge-centred and has a moderate plume flux. It also shows large spatial variability in $^3He/^4He$ ratios. The Hawaii hotspot has the largest plume flux and is situated beneath a fast moving

plate and old lithosphere far away from any plate boundaries. Samoa has a moderate plume flux and is located on a fast moving plate near the Tonga Trench. The Canary Island hotspot has a small plume flux and is situated on the oldest lithosphere in the ocean basins, adjacent to a continent on the very slow moving African plate. Réunion is an intraplate hotspot located on a slow moving plate and the Galápagos hotspot is near a spreading ridge that is migrating away from the hotspot (GRAHAM, 2002). $^{3}He/^{4}He$ ratios of these localities are shown in Table 3. Not only do the different hotspots vary significantly in their $^{3}He/^{4}He$ ratios, but also within one plume there are large spatial variations. In the Galápagos plume, for example, $^{3}He/^{4}He$ ratios change from high values in the west and south to MORB-like values in the east (GRAHAM, 2002). Examples for a temporal variability of the $^{3}He/^{4}He$ ratios include Samoa and Hawaii. These localities show extensive volcanism that is consistent with the existence of mantle plumes due to thermal upwellings from regions deep in the earth. These mantle plumes may have been remained partly isolated over geological time and could thereby be less degassed compared with the shallower mantle source regions for MORBs (GRAHAM, 2002). If the OIB source is less degassed in comparison to the MORB source, and is hence rich in primordial noble gases like ^{3}He, one would expect the helium concentrations of OIBs with high $^{3}He/^{4}He$ to be higher than those of MORBs, if they reflect the concentrations of their mantle sources. However, as inferred from glasses derived from Loihi Seamount, Hawaii, for instance, helium abundances are generally lower than those of MORB glasses. ANDERSON (1998a) termed this observation the “helium paradox” (FISHER, 1985; FISHER, 1989; STAUDACHER and ALLÈGRE, 1989; HONDA et al., 1993b; ANDERSON, 1998a; ANDERSON, 1998b). Several mechanisms have been invoked to explain the helium paradox. HILTON et al. (1997) propose extensive degassing prior to eruption of plume melts to account for the lower helium concentrations of OIBs. GRAHAM (2002) furthermore states that the helium paradox is a “manifestation of shallow level processes and has little bearing on mantle source characteristics“. PARMAN (2005) and PARMAN et al. (2007) suggest an alternative model for the helium isotopic evolution in which a less degassed reservoir for OIBs becomes redundant. In this alternative model these authors infer that helium might be more compatible than U and Th during mantle melting and that the mantle residues can preserve high $^{3}He/^{4}He$ ratios and will still have low helium concentrations (HOPP and TRIELOFF, 2008).

Table 3: Variability of $^{3}He/^{4}He$ ratios for different ocean island localities.

Location	$^{3}He/^{4}He$
Iceland[1]	5-40 R_A
Hawaii[2]	8-35 R_A
Samoa[3]	11-24 R_A
Canary Islands[4]	5.5-8.9 R_A
Réunion[5]	11-30 R_A
Galápagos[6]	up to 30 R_A

[1] KURZ et al., 1985; HILTON et al., 1990; MARTY et al., 1991; POREDA et al., 1992b; BURNARD et al., 1994; HILTON et al., 1998; HARRISON et al., 1999; HILTON et al., 1999; BREDDAM et al., 2000; DIXON et al., 2000; BREDDAM and KURZ, 2001; MOREIRA et al., 2001; ALTHAUS et al., 2003; KURZ et al., 2004

[2] KURZ et al., 1982a; KANEOKA et al., 1983; KURZ et al., 1983; HIYAGON et al., 1992; HONDA et al., 1993a; HILTON, 1997; VALBRACHT et al., 1997; ALTHAUS et al., 2003; KURZ et al., 2004

[3] FARLEY and CRAIG, 1992a; POREDA et al., 1992b

[4] GRAHAM et al., 1996; HILTON et al., 2000a

[5] KANEOKA et al., 1986; STAUDACHER et al., 1986; GRAHAM et al., 1990; MARTY et al., 1993; HANYU et al., 2001

[6] GRAHAM et al., 1993; KURZ and GEIST, 1999

The study of MORBs and OIBs has revealed that in general the Earth's mantle is characterized by elevated $^{21}Ne/^{22}Ne$ and $^{20}Ne/^{22}Ne$ ratios (e.g. GRAHAM, 2002). The different correlations between $^{21}Ne/^{22}Ne$ and $^{20}Ne/^{22}Ne$ in MORBs and OIBs are shown in Figure 1. The solar and atmospheric compositions are given in the diagram. The latter is passed by all correlation lines due to the omnipresent atmospheric component in all mantle-derived and crustal materials. OIBs, represented by the Loihi-Kilauea line defined by HONDA et al. (1991), and MORBs, represented by the MORB line defined by SARDA et al. (1988), approach the solar $^{20}Ne/^{22}Ne$ value, whereas the atmospheric component is fractionated from the solar composition, resulting is a much lower $^{20}Ne/^{22}Ne$ value. MORBs and OIBs are influenced in their isotopic composition by addition of nuclear Ne to the primordial Ne, resulting in a shift of $^{21}Ne/^{22}Ne$ to higher values, as indicated by the pink line in Figure 1. The isotopic neon composition of the mantle sources of oceanic basalts can therefore be considered as a mixture between air, nucleogenic and primordial end-members (e.g. HONDA et al., 1993a). The systematic differences in the neon isotope composition of MORBs and OIBs are due to differences in the nucleogenic ^{21}Ne production and the content

of primordial Ne in their mantle sources (GRAHAM, 2002). The MORB source is thought to have degassed much of its primordial components and hence shows a relative enrichment in the nucleogenic component. OIBs on the other hand are thought to be more primitive, due to a lesser degree of degassing. OIBs erupting in plume-related localities such as Hawaii, Iceland or Réunion, show due to a lower (less nucleogenic) $^{21}Ne/^{22}Ne$ ratio, a much steeper trend in the Ne three-isotope diagram compared to MORBs. The MORB mantle source presumably has a lower time-integrated $^{3}He/(U+Th)$ and $^{22}Ne/(U+Th)$ than the OIB mantle source at least for settings like Hawaii and is furthermore depleted in trace elements in comparison to some OIB mantle sources. This led to the assumption that the mantle source for Hawaii and other OIBs like Iceland or Réunion contains more primordial ^{3}He and ^{22}Ne compared to the MORB source (GRAHAM, 2002). The steeper slope of the OIB lavas in the Ne three-isotope diagram is attributed to a less degassed lowermost mantle, resulting in a lower $^{21}Ne/^{22}Ne$ for a given $^{20}Ne/^{22}Ne$, the former being less sensitive to an isotopic shift induced by addition of nucleogenic ^{21}Ne (SHAW et al., 2001).

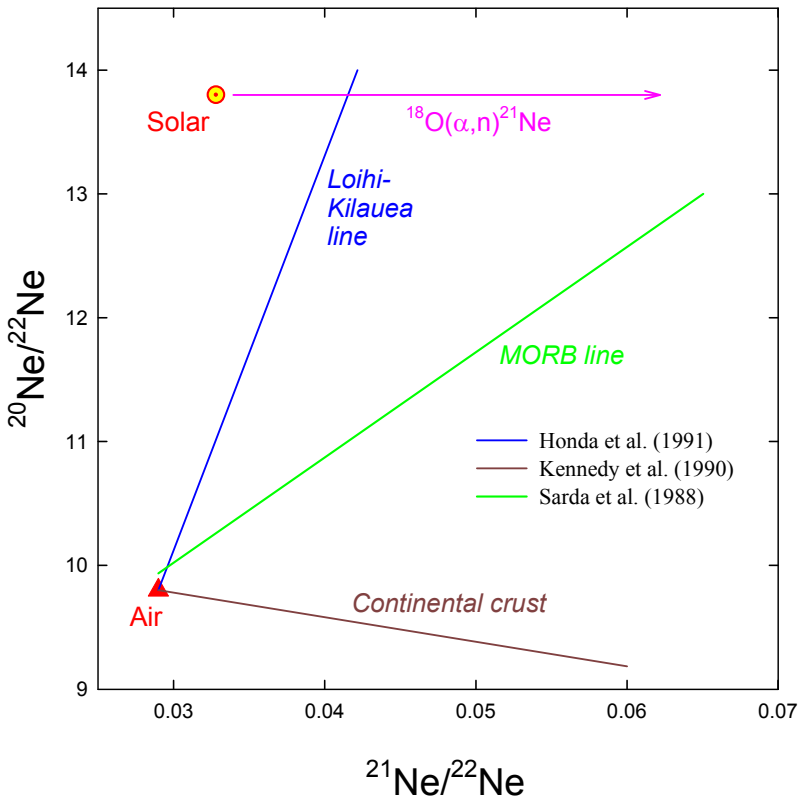

Figure 1: The Ne three-isotope diagram ($^{20}Ne/^{22}Ne$ vs. $^{21}Ne/^{22}Ne$). Data sources are MORB - Sarda et al. (1988); OIB – Honda et al. (1991); Crust – Kennedy et al. (1990).

A still discussed issue in neon-isotope systematics is the nature of the initial solar Ne component within Earth. The elevated $^{21}Ne/^{22}Ne$ and $^{20}Ne/^{22}Ne$ ratios of mantle-derived materials can either be explained by the presence of a solar neon component as represented by solar wind ($^{20}Ne/^{22}Ne$= 13.6 (WIELER, 2002)) or by a neon-B-like component (solar-type Ne in meteorites with $^{20}Ne/^{22}Ne$= 12.5 (TRIELOFF et al., 2000)). Assuming a coupling of He and Ne in gases extracted from mantle-derived samples due to the linked nuclear production of ^{21}Ne and ^{4}He ($^{4}He/^{21}Ne^{*}$ = 2.2 ±0.1*10^{7}) (YATSEVICH and HONDA, 1997), as proposed by the solar hypothesis from of HONDA et al. (1993b), an increase in $^{21}Ne/^{22}Ne$ should be accompanied by a decrease in $^{3}He/^{4}He$. However, SHAW et al. (2001) showed for the Manus Basin a decoupling of He and Ne isotopes as did NIEDERMANN et al. (1997) for the East Pacific Rise (EPR). The latter view has recently been challenged by KURZ et al. (2005), who claimed a coupling of He and Ne for the EPR despite data that agree with those of NIEDERMANN et al. (1997). More recent work by STRONCIK et al. (2008) revealed a He-Ne decoupling on Mid-Atlantic Ridge glasses. According to DIXON et al. (2000) and DIXON (2003), helium and neon heterogeneities in Icelandic basalts are due to processes during generation and eruption of magmas like shallow-level elemental fractionation and binary mixing.

The high $^{40}Ar/^{36}Ar$ ratios of MORBs are the result of a source strongly degassed in ^{36}Ar which has furthermore experienced ingrowths of ^{40}Ar with time. Terrestrial $^{40}Ar/^{36}Ar$ ratios exhibit a large range, caused by contamination of the magmatic component with atmospheric argon from e.g. seawater, altered wall rock, or air itself. Due to this notorious air contamination of MORBs and OIBs, measured $^{40}Ar/^{36}Ar$ ratios should be considered a minimum estimate for their source (GRAHAM, 2002).
Maximum measured values for the $^{40}Ar/^{36}Ar$ ratio in ocean island basalts reach up to 8000 and 8300 for olivine phenocrysts from Juan Fernandez and basalt glasses from Loihi Seamount (FARLEY and CRAIG, 1994; TRIELOFF et al., 2000), hence the mantle sources of localities like Iceland, Hawaii and Réunion supposedly have ratios of $^{40}Ar/^{36}Ar \geq 8000$ (GRAHAM, 2002). These assumed values for argon isotopes in OIBs may however reflect contamination with MORB Ar, which would mean that some observed Ar ratios around 300 may represent the OIB source best (OZIMA and PODOSEK, 2002).

The krypton isotopic composition of oceanic basalts is, due to the minor contribution of ^{83}Kr, ^{84}Kr and ^{86}Kr from spontaneous fission of ^{238}U to the relatively high natural abundance

(11.5%, 57% and 17.3%, respectively for ^{83}Kr, ^{84}Kr and ^{86}Kr), typically the same as modern air. Krypton isotopes are thus not very diagnostic of mantle processes (GRAHAM, 2002).

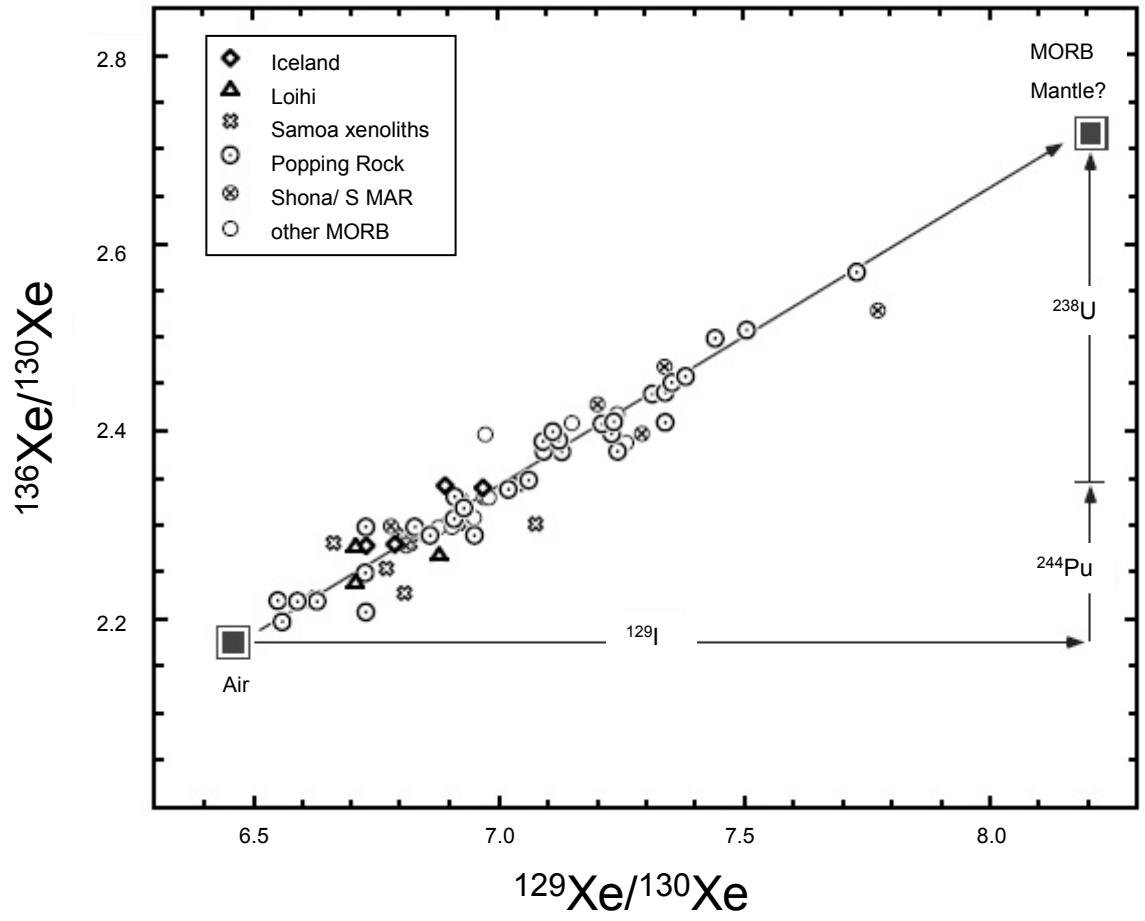

Figure 2: ^{136}Xe/^{130}Xe versus ^{129}Xe/^{130}Xe in MORB and OIB samples, figure taken from GRAHAM (2002).

Resolving isotopic Xe variations in mantle-derived materials is difficult, due to the ubiquitous presence of atmospheric xenon. Elevated ^{129}Xe/^{130}Xe and ^{136}Xe/^{130}Xe have been distinguished in MORBs (STAUDACHER and ALLÈGRE, 1982; KURZ et al., 1998). The largest and most precise excesses of ^{129}Xe and ^{136}Xe have been determined for the Mid-Atlantic Ridge (MAR) popping rock (^{129}Xe/^{130}Xe up to 7.73; ^{136}Xe/^{130}Xe up to 2.57; atmosphere 6.48 and 2.17, respectively). These excesses are derived from the extinct radioactivity of ^{129}I and from spontaneous fission of ^{238}U and extinct ^{244}Pu, respectively. The xenon composition in MORBs reflects mixing of air and a depleted mantle component. OIBs, on the other hand, exhibit much smaller Xe anomalies than MORBs, which is probably due to a higher degree of contamination. The OIB source may theoretically show a trend different from MORBs, due to

different fissiogenic contributions from ^{238}U and ^{244}Pu. However, as for now, a systematic trend of OIBs is not clearly resolved. The available data for Xe anomalies in OIBs from TRIELOFF et al. (2000), plot on the MORB correlation line. However, if considered in combination with $^{20}Ne/^{22}Ne$, samples from Iceland and Loihi seem to define a shallower slope compared with MORB. The data set shows too much scatter though for defining an extrapolated signal for the OIB source. Hence, at the present time, it remains a matter of speculation whether OIB and MORB sources are different regarding their Xe isotope signature (GRAHAM, 2002).

Helium-Neon-Argon Systematics

The measured noble gas concentrations, corrected for atmospheric contamination, can be used to estimate the nucleogenic (Ne^*) and solar Ne (Ne_S) amounts as well as the radiogenic Ar (Ar^*) amount of each sample as described by GRAHAM (2002). The estimated abundances are then related to the measured helium abundances ($^3He/^{22}Ne_S$, $^4He/^{21}Ne^*$ and $^4He/^{40}Ar^*$). In order to estimate the nucleogenic and solar Ne amounts it has to be considered, that mantle neon is a mixture of primordial solar (with $^{20}Ne/^{22}Ne$ ratio of 13.6 or 12.5), nucleogenic and atmospheric neon, as opposed to the calculation of radiogenic Ar that is derived from the mantle ($^{40}Ar^*$), where primordial ^{40}Ar is negligible (GRAHAM, 2002).

Since ^3He and ^{22}Ne are primordial, the $^3He/^{22}Ne_S$ of unfractionated mantle gases should reflect the primordial ratio. The mean primordial $^3He/^{22}Ne_S$ ratio for MORBs and OIBs is 7.7 ± 2.6 (HONDA and MCDOUGALL, 1998; HONDA and PATTERSON, 1999), which is about twice the modern-day solar wind value of ~3.8 (BENKERT et al., 1993). The higher values of mantle-derived materials indicate a fractionation of helium and neon from the solar composition, assuming an initial solar isotope composition of the solid Earth. According to HONDA and MCDOUGALL (1998) this elemental fractionation was probably caused by a solubility-controlled degassing process early in Earth's evolution resulting in a relative enrichment in helium. However, degassing processes during generation and eruption of magmas also affect helium and neon differently and lead to a decoupling of their isotopic systematics.

Both, ^4He and ^{21}Ne are produced by U and Th decay, ^4He is a daughter isotope of the radionuclides ^{235}U, ^{238}U, and ^{232}Th, whereas ^{21}Ne is produced by natural nuclear processes subsequent to U and Th decay (Table 1). The nucleogenic ^{21}Ne to radiogenic ^4He production ratio of the mantle has been almost constant over Earth's history, hence the $^4He/^{21}Ne^*$ of

unfractionated mantle gases is expected to be the same as the estimated production ratio of 2.2 $\pm 0.1 * 10^7$ (YATSEVICH and HONDA, 1997).

The $^4He/^{40}Ar^*$ production ratio is a function of accumulation time and the K/U and Th/U ratios and varies between 1.6 and 4.2 (HONDA and PATTERSON, 1999; GRAHAM, 2002). Mantle-derived materials showing $^4He/^{40}Ar^*$, $^3He/^{22}Ne_S$ and $^4He/^{21}Ne^*$ higher than the production and primordial ratios, respectively, suggest that degassing processes have led to a helium enrichment compared with neon and argon.

1.2.3 Noble Gas State of the Earth's Crust and Atmosphere

Trapped noble gases in crustal rocks are either of atmospheric origin, or derived from in situ radiogenic and nucleogenic production. Noble gases are furthermore introduced into the continental crust from the mantle due to magmatic activity (BALLENTINE and BURNARD, 2002). Cosmogenic neon and helium are moreover to be considered near the Earth's surface, and extraterrestrial noble gases carried by cosmic dust accumulate in deep ocean bottom sediments (e.g. OZIMA and PODOSEK, 2002).

Cosmic-Ray Produced Noble Gases

In situ production of cosmogenic noble gases (^3He, ^{21}Ne) in mineral grains is due to bombardment by secondary cosmic rays, which induce spallation processes in the target mineral. The production mechanisms of cosmogenic nuclides besides spallation processes include stopped and fast muon induced reactions with target elements in the mineral lattice. Production rates of cosmogenic nuclides are contingent on the exposure time and intensity of the cosmic radiation, which in turn depends on the latitude and elevation and a potential shielding of the rock surface. The mean cosmic ray attenuation length is about 60 cm for rocks with a density of $2.7 g/cm^3$. About 63% of the cosmogenic nuclides are produced within the mean attenuation length (LAL, 1991). Cosmic ray muons penetrate much deeper into the rock and may produce for example ^3He and ^{21}Ne. Hence, for the surface samples analysed in this study a potential cosmogenic contribution has to be considered. Noble gases that are not trapped in the mineral lattice but in fluid inclusions are probably not altered significantly by these processes. These noble gases can be extracted by crushing of the mineral grains, a method that is preferable for samples that reveal cosmogenic contamination when the noble gases are thermally extracted.

Radiogenic, Nucleogenic, and Fissiogenic Noble Gases in the Crust

The dominant source of ^{4}He in the crust is the α-decay of U and Th, whereas ^{3}He is produced by thermal neutron capture of ^{6}Li ($^{6}Li(n,\alpha)^{3}H$ $(\beta^{-})^{3}He$). The average crust is characterized by a $^{3}He/^{4}He$ ratio of about 10^{-8}, which is considerably lower than compared to the well defined upper mantle ratio of about 10^{-5} (OZIMA and PODOSEK, 2002).

The production of Neon isotopes in the crust as a result of nuclear reactions (Table 4) can make a significant contribution to the neon isotopic composition in the crust, due to the low abundance of neon relative to U and Th (KENNEDY et al., 1990). ^{21}Ne and ^{22}Ne are produced in significant amounts in the crust mainly through the reactions of oxygen and fluorine with α particles from the radioactive decays of U and Th, while the nucleogenic production of ^{20}Ne can be neglected, leaving the ^{20}Ne concentration mainly to primordial origin (OZIMA and PODOSEK, 2002). The crustal neon composition is distinct from air neon, due to a clear excess of $^{21,22}Ne$ relative to ^{20}Ne resulting in $^{20}Ne/^{22}Ne$ ratios below the air value (9.8), in contrast to mantle-derived materials with $^{20}Ne/^{22}Ne \geq 9.8$. The array for the continental crust in the Ne three-isotope diagram (Figure 1) reflects mixing between atmospheric and nucleogenic Ne.

Table 4: Nucleogenic neon production via different reactions in the mantle and crust (YATSEVICH and HONDA, 1997).

Isotope	***Reaction***	***Production over 4.5 Ga, % of total for given isotope***	
		Mantle	Crust
^{20}Ne	$^{17}O(\alpha,n)^{20}Ne$	99.78	99.89
	$^{23}Na(p,\alpha)^{20}Ne$	0.22	0.11
^{21}Ne	$^{18}O(\alpha,n)^{21}Ne$	96.43	99.94
	$^{24}Mg(n,\alpha)^{21}Ne$	3.57	0.06
^{22}Ne	$^{19}F(\alpha,n)^{22}Na(\beta^{+})^{22}Ne$	27.25	78.57
	$^{19}F(\alpha,p)^{22}Ne$	7.40	21.30
	$^{25}Mg(n,\alpha)^{22}Ne$	65.35	0.13

^{40}Ar in the Earth's crust is produced by the decay of ^{40}K. The decay of ^{40}K is branched, producing ^{40}Ca by β^- decay and ^{40}Ar by electron capture, the former being the main process of disintegration. The production of ^{36}Ar in the crust through β-decay of ^{36}Cl is small compared to the ambient background of atmosphere-derived ^{36}Ar. ^{38}Ar is produced through the reaction ^{35}Cl(α,p)^{38}Ar. The production rates for average upper crust of ^{36,38,40}Ar are 0.19 atoms $g^{-1}yr^{-1}$, $6*10^{-4}$ atoms $g^{-1}yr^{-1}$, and $2.93*10^{6}$ atoms $g^{-1}yr^{-1}$, respectively (BALLENTINE and BURNARD, 2002).

Crustal xenon (^{129,131,132,134,136}Xe) is dominantly produced through spontaneous fission of ^{238}U. Xe from extinct radioactivity of ^{244}Pu and ^{129}I is not produced in the crust, but can be carried in as components of magmatic or atmosphere-derived fluids (BALLENTINE and BURNARD, 2002).

2 Analytical Determination of Noble Gas Isotopes with the VG 5400 Mass Spectrometer

2.1 Introduction

Sector field mass spectrometry uses a static electric or magnetic sector field or a combination of both as mass analyser. The 90° sector field mass spectrometer VG 5400 (Micromass/GV) at GFZ Potsdam, designed for isotopic analysis of He, Ne, Ar, Kr and Xe, uses a magnetic field to deflect ions through a circular trajectory. Ions are produced in a Nier-type electron impact ion source and detection is accomplished by an off-axis Faraday cup for ion currents above ~10^{-13} A and an axial electron multiplier for ion currents below that.

2.2 Ion Separation in a Magnetic Field

Mass spectrometers use the difference in mass-to-charge ratio (m/e) of ionized atoms to separate them from each other. Ions with equal charge leave the exit slit of the ion source with equal kinetic energy.

$$E = \frac{1}{2} m \cdot v^2 = eU \qquad (1)$$

(E is the energy of the ion, m its mass, v its velocity, e its charge and U is the acceleration potential). Ions are then deflected onto a circular trajectory when entering the magnetic field. The following equation applies for a magnetic field perpendicular to the ion velocity:

$$e(B \times v) = m \frac{v^2}{r} \qquad (2)$$

(B is the magnetic field strength, r is the trajectory radius). Combining equations 1 and 2 results in the mass spectrometer equation:

$$\frac{m}{e} = \frac{B^2 r^2}{2U} \qquad (3)$$

By adjusting the magnetic field or the acceleration voltage it is thus possible to achieve any arbitrary radius.

2.3 Ion Optics

Ions are generated from gas atoms with initial random energy in ultrahigh vacuum in an ion source and are subsequently accelerated into a directed beam by a potential, sufficient to give the ions a coherent energy. In a Nier-type electron impact ion source (such as the bright source used in the VG5400), the electron emission is controlled by the trap current which regulates the filament current. The ions are extracted from the ionisation cage and accelerated by a 4.5 kV high voltage. The ion source is typically operated with an electron voltage of ~80 V and a trap current of 400 μA for He analysis and 200 μA for Ne, Ar, Kr, and Xe analysis.

Coming from the ion source, the ions pass a pair of beam defining slits and enter into the magnetic sector field. Once inside the magnetic field, the ions in the beam are deflected and dispersed according to their mass to charge ratio. A resolving slit at the exit of the analyser allows only the ions of interest to pass through into the detector. The relative abundance of each ion species is determined by its corresponding ion current, captured by a Faraday cup or a multiplier detector (DICKIN, 1997).

The magnetic sector field is never perfect, focusing aberrations occur due to field imperfections, inappropriate choice of field shape, and fringing fields (COTTRELL and GREATHEAD, 1986). A schematic diagram of the ion optics geometry following the Nier-type design is shown in Figure 3.

The VG5400 is a Nier-type mass spectrometer with “extended geometry” (Figure 3). It uses pole pieces set at a slightly oblique angle to the beam, generating fringing fields which cause focussing of the ion beam in the y and z planes (see Figure). The focussing of the y direction is achieved by increasing the distance from the magnet pole exit to the principal focus in the y plane, hence this design is referred to as “extended geometry” (DICKIN, 1997). This configuration improves the transmission and accuracy of the machine and permits for a magnet with 27 cm beam radius a mass resolution equivalent to a conventional mass spectrometer with 54 cm beam radius (DICKIN, 1997).

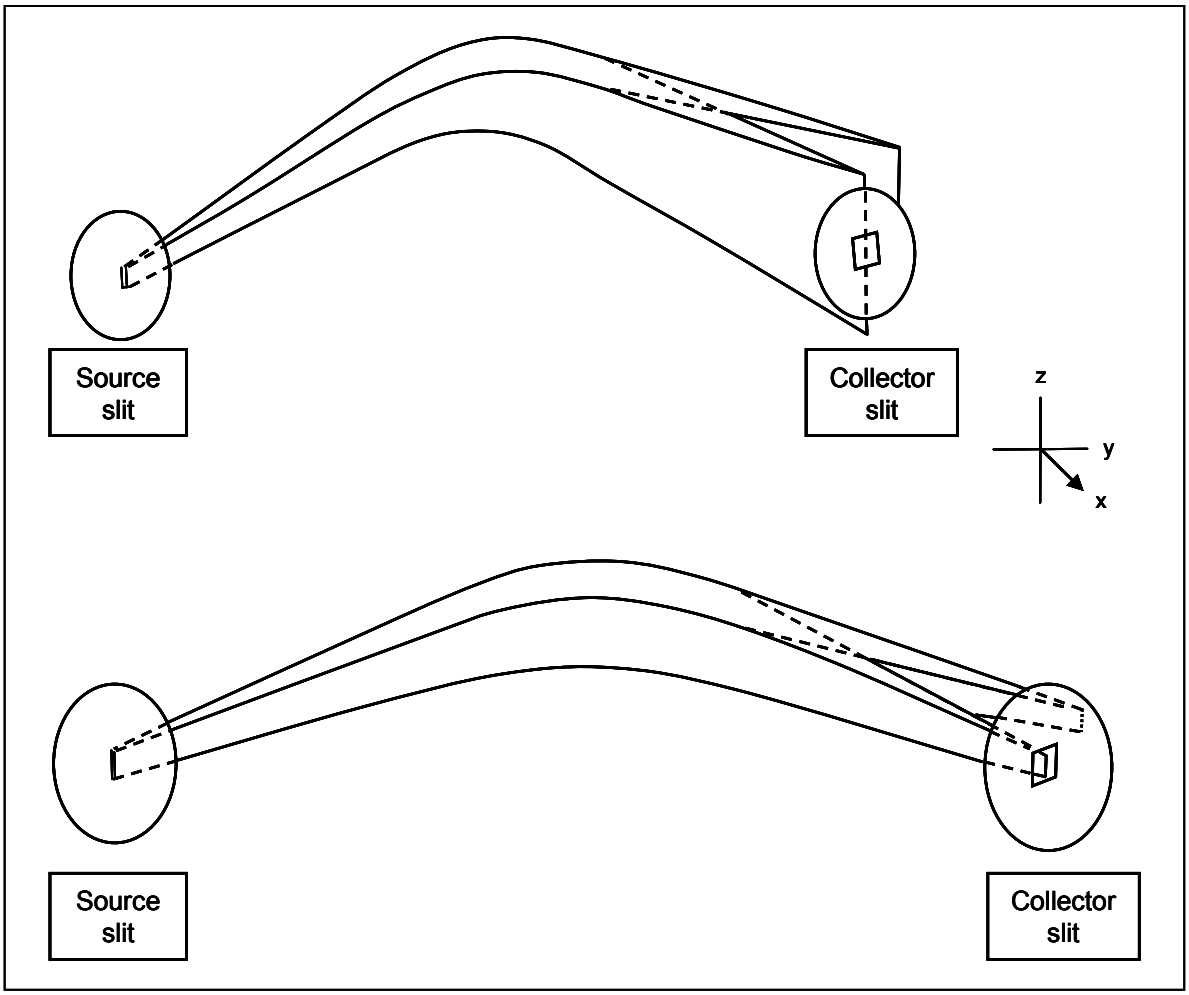

Figure 3: Schematic figure of the ion optics of a Nier-type mass spectrometer (upper panel) and of an extended geometry (lower panel) (DICKIN, 1997).

2.4 Detectors and Isobaric Interferences

The mass spectrometer is equipped with two detectors: an axial electron multiplier with a mass resolution (defined as m/Δm) of ≥ 600 on the 5% level and a Faraday cup located to the high mass side of the multiplier which has a resolution of ~ 200. Multiplier signals are processed in ion counting mode (NIEDERMANN et al., 1997). The mass resolution of the Nier-type mass spectrometer with "extended geometry" allows resolving isobaric interferences, for example $^{3}He^{+}$ (3.016 amu), from HD^{+} (3.022 amu) which in turn allows accurate determinations of the $^{3}He/^{4}He$ ratio. However, a few important interferences remain which cannot be resolved ($^{12}C^{3+}$ at m/e = 4, $^{40}Ar^{2+}$ at m/e = 20, $^{12}C^{16}O_2^{2+}$ at m/e = 22, $^{12}C_3^{+}$ and $H^{35}Cl^{+}$ at m/e = 36, and $H^{37}Cl^{+}$ at m/e = 38). Contributions of $^{12}C^{3+}$ to the mass 4 peak are only important for ^{4}He abundances near the blank level. However, by adjusting the magnetic

field to a position in the low mass side of the combined peak, acceptable results are achieved for ^4He. Accurate interference corrections are required at m/e = 20 and m/e = 22 for reliable Ne data. Therefore, to correct for $^{40}Ar^{2+}$ and CO_2^{2+}, the signals of H_2^+, $^4He^+$, CH_4^+, $^{40}Ar^+$, and CO_2^+ are monitored together with neon isotopes during each measurement cycle. The charge state ratios $^{40}Ar^+/^{40}Ar^{2+}$ and CO_2^+/ CO_2^{2+} depend on the mass spectrometer background (represented by H_2^+, $^4He^+$, CH_4^+, CO_2^+) and are fitted by a second order polynomial (Figure 4) (NIEDERMANN et al., 1997). For more detail see NIEDERMANN et al. (1997).

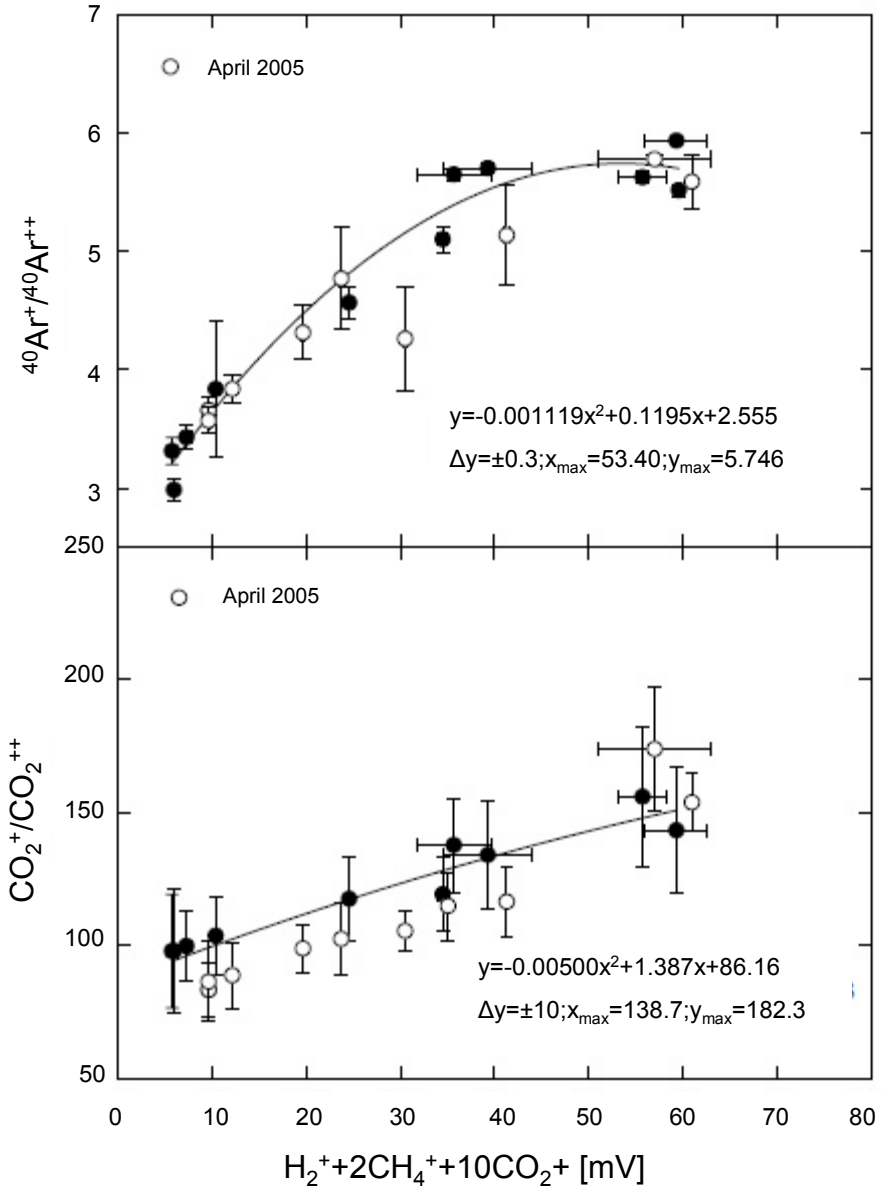

Figure 4: Dependence of charge state ratios $^{40}Ar^+/^{40}Ar^{2+}$ and CO_2^+/CO_2^{2+} on the parameter x = H_2^+ + 2CH_4^+ + 10 CO_2^+. $H_2^+$and CH_4^+ are detected on the Faraday cup and CO_2^+ on the electron multiplier.

For correcting the HCl^+ interferences on m/e = 36 and 38, $H^{35}Cl^+/^{35}Cl^+$ and $H^{37}Cl^+/^{35}Cl^+$ ratios are determined to deduce a correction factor. This is achieved by measuring the m/e=35, 36, 38 and 40 signals and extrapolating to a virtual point in time $-t_0$, when the ^{40}Ar concentration would equal zero. The extrapolated values for m/e = 36 and 38 at $-t_0$ then equal the concentrations of $H^{35}Cl^+$ and $H^{37}Cl^+$, respectively. The $H^{35}Cl^+/^{35}Cl^+$ and $H^{37}Cl^+/^{35}Cl^+$ ratios are constant for constant ion source conditions and do not depend on background pressure, but may show long-term drift. Hence the correction factors are determined in regular intervals. During all Ar measurements of samples, standards, and blanks, $^{35}Cl^+$ is monitored and together with the predetermined correction factor, the values for $H^{35}Cl^+$ and $H^{37}Cl^+$ can be deduced. Those values are used to correct the measured values for m/e = 36 and 38. For more detail see WIERSBERG (2002). For the presented Kr and Xe data, no unresolved isobaric interferences are present.

2.5 Sensitivity and Discrimination

In order to determine the gas concentration and isotope composition of a sample, the sensitivity and mass discrimination of the mass spectrometer have to be known. The sensitivity can be defined as the relationship of a measured current to a gas amount. The discrimination is the instrumental-induced isotope fractionation. Furthermore, the multiplier gain, which is the (nominal) amplification factor of the multiplier to the Faraday cup, has to be determined. For calibration, a pipette of an artificial gas mixture is used. For Ne and Ar, the isotope ratios in the calibration gas are atmospheric within uncertainties. The ^{20}Ne and ^{36}Ar isotopes are used for determining the multiplier gain. The sensitivity ε can be deduced from the known concentration of a noble gas in the calibration pipette and the measured ion current.

The discrimination D is defined as follows:

$$D = \frac{\left(\frac{A}{B}\right)_{measured}}{\left(\frac{A}{B}\right)_{true}} \qquad (4)$$

(A and B are different isotopes of the same element).

2.6 Gas Extraction, Gas Purification, Gas Measurement

In this study, noble gases were extracted through stepwise heating or crushing of the olivine sample. The mechanical gas extraction was performed using an ultrahigh vacuum crushing device. Thermal gas extraction was accomplished using a high vacuum metal extraction furnace with a cylindrical heating element made of graphite and a tantalum crucible, allowing temperatures up to 2000°C. Temperature control was provided by a W-Re thermocouple.

The sample material typically consisted of 1-2 g pure olivine minerals which were wrapped in Al or Mo foil for thermal gas extraction or filled into the sample chamber of the crushing device for mechanical gas extraction. All samples were treated with acetone in an ultrasonic bath for 10 minutes prior to loading. Thermal extraction was done in two or three temperature steps, the maximum extraction temperature always being 1750°C. Samples were dropped from a carrousel into the molybdenum liner fitted within the Ta crucible. Prior to the first sample measurement, the carrousel was heated at 100°C and evacuated for several days, in order to remove adsorbed gases.

The released gas consists mainly of reactive gases such as H_2O, N_2, O_2, CO_2, H_2, and C_xH_y and only to a very small fraction of noble gases. Thus a purification line is attached to the extraction furnace, which is equipped with a cold trap, two Ti sponges, and two SAES (ZrAl) getters. The cold trap is cooled with dry ice and condenses water vapour. The Ti sponges adsorb N_2, O_2, and CO_2 at 400°C. Since the capacity of the sponges is limited, the process is later reversed at 750°C or 850°C when the sponges are evacuated. One of the SAES getters is operated at room temperature to pump mainly hydrogen, the other one at ~ 250°C to pump other reactive gases (CO_2 and hydrocarbons). During He measurements a liquid N_2-cooled steel frit is used, which is supplemented with a liquid N_2-cooled charcoal for Ne measurements. This further reduces the Ar, Kr, and Xe as well as methane and CO_2 background during the He and Ne measurements.

Attached to the purification line are two cold heads. Ar, Kr, and Xe are adsorbed to a stainless steel frit in the first cryostatic cold head at 50K. Ne and He are adsorbed to an activated charcoal in the second cold head at 11K. Subsequently, the noble gases are sequentially released and measured separately. The desorption temperatures for He and Ne from the charcoal are 35K and 120K and for Ar, Kr, and Xe from the stainless steel frit are, 80K, 100K, and 150K respectively.

Each noble gas is measured separately over 11 measuring cycles, taking about 15-30 minutes. The measured gas is influenced by ion implantation into the metal walls of the mass spectrometer and subsequent release of earlier implanted ions, so that memory effects can

result in both, increasing or decreasing trends during a measurement. The measured data are therefore extrapolated to the time t=0 which equals the time of gas inlet into the mass spectrometer. The same is done for changing isotope ratios during a measurement, which usually tend towards the atmospheric value.

2.7 Blanks

Between sample measurements, analytical blanks were run regularly at the same temperatures used for gas extraction. Blanks are for instance caused by gases extracted from the metallic walls of the crucible and liner and therefore by the history of the crucible and liner, the extraction temperature, and by reactions of the mineral melt with the liner material, which in turn can contain different contaminants due to the conditions of manufacturing.

2.8 Data Evaluation

The data evaluation comprises the processing of sample, blank and standard measurements as well as additional calibrations. Sensitivity, mass discrimination and multiplier gain are deduced from standard measurements (Chapter 2.5) whereas factors for the interference correction for Ne and Ar are determined from calibrations (Chapter 2.4). Furthermore, analytical blanks are determined regularly. These parameters allow the calculation of accurate noble gas concentrations and isotopic compositions for the respective measurements, which are combined in case of stepwise heating to the total noble gas composition of a sample.

2.9 Uncertainties and Error Propagation

No measurement is ever absolutely accurate, random as well as systematic errors are inevitable. Systematic errors are biases in measurements which shift the values systematically in a certain direction. Such errors like for example uncertainties in the isotope ratios of reference gases can only be accounted for by error estimation because they do not follow statistical laws. However these systematic errors are usually small compared to statistical errors. A systematical error which can be accounted for in noble gas mass spectrometry is the time-depending variation of values during a measurement. This error can be avoided by extrapolation to the time of gas inlet into the mass spectrometer.

Statistical or random errors due to precision limitations can be evaluated through statistical analysis and can be assessed by error propagation. The statistical distribution of measured values x can be described by the general formula $f(x)$ of the Gaussian distribution (normal distribution):

$$f(x) = \frac{1}{\sigma\sqrt{2\pi}} e^{-\frac{1}{2}\left(\frac{x-x_0}{\sigma}\right)^2} \qquad (5)$$

(x_0 equals the true value of the measurement x, σ is the standard deviation).

The true value of the measurement x is indeterminable; an approximation has to be done by using the "least squares method of Gauss". It is a method for linear regression that determines the values of unknown quantities in a statistical model by minimizing the sum of the residuals (difference between the predicted and observed values) squared. This method is applied to deduce the most probable value out of the 11 cycles during a noble gas measurement.

The standard deviation σ is a measure of the spread of the measured values and is defined as the square root of the variance. The standard deviation of repeated measurements can describe the precision and reproducibility of a measurement, but says nothing about the accuracy of the measured value which can be affected by systematical errors.

If a measurement R is determined from several individual measured values x, y, z, the absolute error ΔR can be determined by error propagation:

$$\Delta R = \sqrt{\left(\frac{\partial R}{\partial x}\Delta x\right)^2 + \left(\frac{\partial R}{\partial y}\Delta y\right)^2 + \left(\frac{\partial R}{\partial z}\Delta z\right)^2} \qquad (6)$$

(Δx, Δy, Δz are the errors of the individual measured values x, y, z).

3 Origin and Characteristics of the Samples

3.1 Geological Setting

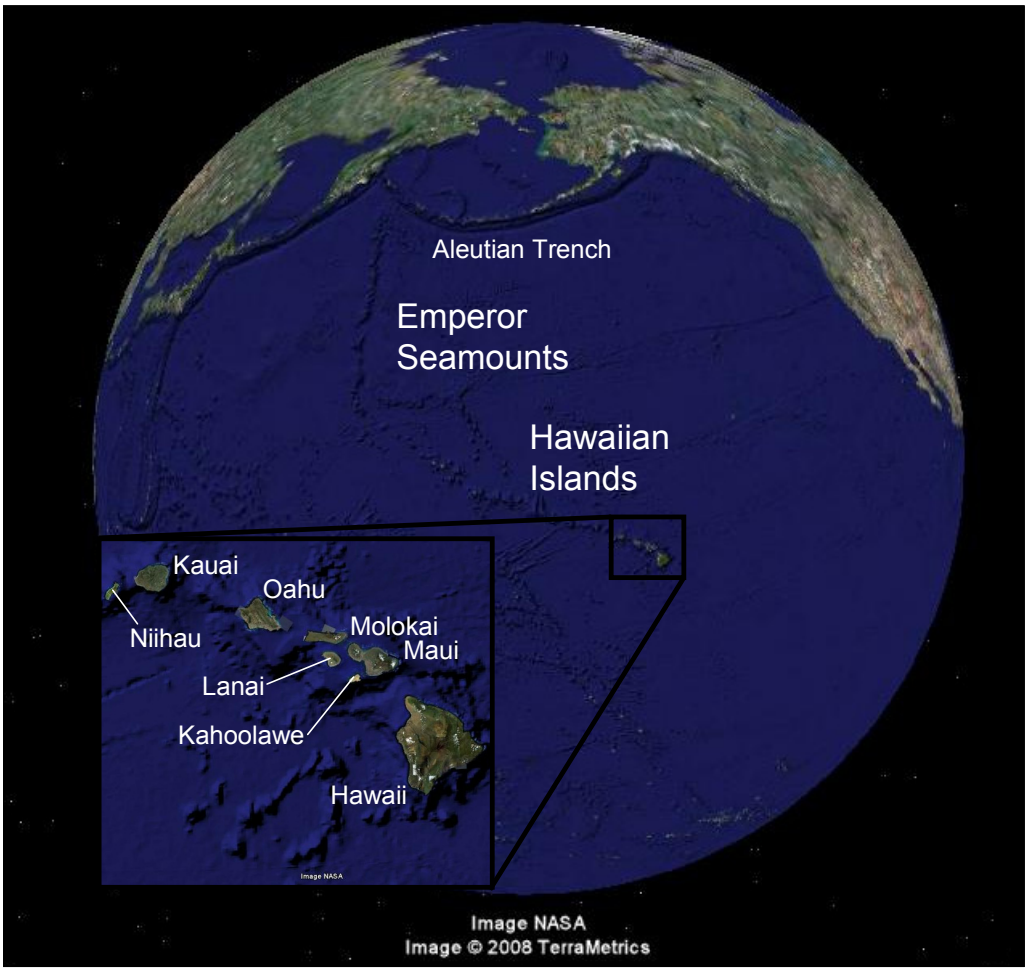

Figure 5: The Hawaiian Emperor Seamount Chain in the northern Pacific Ocean.

The Hawaiian Islands form a volcanic chain in the northern Pacific Ocean between latitudes 19°N and 29°N, trending northwest from the Island of Hawaii to Kure Island. The volcanic chain continues with a sharp bend to the north forming the Emperor Seamount Chain which stretches on to the Aleutian Trench, where the Pacific Plate is being subducted under the North American Plate. The principal Hawaiian Islands (Island of Hawaii, Maui, Kahoolawe, Lanai, Molokai, Oahu, Kauai, Niihau) lie at the southeastern end of the chain, from where the age increases progressively to the northwest. The volcanism in Hawaii is interpreted in terms of the northwestward migration of the fast-spreading Pacific plate over a stationary hotspot in

the mantle beneath, which is recorded by the Hawaiian-Emperor seamount chain and the Hawaiian Islands. Mauna Kea, Mauna Loa, Kilauea, and Loihi Seamount are the youngest and still active volcanoes of the Hawaiian Islands and provide information on how the volcanoes of the chain formed (SHARP and RENNE, 2005).

3.1.1 The Plume Theory

J. Tuzo Wilson made seminal contributions to the development of the plate-tectonics theory in the 1960s and 1970s and suggested in 1963 that the Hawaiian island chain was formed due to the movement of a tectonic plate over a fixed "hotspot" (upper-mantle-fixed lava source) in the Earth's mantle (WILSON, 1963). W. Jason Morgan further developed the hypothesis of hotspots and postulated that Hawaiian volcanism is caused by the movement of the Pacific plate over a fixed hotspot, which is caused by thermal upwellings from the Earth's mantle (MORGAN, 1971). Morgan coined the phrase "deep mantle plume" for this theory, in which heat from the core is transported to the Earth's surface by convection in the mantle. Morgan applied the mantle plume theory not only to Hawaii but also showed that island chains like the Tuamotu Line and the Austral-Gilbert-Marshall island chain can be generated by the motion of a rigid Pacific plate rotating over fixed hotspots (MORGAN, 1971). Although the plume theory is controversial, many authors favour the explanation that deep mantle plumes arise from a thermal boundary layer, which may be as deep as the core mantle boundary. This topic remains however strongly debated despite detailed seismic topography studies that underline the deep origin of at least some hotspots. As P-wave velocity images show, there are six well-resolved plumes that extend into the lowermost mantle (Ascension, Azores, Canary, Easter, Samoa, and Tahiti) as well as less well-resolved plumes like Hawaii, which may also reach into the lowermost mantle (MONTELLI et al., 2004). According to MONTELLI et al. (2004) the plumes must have diameters of several hundred kilometres; otherwise they cannot be resolved by the imaging techniques. Furthermore MONTELLI et al. (2004) conclude that the convection in the lower mantle is slow, indicating that the role of plumes in heat-transport from the core to the Earth's surface is larger than suggested earlier (SLEEP, 1990). Besides the deep plumes, shallow plumes have been identified that are imaged only in the upper mantle. These include Iceland, Galápagos, and Juan de Fuca/Cobb with imaged bases near the 670 km-discontinuity (MONTELLI et al., 2004). COURTILLOT et al. (2003) developed five criteria for `primary` plumes that originate deep in the mantle and found that seven hotspots are candidates for deepest, primary plumes: they are Hawaii, Easter and Louisville in the Pacific hemisphere, and Iceland, Afar, Réunion and Tristan da Cunha in the Indo-Atlantic

hemisphere. The criteria used are the presence of a linear chain of volcanoes with monotonous age progression and an associated flood basalt province, a large buoyancy flux, a high $^{3}He/^{4}He$ ratio, and a significantly low shear wave velocity in the underlying mantle.

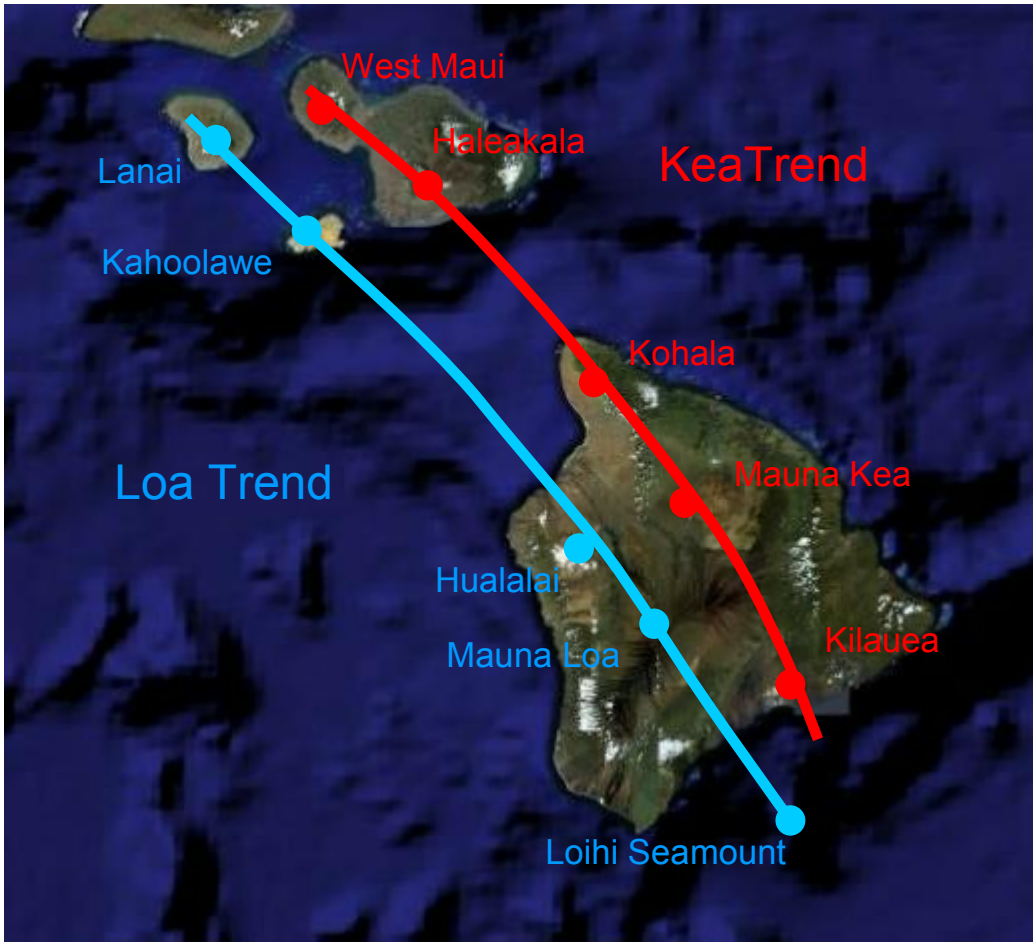

Figure 6: Map showing the Loa and Kea trends, after ABOUCHAMI et al. (2005). The subdivision into the Loa and Kea trends is based on different but overlapping radiogenic isotope characteristics and includes all volcanoes from the Island of Hawaii, Maui, Lanai and Kahoolawe.

The Hawaiian volcanoes are distinguished into two volcanic trends, the Loa trend and the Kea trend. This subdivision was first proposed by JACKSON et al. (1972), based on the parallel loci of the recent Hawaiian volcanoes and was supported by studies that found different but overlapping radiogenic isotope characteristics of the two trends ((JACKSON et al., 1972; TATSUMOTO, 1978; WEST and LEEMAN, 1987; HAURI et al., 1996; KURZ et al., 1996; LASSITER et al., 1996; ABOUCHAMI et al., 2000; ABOUCHAMI et al., 2005). According to ABOUCHAMI et al. (2005), the Loa-Kea subdivision does not hold for the volcanoes following to the northwest and therefore only includes volcanoes from the Island of Hawaii,

Maui, Lanai and Kahoolawe. The Loa trend volcanoes therefore include Loihi, Mauna Loa, Hualalai, Kahoolawe and Lanai, while the volcanoes Kilauea, Mauna Kea, Kohala, Haleakala and West Maui belong to the Kea trend (Figure 6).

3.1.2 Island of Hawaii

The idealized evolution model of Hawaiian volcanoes envisages four different stages with changing magma supply rates and composition. According to this general model, the four major eruptive stages are the preshield, shield, post-shield, and rejuvenated stage. The preshield stage, which is thought to last approximately 200,000 years (USGS, 1998), comprises the earliest phase of submarine activity. A known example today is Loihi Seamount which consists of alkalic basalt and basanite in this stage. During the shield stage, most of the total volume of the volcanoes is produced. The shield stage, in which ~95 % of the volcanoes volume is produced during roughly 500,000 years (USGS, 1998), includes submarine eruption of tholeiitic basalt which is followed by the subaerial shield forming eruptions (CLAGUE and DALRYMPLE, 1987). The shield stage lavas are dark in colour and form relatively long and thin flows, with sparse to abundant amounts of olivine phenocrysts and sometimes plagioclase (LANGENHEIM and CLAGUE, 1987). Alkalic lavas are produced during the approximately 250,000 years of post-shield stage (USGS, 1998), which make up less than 1% of the total volume of the volcanoes. The lava of the post-shield stage is generally lighter coloured than shield stage lavas, containing pyroxene, olivine, and plagioclase phenocrysts. While pyroclastic deposits are a minor constituent during the shield stage, they appear to be more abundant during the post-shield stage (LANGENHEIM and CLAGUE, 1987). These two stages are not only characterized by eruptions confined to the summit area, but also by eruptions along rift zones that extend down the flanks of the volcanoes. Between the post-shield and the rejuvenated stage lies a relatively long period without volcanic activity during which the volcano is exposed to erosion. After this quiescence, a very small amount of silica-poor lava erupts from isolated vents that are unassociated with the preexisting rift zones (LANGENHEIM and CLAGUE, 1987). This phase of very low eruption rates may comprise a period of several million years (USGS, 1998). Lavas of the rejuvenated stage are dark-coloured, forming thick flows with few or no phenocrysts; pyroclastic deposits are common during this stage.

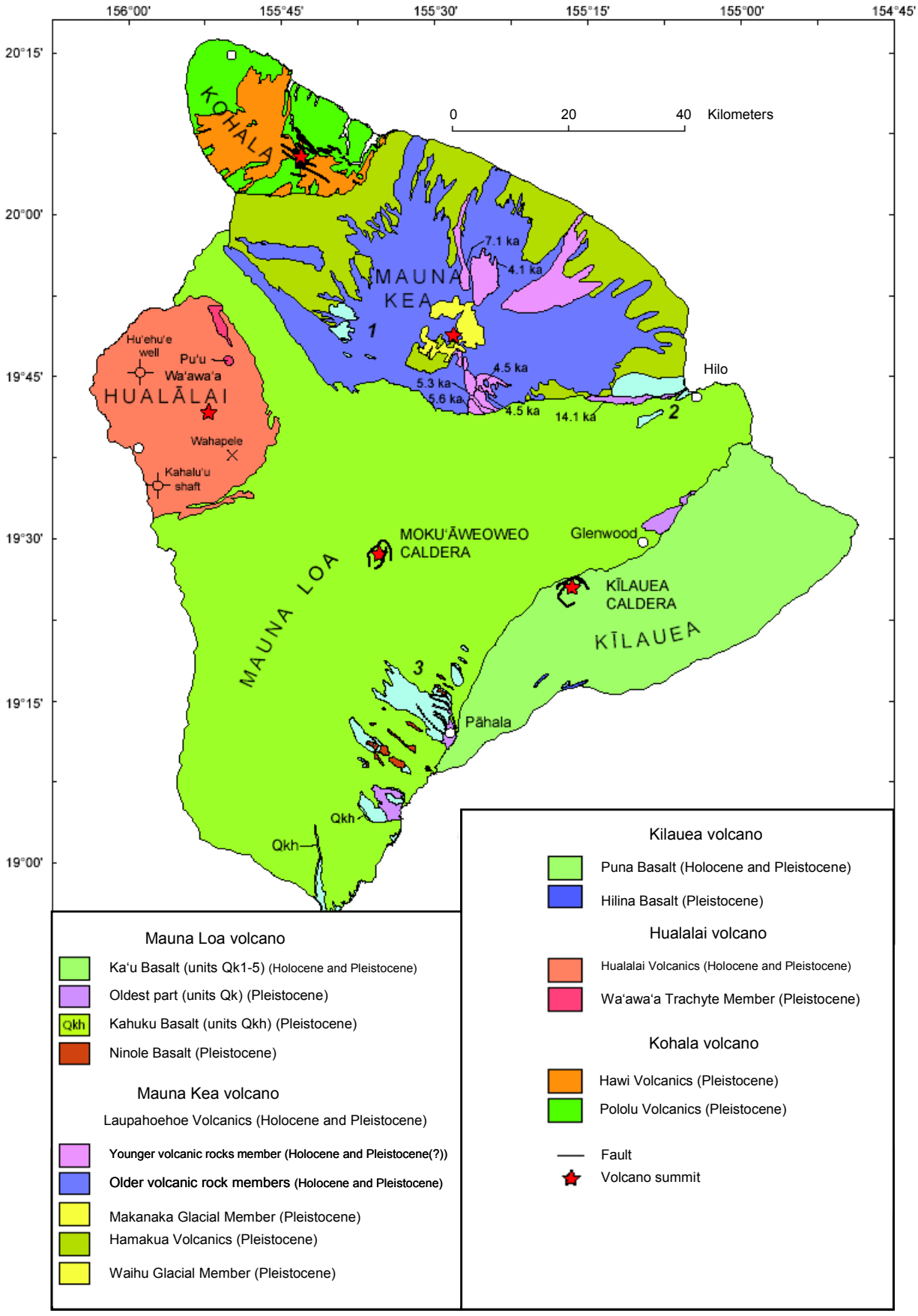

Figure 7: Map showing stratigraphic formations for the five volcanic centres on the Island of Hawaii (SHERROD et al., 2007).

The youngest and southernmost island in the Hawaiian archipelago, the Island of Hawaii ("Big Island") consists of seven volcanoes which are, in order of growth, Mahukona, Kohala, Mauna Kea, Hualalai, Mauna Loa, Kilauea, and Loihi seamount (MOORE and CLAGUE, 1992). Mahukona is a submarine volcano on the northwest flank of the Island of Hawaii, the main shield-building stage of volcanism ended about 470,000 years ago. The summit of the volcano subsided below sea level between 435,000 and 365,000 years ago (CLAGUE and MOORE, 1991). Mahukona, Kohala, Mauna Kea and Hualalai have completed their shield building stage. Mauna Kea and Mauna Loa rise more than 9000 m above the sea floor and are thereby rising higher above their base as any other mountain worldwide.

Kilauea Volcano is the youngest subaerial volcano of the Island of Hawaii and consists of shield-stage tholeiitic lavas which are divided into the Hilina Basalts (older) and the Puna Basalts (younger), the later covering almost the entire surface of Kilauea. However, preshield-stage alkalic basalts, which are as old as 275 ka, are for example exposed on Kilauea's southern submarine slope (SHERROD et al., 2007). According to CLAGUE and DALRYMPLE (1987), the Hilina Basalts are older than 31 ka with a maximum age of 100 ka whereas most of the Puna Basalt was erupted during the last 17,000 years. The Hilina deposits consist of lava flows of tholeiitic basalt containing phenocrysts of olivine, plagioclase, and, rarely, pyroxene. Lava flows are intercalated with basaltic ash deposits. Puna Basalt deposits contain various amounts of olivine, plagioclase, and, rarely, pyroxene phenocrysts. The deposits consist of lava flows, vent deposits, littoral deposits, and tephra deposits of tholeiitic basalt and rare transitional and alkalic basalt (WOLFE and MORRIS, 1996).

The deposits of **Mauna Loa** Volcano are all shield-stage tholeiitic lavas, divided into the Ninole Basalts, Kahuku Basalts and the Kau Basalts. The tholeiitic Ninole Basalts are the oldest unit, being as old as 100-200 ka (possibly up to as 300 ka), and consist of lava flows exposed as erosional remnants on scattered hills in the southern part of Mauna Loa's southern flank. Kahuku Basalts are older than 31 ka, consisting of lava flows of tholeiitic basalt. The youngest unit, the Kau Basalts, erupted during the last 10,000 years. This unit contains various amounts of olivine, plagioclase, and, rarely, pyroxene phenocrysts. The deposits consist of lava flows, vent deposits, littoral deposits, and tephra-fall deposits of tholeiitic basalt and rare transitional and alkalic basalt (WOLFE and MORRIS, 1996).

Mauna Kea Volcano has passed through the primitive shield-building stage into the late stage, with the shield stage lavas almost completely buried by the post-shield stage lavas (MACDONALD et al., 1983). The exposed rocks have been divided into the older Hamakua Volcanic Series and the younger Laupahoehoe Series (MACDONALD et al., 1983). The

basalts of the Hamakua Volcanics (upper and lower members) are between ~70 ka and 300 ka in age and are associated with glacial deposits (SHERROD et al., 2007). The basaltic volcanic rocks consist of lava flows, cinder cones of alkalic and transitional basalt and minor hawaiite, tholeiitic basalt and strongly undersaturated basalt. The lavas contain a variable amount of olivine, plagioclase, and clinopyroxene phenocrysts. The glacial member is composed of diamict and gravel. The Hamakua Volcanic Series was lately postulated to be completely the result of post-shield volcanic activity (RHODES, 1996; WOLFE and MORRIS, 1996), in contrast to older interpretations which favoured the classification that the lower member is derived from shield stage volcanism and the upper member from post-shield volcanism (MACDONALD et al., 1983; LANGENHEIM and CLAGUE, 1987). The Laupahoehoe Series was erupted during post shield volcanic activity and is further divided into a younger volcanic rock member (4.4-7.1 ka) and an older volcanic rock member (14-65 ka). Volcanic rocks of the Laupahoehoe Series are composed of hawaiite, mugearite, and benmorite and associated glacial deposits. The lavas are generally aphyric, with the groundmass being plagioclase-rich, and ultramafic xenoliths occur locally. The younger volcanic member is characterized by lava flows, scoria cones and tephra-fall deposits of hawaiite and mugearite. The older volcanic rock member consists of lava flows, scoria cones, and tephra-fall deposits of hawaiite, mugearite, and benmorite (WOLFE and MORRIS, 1996).

Kohala Mountain, the oldest of the volcanoes on Big Island, forms the northwestern end of the Island of Hawaii and consists of an oval shield volcano. While the western and northern sides are characterized by a gentle topography, the northeastern and southeastern sides are heavily truncated by a series of great sea cliffs. The southern flank of the volcano is buried by Mauna Kea deposits (MACDONALD et al., 1983). The rocks of Kohala Volcano have been divided into the older shield stage Pololu Volcanic Series (younger than 0.78 Ma) and the younger post-shield-stage Hawi Volcanic Series (0.26-0.14 Ma) (SHERROD et al., 2007). The Pololu Volcanic Series consists of mostly basaltic lava flows of tholeiitic, transitional and alkalic composition, cinder cones and a lava dome. The tholeiitic lavas have an age of approximately 700 ka, the transition from eruption of tholeiitic basalt to eruption of transitional and alkalic basalt has occurred by about 400 ka and continued until at least 250 ka. The Hawi Volcanic Series consists of lava flows, scoria cones, lava domes, and tephra-fall deposits of hawaiite, mugearite, benmorite, and trachyte.

Hualalai on the west side of the island is a dormant volcano in the late stage of the eruptive cycle, which last erupted A.D. 1801-1802 (SHERROD et al., 2007). Hualalai lavas are in a less advanced stage of magmatic evolution than those of Mauna Kea and in a more advanced

stage than Mauna Loa (MACDONALD et al., 1983). Tholeiitic shield-stage lavas are found offshore along the northwest rift zone of Hualalai (CLAGUE, 1982; CLAGUE, 1987; HAMMER et al., 2006). The post-shield Hualalai Volcanics (0 - >10 ka), which completely cover the subaerial edifice, consist of lava flows and vent deposits of alkalic basalt, hawaiite, and trachyte deposits (SHERROD et al., 2007). The Waawaa Trachyte Member (92-114 ka) (CLAGUE, 1987; COUSENS et al., 2003) comprises a large cone of trachyte pumice and a trachyte lava flow on the north slope of Hualalai.

3.1.3 Maui

Maui consists of two major volcanoes, West Maui and the younger Haleakala (East Maui). While West Maui seems to be extinct, Haleakala volcano has been dormant since the most recent eruption about A.D. 1449 and 1633 (SHERROD et al., 2003). West Maui and Haleakala are connected by the Maui Isthmus, which was formed by lavas from Haleakala Volcano (MACDONALD et al., 1983).

Haleakala Volcano deposits have been divided into the Honomanu Volcanic Series, the Kula Volcanic Series and the Hana Volcanic Series. Honomanu Basalts range in age from about 1.1 to 0.97 Ma (CHEN et al., 1991). The primitive shield is composed of lava flows of tholeiite, tholeiitic olivine basalt, and oceanite associated with very minor amounts of pyroclastic material (Honomanu Volcanic Series). Post-shield volcanism is characterized by the Kula Volcanic Series, predominantly composed of hawaiite with lesser amounts of alkalic olivine basalt and ankaramite. Kula Volcanics mantle most of Haleakala and the oldest dated lava flows have an age of 0.93 ± 0.33 Ma (CHEN et al., 1991), while rocks from the rim of the crater yield ages of about 0.15 Ma (SHERROD et al., 2003). After a period of erosion, lava flows, associated cinder cones and ash deposits erupted from the Southwest Rift and the East Rift, forming the Hana Volcanic Series which is also part of the post-shield-stage volcanism. Alkalic olivine basalts and basaltic hawaiites are the predominant rock types of the Hana Volcanics. Haleakala is, besides those on the Island of Hawaii, the only volcano on the Hawaiian islands, showing recent activity (SHERROD et al., 2007).

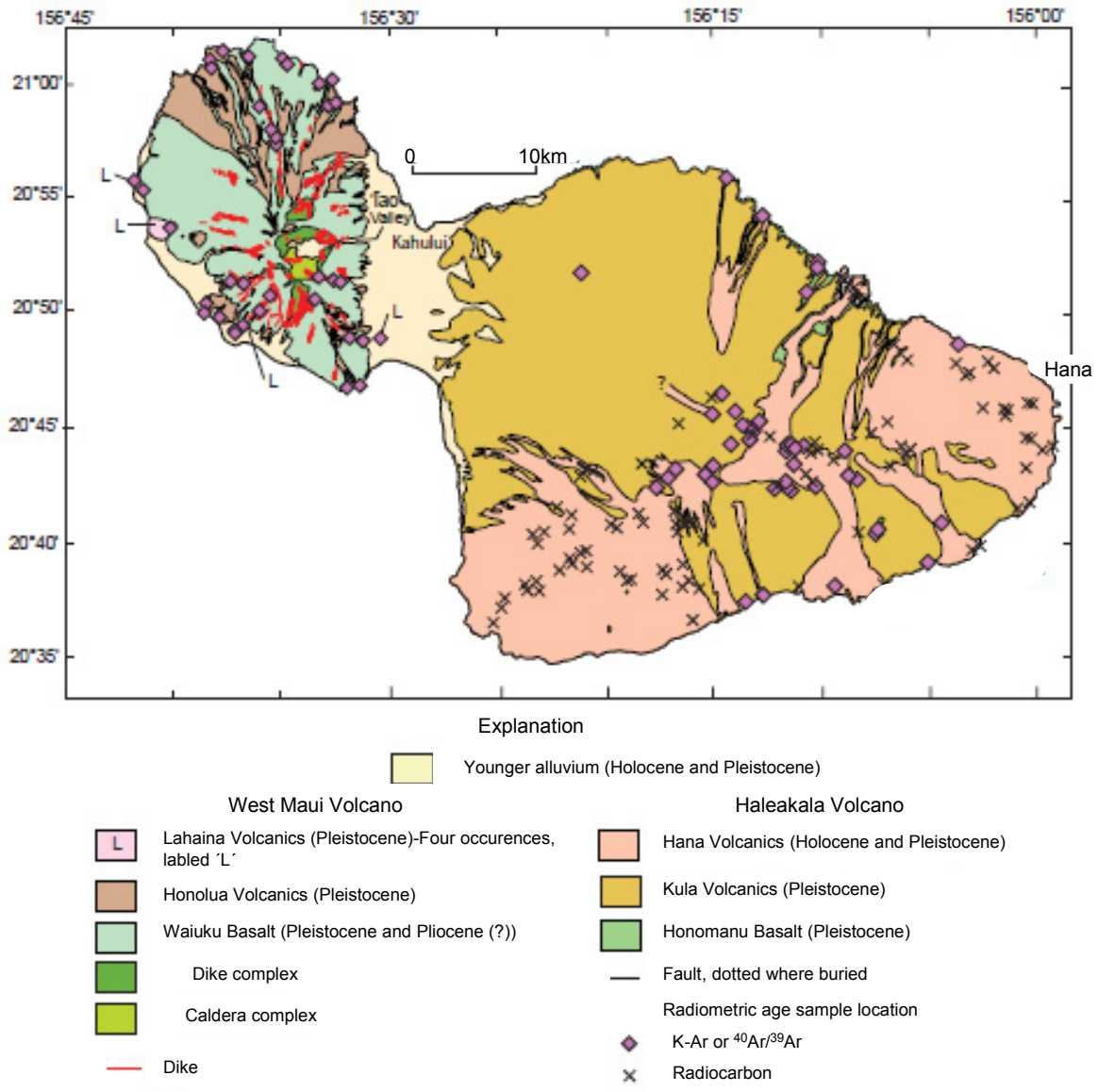

Figure 8: Geologic map of Maui (SHERROD et al., 2007).

3.2 Sample Sites

In this study, samples from the Hawaii Scientific Drilling Project (HSDP) drill core, surface samples from Mauna Kea, Mauna Loa, Kilauea, Hualalai, Kohala, and Haleakala, as well as samples from a bore hole drilled beneath the summit of Kilauea volcano in 1973, funded by the National Science Foundation (NSF well), have been investigated (Table 5).

Major and trace elements have been determined for the complete sample set. In addition, Kohala and Haleakala samples have been analysed for their Sr, Nd and Pb isotope characteristics. The noble gas composition was determined for HSDP and NSF well samples

and for suitable surface samples showing the least influence of alteration and a sufficient amount of olivine for the noble gas analysis.

Table 5: Samples analysed for their noble gas elemental and isotopic composition.

Sample	***Origin***	**Drilling depth/Location**
SR0517-8,5	HSDP-2a	1296 m
SR0626-5,7	HSDP-2a	1593 m
SR0720-17,0	HSDP-2a	1919 m
SR0760-12.8	HSDP-2a	2115 m
SR0952-1,9	HSDP-2a	3002 m
SR979-1,9	HSDP-2a	3096 m
R008 2.7-3.4	HSDP-2b	3117 m
R021 0-0.5	HSDP-2b	3139 m
R050 5.5-6.6	HSDP-2b	3171 m
R060 5.5-6.5	HSDP-2b	3192 m
R125 4.1-4.7	HSDP-2b	3317 m
R129 8.5-9.0	HSDP-2b	3324 m
CR1-4A	NSF well	10.7-14.0 m
CR2-2A	NSF well	26.2-32.3 m
CR11-5A	NSF well	154.9-157.4 m
CR11-5B	NSF well	154.9-157.4 m
CR14-5D	NSF well	324.2-327.3 m
0310KO1	Kohala Volcano, Island of Hawaii	20°08´13.05´´N 155°53´23.21´´W
0410KO4	Kohala Volcano, Island of Hawaii	20°09´13.80´´N 155°53´28.38´´W
0510KO14	Kohala Volcano, Island of Hawaii	20°06´56.40´´N 155°34´25.80´´W
0610KO15	Kohala Volcano, Island of Hawaii	20°03´30.00´´N 155°49´43.20´´W
1310HA2	Haleakala Volcano, Maui	20°43´48.60´´N 155°59´34.20´´W
1310HA5C	Haleakala Volcano, Maui	20°37´55.11´´N 156°11´16.26´´W

Table 5: continued

Sample	*Origin*	Drilling depth/Location
1310HA4	Haleakala Volcano, Maui	20°38´54.00´´N 156°04´58.20``W
1410HA9B	Haleakala Volcano, Maui	20°45´06.00´´N 155°16´28.20´´W
1410HA13	Haleakala Volcano, Maui	20°46´16.20´´N 156°18´13.20´´W
MLO4	Mauna Loa, Island of Hawaii	19°54´27.72´´N 155°52´46.67´´W
KIL1	Kilauea, Island of Hawaii	19°29´15.00´´N 154°55´28.38´´W
HUA1B	Hualalai, Island of Hawaii	19°38´41.64´´N 155°59´24.97´´W
MKEA3	Mauna Kea, Island of Hawaii	20°0´19.80´´N 155°15´48.35´´W

3.2.1 Hawaii Scientific Drilling Project

With the achievements of the Hawaii Scientific Drilling Project (HSDP), which is part of the International Continental Scientific Drilling Project (ICDP), it is possible to document the temporal evolution of a single volcano by means of 3340 m of drill core. Drilling of the HSDP main hole started in 1999 (HSDP-2a) near the city of Hilo on a flank of Mauna Loa volcano. A second drilling phase started in 2003, when the hole was re-opened and casing and cementing of the hole was performed. The third coring phase was executed in 2004/2005 (HSDP-2b) when the existing hole was deepened to a depth of 3340 m. The upper 245 m of the drill core consist of Mauna Loa subaerial tholeiite, followed by ~3100 m of material from Mauna Kea. The upper ~ 800 m of the Mauna Kea section consist of subaerial lavas, the lower ~2300 m submarine Mauna Kea section includes hyaloclastites and pillow lavas and minor intrusives. All Mauna Kea lavas, with the exception of a thin covering of post-shield subaerial lavas at the top of the Mauna Kea section, are tholeiitic.

In this study we analyzed 6 samples from the second coring phase (HSDP-2a) and 6 samples from the third coring phase (HSDP-2b) (Table 5). All samples are derived from the submarine Mauna Kea section of the drill core and are composed of olivine-phyric basalt.

3.2.2 NSF Well

The NSF well is located at an elevation of 1103 m above sea level on the southwest rim of the caldera beneath the summit of Kilauea Volcano (Figure 9). The borehole was drilled in 1973 to a total drilling depth of 1262 m (4141ft) (KELLER et al., 1979). Since the water table was encountered at a depth of 488 m, samples for noble gas analysis were taken from above this depth in order to avoid altered material. Samples from Units I and III have been analysed in this study. Olivine basalt from Unit I comprises the upper 183 m of the drill core and consists of pahoehoe and interbedded ash and is part of the Puna Volcanic Series. Unit III from 323 to 445 m drilling depth comprises unaltered olivine basalt which is interpreted to reflect local ponding of lavas (KELLER et al., 1979).

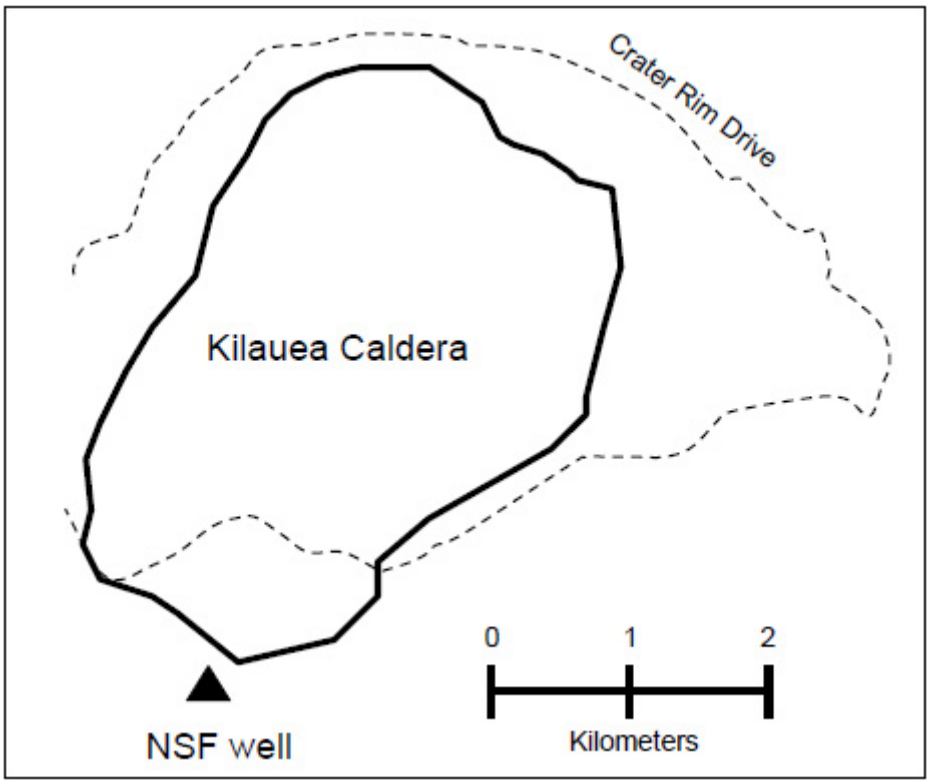

Figure 9: Map of the Kilauea caldera and the location of the NSF well.

3.2.3 Surface Samples

Additionally to the drill core samples from Mauna Kea and Kilauea, surface samples from various Hawaiian volcanoes were analysed (Table 5). Besides single surface samples from each of Mauna Kea, Mauna Loa, Kilauea, and Hualalai, several surface samples each from the volcanoes Kohala and Haleakala were analysed.

4 Results

4.1 Major and Trace Elements

The results of the major and trace element analyses of lavas from Mauna Kea, Kilauea, Kohala, and Haleakala volcanoes are compiled in Table A2 (Appendix).

The analysed samples from the HSDP drill core and one surface sample range in SiO_2 from 45 to 50% and vary widely in MgO content (7.3-18.9%). Abundances of TiO_2, K_2O and P_2O_5 range from 1.7-2.6%, 0.19-0.40%, and 0.18-0.25%, respectively. The analysed samples are tholeiitic basalts erupted during the shield building stage and form a linear array in the Total Alkali-Silica (TAS) diagram (Figure 10).

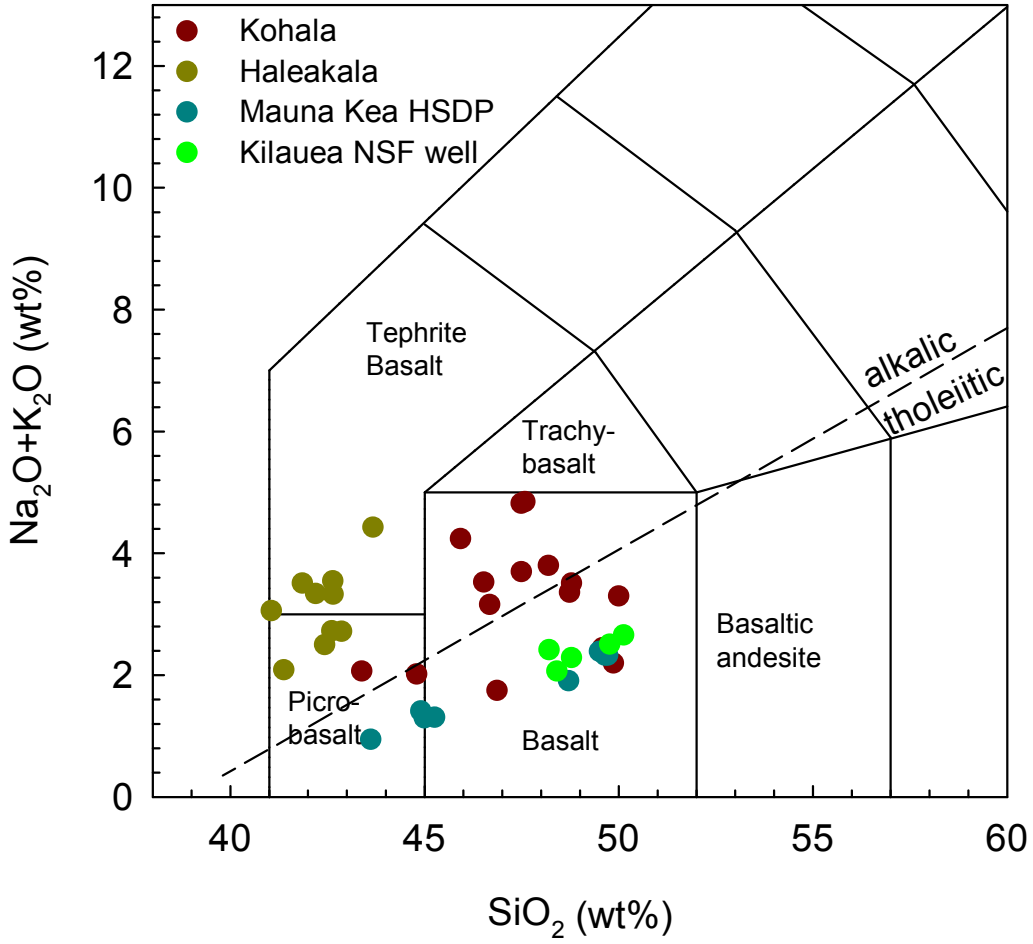

Figure 10: The Total Alkali-Silica (TAS) diagram (LE BAS et al., 1986), for the analysed samples from different Hawaiian volcanoes, showing the boundary between the tholeiitic and alkalic fields (diagonal dashed line) (MACDONALD and KATSURA, 1964). Samples from Haleakala are alkalic, Mauna Kea and Kilauea lavas are tholeiitic.

The analysed samples from the NSF well are tholeiitic basalts erupted during the persistent shield-stage of Kilauea volcano and form a linear array in the TAS diagram (Figure 10). The analysed samples range in SiO_2 from 48 to 50 wt% and in MgO from 7.5-13.0%. The abundances of TiO_2, K_2O, and P_2O_5 range from 2.0-3.2%, 0.32-0.47%, and 0.18-0.25%, respectively.

Analysed samples from Kohala volcano are from the shield stage (Pololu Volcanics), ranging compositionally from tholeiitic to transitional and alkalic basalt. The term transitional is used for lavas from Kohala that plot near the alkalic-tholeiitic compositional boundary in the TAS diagram (Figure 11). The SiO_2 content of lavas from Kohala ranges from 43 to 50 wt%, most of the lavas have > 45% SiO_2. Abundances of MgO, TiO_2, K_2O, and P_2O_3 range from 4.9-13%, 1.9-3.5%, 0.09-1.3%, and 0.19-0.63%, respectively.

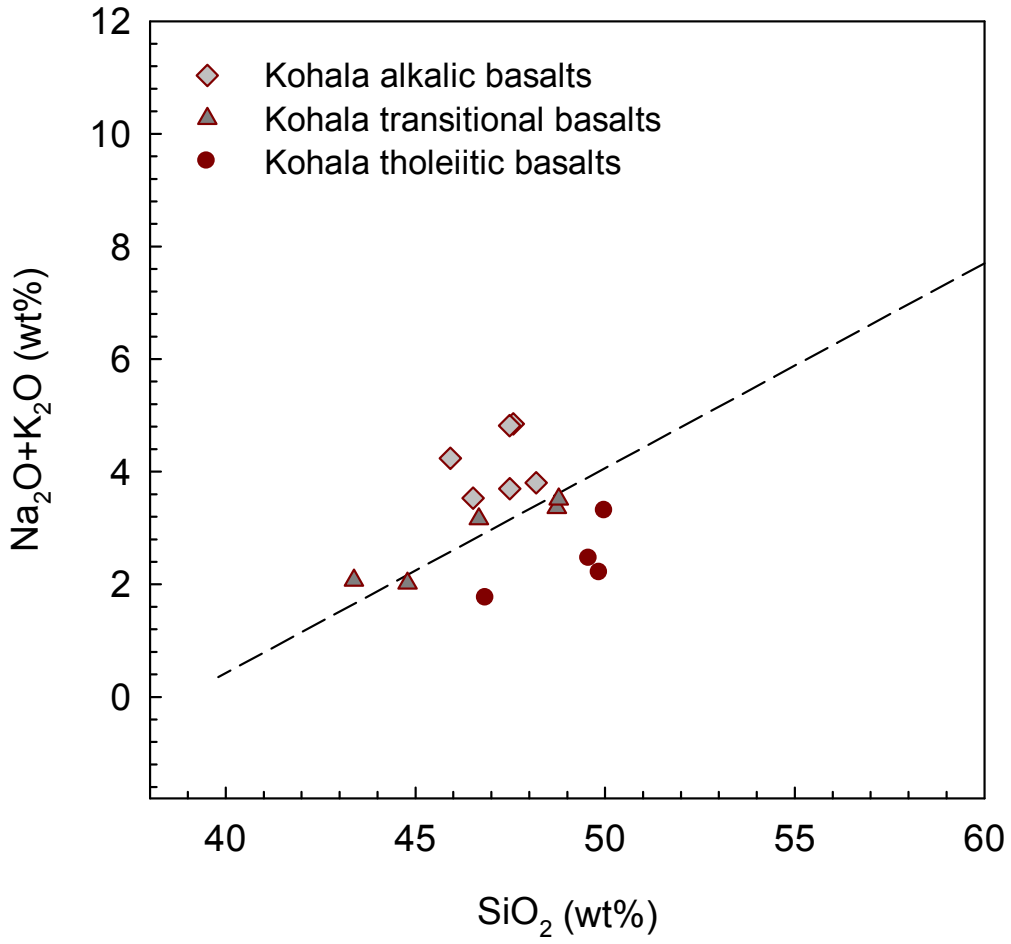

Figure 11: The Total Alkali-Silica (TAS) diagram (LE BAS et al., 1986), for the analysed Kohala lavas. Data are divided into an alkalic and a tholeiitic group as well as a transitional group with intermediate composition.

All analysed samples from Haleakala volcano were erupted during the post-shield stage and are alkalic (Figure 10). Abundances of SiO_2 range from 41-44 wt%, MgO contents vary between 6.9 and 13.8%. The abundances of TiO_2, K_2O, and P_2O_5 range from 2.4-3.7%, 0.44-1.19%, and 0.31-0.48%, respectively. Samples 1410HA12, 1410HA10, 1410HA9 and 1410HA13 are from the older Kula volcanic series, while the remaining samples (1310HA2, 1310HA4, 1310HA5, 1310HA6, 1310HA7, 1310HA8) are from the younger Hana volcanic series. Samples from Kula and Hana are characterized by different major element systematics. There is an obvious bi-modal distribution in MgO contents reflecting the different volcanic stages during which the samples were erupted. The older samples (Kula) are characterized by a higher and less variable MgO content and lower Al_2O_3/CaO and CaO/MgO, but higher CaO/Na_2O compared to the younger samples from the Hana volcanic series. Samples from the Hana and Kula volcanics are also distinguished in their trace element abundances. The younger samples (Hana) have higher concentrations in La, Nb, Sr, P_2O_5, Zr, Ba, and Th with lower MgO contents.

The MgO content of the analysed samples varies widely from 4.9 to 18.9 wt%. Abundances of MgO are inversely correlated with other major element oxides (e.g. SiO_2, CaO and Al_2O_3) (Figure 12), reflecting olivine fractionation or accumulation (FREY and RHODES, 1993). Concentrations of Ni and Cr, elements that are compatible in olivine and Cr- spinel, are positively correlated with the MgO content. Abundances of incompatible trace elements such as Nb, Zr, P_2O_5, are positively correlated (Figure 13), as has been seen in other Hawaiian shield volcanoes. Frey et al. (1994) interpreted these correlations to reflect magmatic processes.

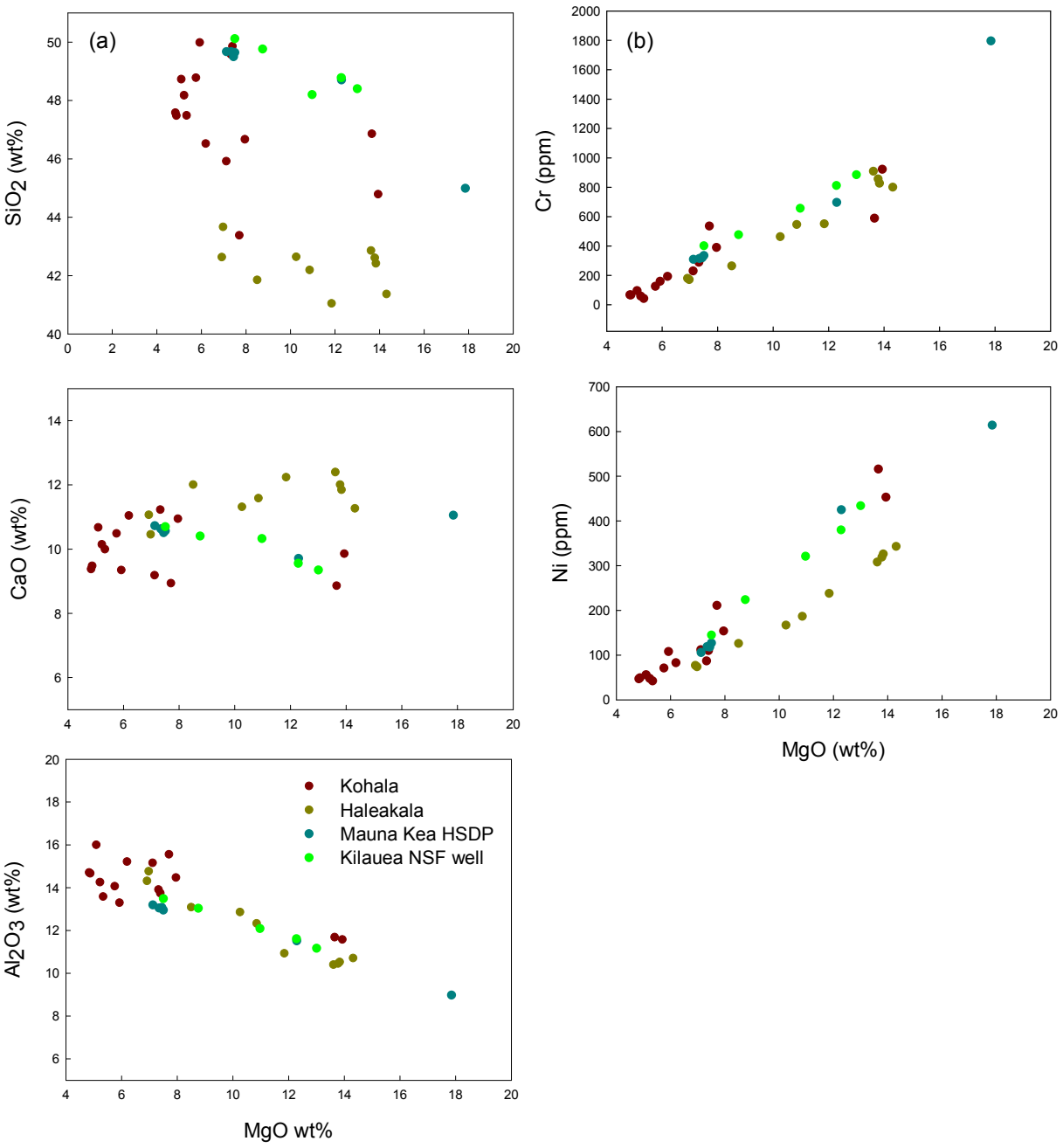

Figure 12: (a) Major oxide abundance (SiO_2, CaO, Al_2O_3) and (b) concentration of compatible trace elements (Cr, Ni) versus MgO content in lavas from Mauna Kea (HSDP), Kilauea (NSF well), Kohala and Haleakala.

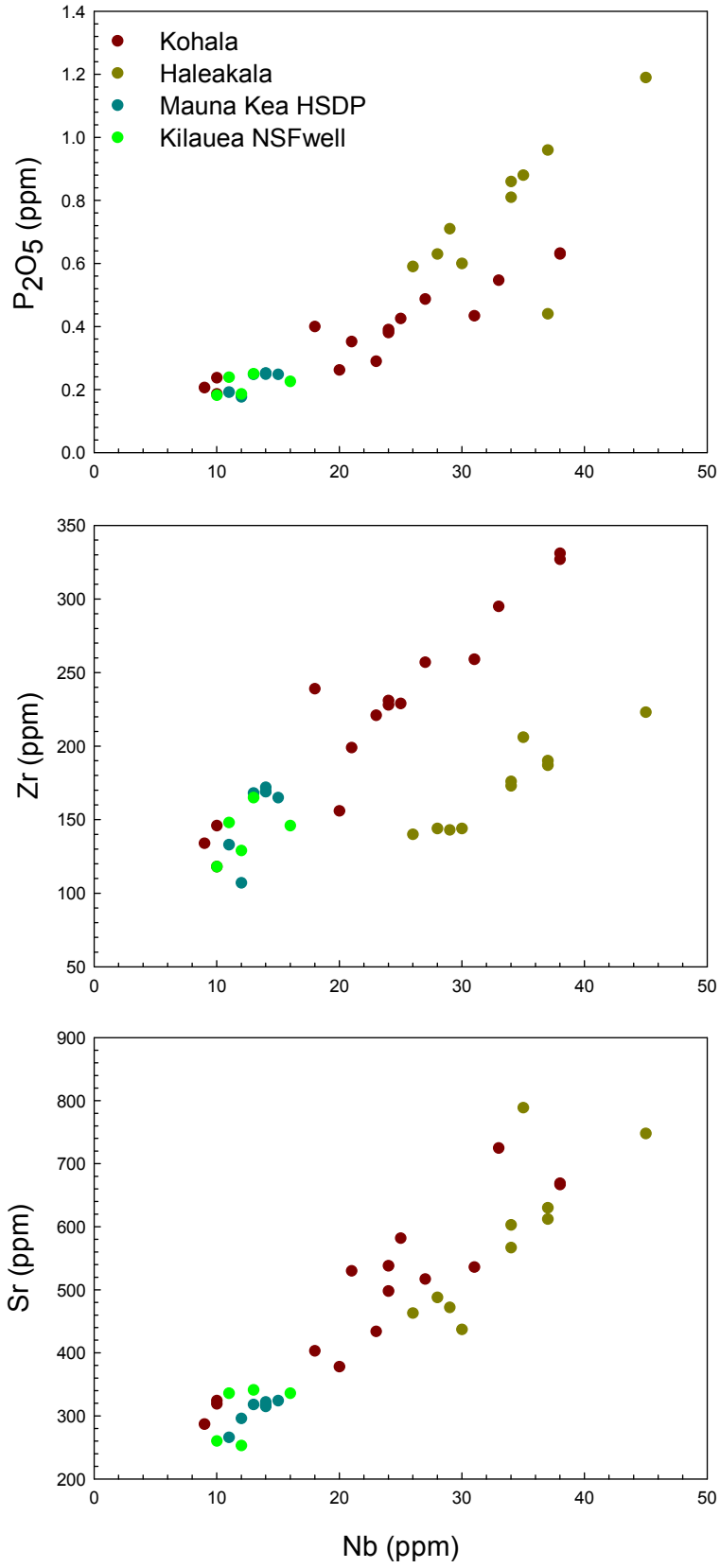

Figure 13: Concentration of incompatible trace elements (Zr, Sr, Nb) and minor oxide (P_2O_5) in lavas from Mauna Kea (HSDP), Kilauea (NSF well), Kohala and Haleakala.

4.1.1 Intershield Comparison

In the following section, compositional differences between the Mauna Kea, Kilauea, Kohala and Haleakala shields are outlined. Analysed samples from Mauna Kea, Kilauea, and Kohala are from the shield stages of the volcanoes, while the samples from Haleakala were erupted during the post-shield stage. Differences between the analysed lavas from these volcanoes are apparent in major and trace element compositions. Mauna Kea, Kilauea, Kohala and Haleakala lavas show distinctly different SiO_2 contents. Haleakala lavas show the lowest SiO_2 content and are slightly overlapping with lavas from Kohala. Kohala lavas span a relatively large range in SiO_2 and overlap to higher SiO_2 abundance with lavas from Mauna Kea and Kilauea. The highest, nearly indistinguishable SiO_2 contents are found in lavas from Mauna Kea and Kilauea. Abundances of Al_2O_3 and CaO are similar in lavas from Mauna Kea, Kilauea, Haleakala and Kohala, but many Kohala lavas have higher Al_2O_3 contents, while the majority of Haleakala lavas have the highest CaO abundances. Abundances of TiO_2, Na_2O, K_2O, P_2O_5 and Fe_2O_3 are overlapping, but are highest in Haleakala and Kohala lavas. Mauna Kea and Kilauea samples are lower in total alkalis compared to Kohala and Haleakala lavas (Figure 10). Most Kohala lavas are alkalic basalts, but some lavas have a tholeiitic composition. Kohala lavas seem therefore to be intermediate between the alkalic Haleakala lavas and the tholeiitic basalts from Mauna Kea and Kilauea. An intrashield comparison reveals that for Kohala and Haleakala the samples with the lowest MgO content have the highest abundance of incompatible trace elements. Kohala samples with MgO between 4.8 and 7.1% and Haleakala samples with MgO between 6.9 and 12.0% show the highest abundances of La, Nb, Sr, P_2O_5, Zr and Ba. The intershield comparison shows that Haleakala and Kohala lavas are higher in incompatible trace elements compared to Mauna Kea and Kilauea. Kohala lavas span moreover the widest compositional range and overlap to higher concentrations with Haleakala lavas and to lower concentrations with Mauna Kea and Kilauea lavas. Ratios of TiO_2/Al_2O_3 and Zr/Nb are used as chemical discriminants to distinguish between the data from the different Hawaiian volcanoes (RHODES, 1996). There are large differences in Zr/Nb ratios of lavas from Haleakala compared to lavas from the other analysed volcanoes. Haleakala lavas have lower Zr/Nb ratios at higher TiO_2/Al_2O_3 values. Kohala lavas are intermediate, but some overlap with Mauna Kea and Kilauea lavas which show generally higher Zr/Nb ratios and lower TiO_2/Al_2O_3 values (Figure 14). Abundances of Ni and Cr are indistinguishable, but many samples from Kohala extend to the lowest concentrations of Ni, Cr and MgO. Mauna Kea, Kilauea and tholeiitic basalts from Kohala show the lowest Th abundances. Lavas from Haleakala along with the alkalic lavas from Kohala have the highest

Th abundances. Transitional basalts from Kohala have intermediate Th concentrations between tholeiitic basalts from Mauna Kea, Kilauea and Kohala and alkalic basalts from Haleakala.

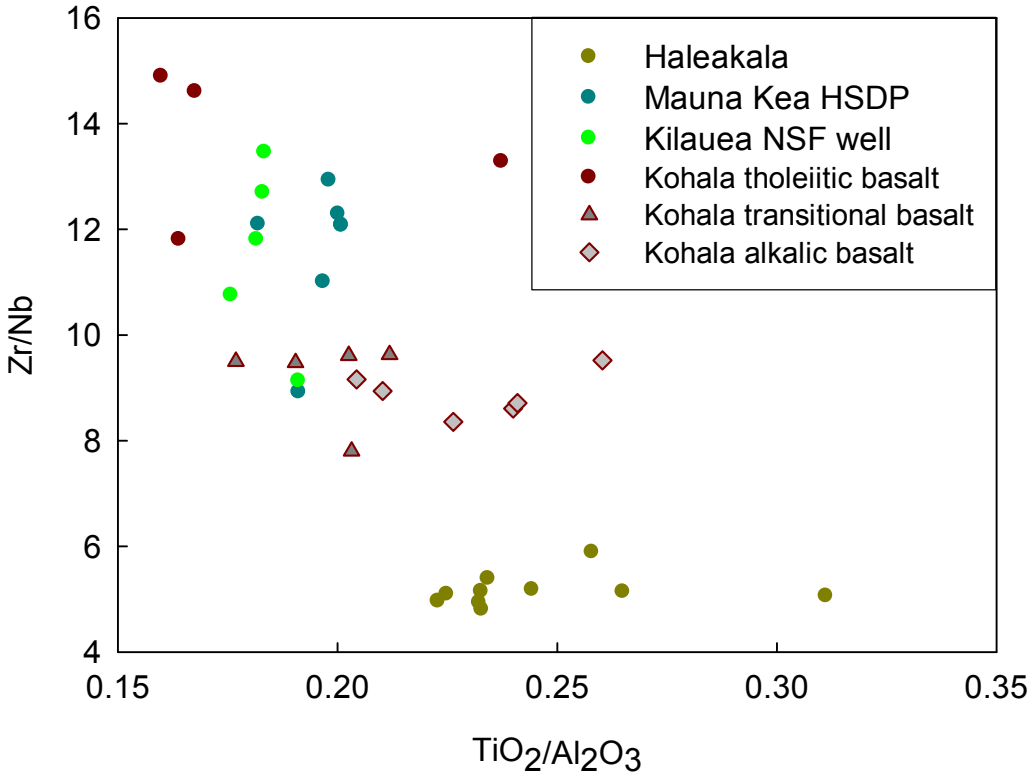

Figure 14: Variations of Zr/Nb versus TiO_2/Al_2O_3 in lavas from Mauna Kea (HSDP), Kilauea (NSF well), Kohala and Haleakala.

4.1.2 Influence of Postmagmatic Alteration

Low-temperature weathering in tropical environments like in Hawaii is known to result in an enhanced mobility of alkali elements and also SiO_2 (FREY et al., 1994; RHODES and VOLLINGER, 2004). The K_2O/P_2O_5 ratio of the analysed lavas is a sensitive indicator of postmagmatic alteration because K is preferentially leached from the basalt, leading to low K_2O/P_2O_5 (<1.4 and often <1.0) values in postmagmatically altered rocks (HUANG and FREY, 2003). The stated magmatic values for K_2O/P_2O_5 or values for unaltered rock vary slightly in literature from values < 1 up to values of 2.2 (WRIGHT and FISKE, 1971; HUANG and FREY, 2003; HASKINS and GARCIA, 2004; RHODES and VOLLINGER, 2004). The HSDP drill core samples show almost no influence of postmagmatic alteration, indicated K_2O/P_2O_5 ratios ranging between 1.1 and 1.6. K_2O/P_2O_5 ratios of the NSF well

samples from Kilauea volcano range between 1.8 and 2.0 and are well within the range of unaltered rock. Surface samples from Kohala and Haleakala volcano The K_2O/P_2O_5 values of Kohala and Haleakala are between 0.48-2.1, and 1.2-2.5, respectively, indicating influence of alteration for some Kohala samples and a minor effect for one Haleakala sample.

4.2 Rare Earth Elements

Analyses of the REE contents of basalts from Mauna Kea, Kohala, Kilauea and Haleakala are presented in Table A4 (Appendix), the data are displayed in Figures 15, 16 and 17. Alkalic lavas from Kohala have the highest LREE abundances, together with lavas from Haleakala. Transitional Kohala lavas have intermediate abundances, whereas tholeiitic Kohala lavas have the lowest LREE abundances of all analysed samples. When comparing the REE pattern of samples from Kohala Volcano with the analysis by LANPHERE and FREY (1987), samples from this study agree with the older shield stage Pololu Volcanics, which show a lesser degree of enrichment in REE than the younger post shield Hawi Volcanics (Figure 16). The samples can furthermore be distinguished into the Upper Pololu Volcanics and the Lower Pololu Volcanics, the former being more enriched in the most incompatible REE. Samples 0510KO13, 0610KO15, 0610KO16 fit well within the pattern of the Lower Pololu Volcanics, while the remaining samples from Kohala agree with lavas from the Upper Pololu Volcanics (Figure 16). Haleakala lavas have high LREE abundances, while their HREE contents are the lowest of all analysed samples. Furthermore, Haleakala lavas from this study agree well with REE patterns of lavas from the Kula Volcanic Series reported by WEST and LEEMAN (1994). REE patterns from Haleakala shield stage lavas (REN et al., 2004) are distinctly different from post-shield stage lavas. Post-shield stage lavas have higher LREE contents, but similar HREE abundances compared to shield-stage lavas (Figure 17). Mauna Kea and Kilauea lavas overlap in REE abundances with the tholeiitic Kohala lavas. Mauna Kea lavas have however the tendency to slightly higher HREE contents compared to Kilauea lavas (Figure 15).

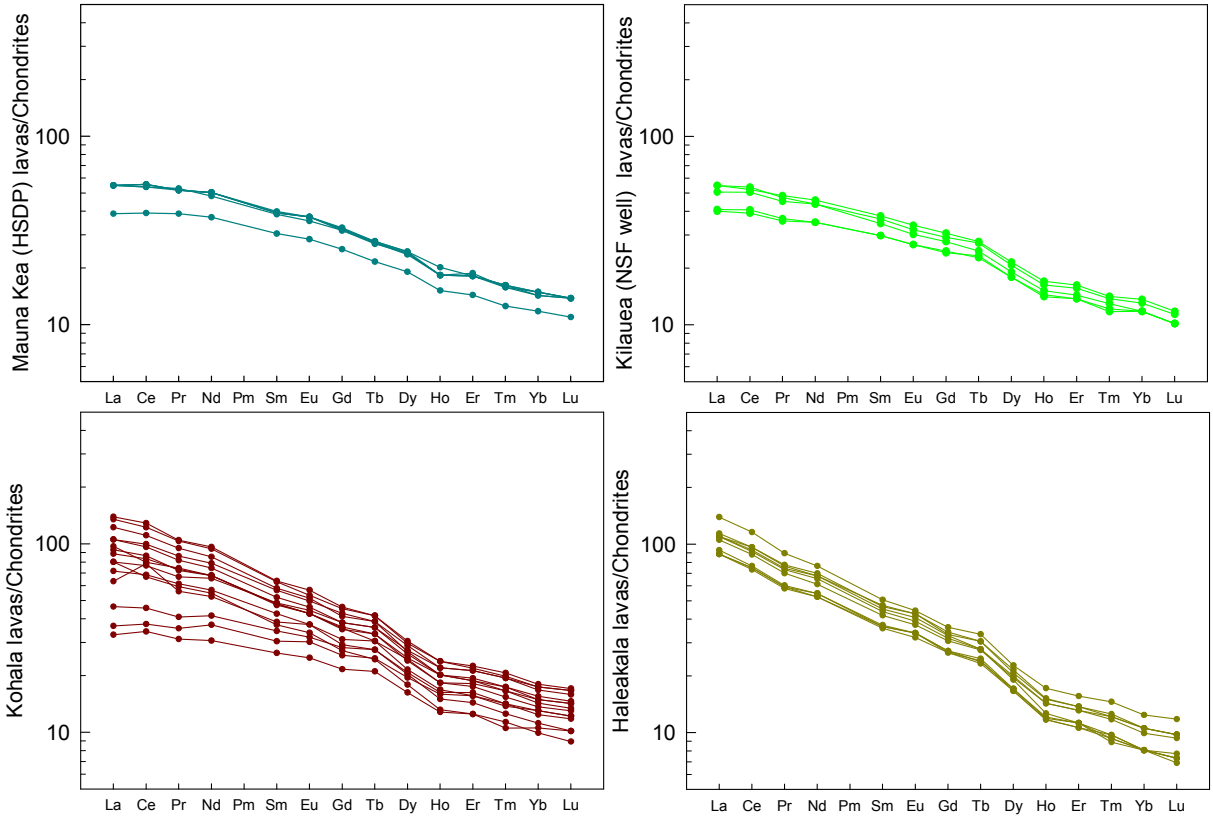

Figure 15: Chondrite-normalized REE concentrations (normalizations from MCDONOUGH and SUN, (1995)) for lavas from Mauna Kea (HSDP), Kilauea (NSF well), Kohala, and Haleakala.

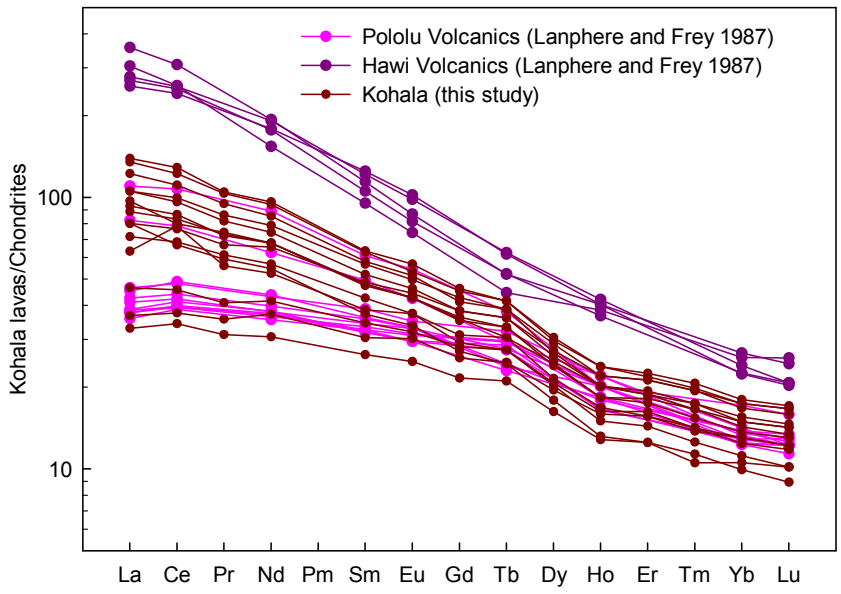

Figure 16: Chondrite-normalized REE concentrations (normalizations from MCDONOUGH and SUN, 1995) of lavas from Kohala. Data from LANPHERE and FREY (1987) are shown for comparison.

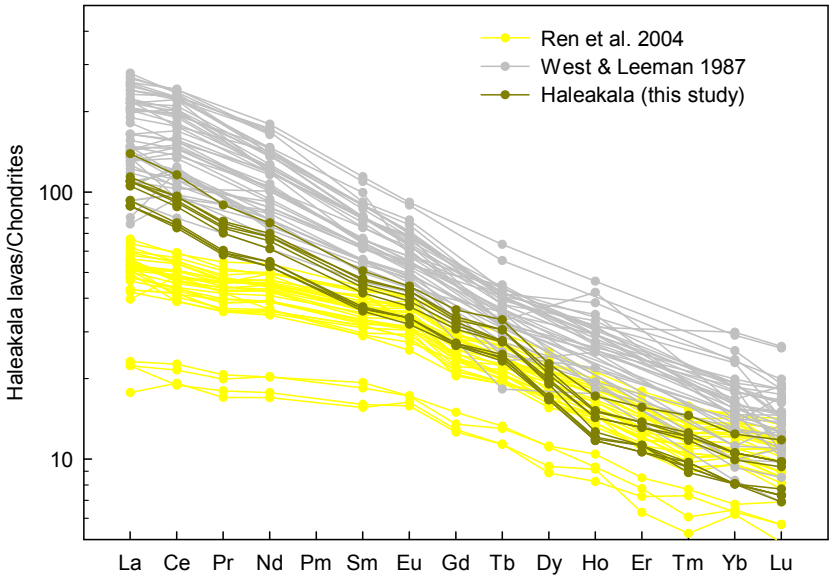

Figure 17: Chondrite-normalized REE concentrations (normalizations from MCDONOUGH and SUN, 1995) of lavas from Haleakala. Data from REN et al. (2004) and WEST and LEEMAN (1987) are shown for comparison.

4.3 Sr, Nd, and Pb isotopic compositions

Samples from Kohala and Haleakala have been analysed for their isotopic composition of Sr, Nd and Pb, the results are compiled in Table 6. $^{206}Pb/^{204}Pb$, $^{207}Pb/^{204}Pb$, and $^{208}Pb/^{204}Pb$ ratios range from 18.17 to 18.60, 15.48 to 15.53, and 37.89 to 38.17, respectively; for samples from Kohala volcano and from 18.18 to 18.33, 15.46 to 15.49, and 37.78 to 37.97, respectively, for those from Haleakala volcano. $^{87}Sr/^{86}Sr$ ratios from Kohala and Haleakala range from 0.70361 to 0.70387 and 0.70318 to 0.70330, respectively. $^{143}Nd/^{144}Nd$ isotope ratios range from 0.51293 to 0.51300 for Kohala and from 0.51302 to 0.51306, for Haleakala.

The isotopic composition of Pb overlaps in the samples from Kohala and Haleakala. When comparing the analysed lavas from Kohala and Haleakala with regard to their Sr and Nd isotope characteristics, a bi-modal distribution becomes obvious (Figure 18). The two volcanoes define two groups, where post-shield Haleakala samples are defined by higher $^{143}Nd/^{144}Nd$ and lower $^{87}Sr/^{86}Sr$ ratios, whereas Kohala samples have lower $^{143}Nd/^{144}Nd$ and higher $^{87}Sr/^{86}Sr$ ratios. This anti-correlation of $^{87}Sr/^{86}Sr$ and $^{143}Nd/^{144}Nd$ isotope ratios is due to the behavior of their parent isotopes during partial melting. The radiogenic isotope ^{87}Sr is produced by the decay of ^{87}Rb while ^{86}Sr is a stable isotope. The Earth's mantle is characterized by a rather low $^{87}Sr/^{86}Sr$ ratio due to the higher incompatibility of Rb compared to Sr during melting events (WHITE, 2005). ^{147}Sm decays by α emission to ^{143}Nd. The

$^{143}Nd/^{144}Nd$ ratio is often reported in the ε notation, which gives the relative deviation of the $^{143}Nd/^{144}Nd$ ratio from the chondritic value (0.512638) in parts in 10^4 (WHITE, 2005). Nd is more incompatible during mantle melting than Sm; hence, partial melting depletes the Earth's mantle more in Nd than in Sm resulting in a high Sm/Nd ratio of the mantle. Due to the different compatibilities of their parent isotopes, Sr and Nd tend to be inversely correlated in the mantle and in mantle-derived melts as a result of magmatic processes which dominate the chemical evolution of the mantle (WHITE, 2005).

$^{143}Nd/^{144}Nd$ and $^{87}Sr/^{86}Sr$ data for Kohala agree well with values for other Hawaiian volcanoes (Figure 18). Fields for other ocean islands are shown for comparison. Data for Iceland, Galapagos, Samoa and Hawaii can be found in the GEOROC database (http://georoc.mpch-mainz.gwdg.de/georoc/). Post-shield Haleakala data show a more depleted character compared to Hawaiian shield-stage data. Data from Kohala fit well within the data for Kea trend volcanoes, which are characterized by higher $^{143}Nd/^{144}Nd$ and lower $^{87}Sr/^{86}Sr$ values compared to Loa trend volcanoes (Figure 18).

As stated above, Haleakala and Kohala lavas overlap in their $^{206}Pb/^{204}Pb$, $^{207}Pb/^{204}Pb$, and $^{208}Pb/^{204}Pb$ values, the bi-modal distribution between the post-shield and shield lavas, as seen in the $^{143}Nd/^{144}Nd$ and $^{87}Sr/^{86}Sr$ data, is not significant. Both, Haleakala and Kohala data, plot within the field for Hawaiian volcanoes (Figure 19). Data for other ocean island are shown for comparison (GEOROC DATABASE). In Figure 20 data for Loa and Kea trend volcanoes are shown in comparison to the analysed Haleakala and Kohala data. The bi-modal distribution of data from Loa and Kea trend volcanoes is most obvious in the $^{208}Pb/^{204}Pb$ versus $^{206}Pb/^{204}Pb$ diagramm. Mauna Kea data Haleakala and Kohala data fit well within data from Kea trend volcanoes. Kea trend volcanoes are more enriched in terms of $^{206}Pb/^{204}Pb$ than Loa trend volcanoes, while they have a more depleted character in their $^{143}Nd/^{144}Nd$ and $^{87}Sr/^{86}Sr$ composition.

Table 6: Pb-Nd-Sr isotope data from Kohala and Haleakala.

	Sample [1]	$^{206}Pb/^{204}Pb$ [2]	$^{207}Pb/^{204}Pb$ [2]	$^{208}Pb/^{204}Pb$ [2]	$^{143}Nd/^{144}Nd$ [3] ($\pm 2\sigma_m$)	$^{87}Sr/^{86}Sr$ [4] ($\pm 2\sigma_m$)
1	0310KO1*	18.843	15.566	38.338	-	0.703678 ±7
2	0310KO1	18.601	15.534	38.175	0.512987±8	0.703670 ±7
3	0410KO4	18.252	15.480	37.892	0.512975±4	0.703702 ±7
4	0610KO15	18.173	15.484	37.953	0.512927±5	0.703874 ±7
5	1310HA2	18.326	15.489	37.973	0.513035±5	0.703302 ±7
6	1410HA9B	18.253	15.472	37.859	0.513058±5	0.703263 ±7
7	1410HA13	18.256	15.480	37.868	0.513055±4	0.703257 ±7
8	1310HA4	18.309	15.480	37.942	0.513023±6	0.703283 ±7
9	0510KO14	18.400	15.498	38.012	0.512995±5	0.703606 ±7
10	0410KO9	18.307	15.483	37.925	0.512984±4	0.703653 ±8
11	1310HA5C	18.183	15.462	37.784	0.513054±4	0.703177 ±7

[1] Pb, Sr, and Nd were determined on the same aliquots. For analytical details see ROMER et al. (e.g. 2005).

[2] Measured ratios corrected for mass fractionation with 0.1 %/a.m.u. as determined from the repeated measurement of NBS 981 Pb reference material. Reproducibility better than 0.1%.

[3] Analysed using dynamic multi-collection on a MAT 262 TIMS. Values normalized to $^{146}Nd/^{144}Nd = 0.7219$. Nd reference material La Jolla gave a value of 0.511847±7 (n=4 analyses) during the measurement period.

[4] Analysed using static multi-collection on a MAT 262 TIMS. Values normalized to $^{86}Sr/^{88}Sr = 0.1194$. Sr reference material NBS 987 gave a value of 0.710288±7 (n=8 analyses) during the measurement period. All ratios were adjusted to a value of 0.710256.

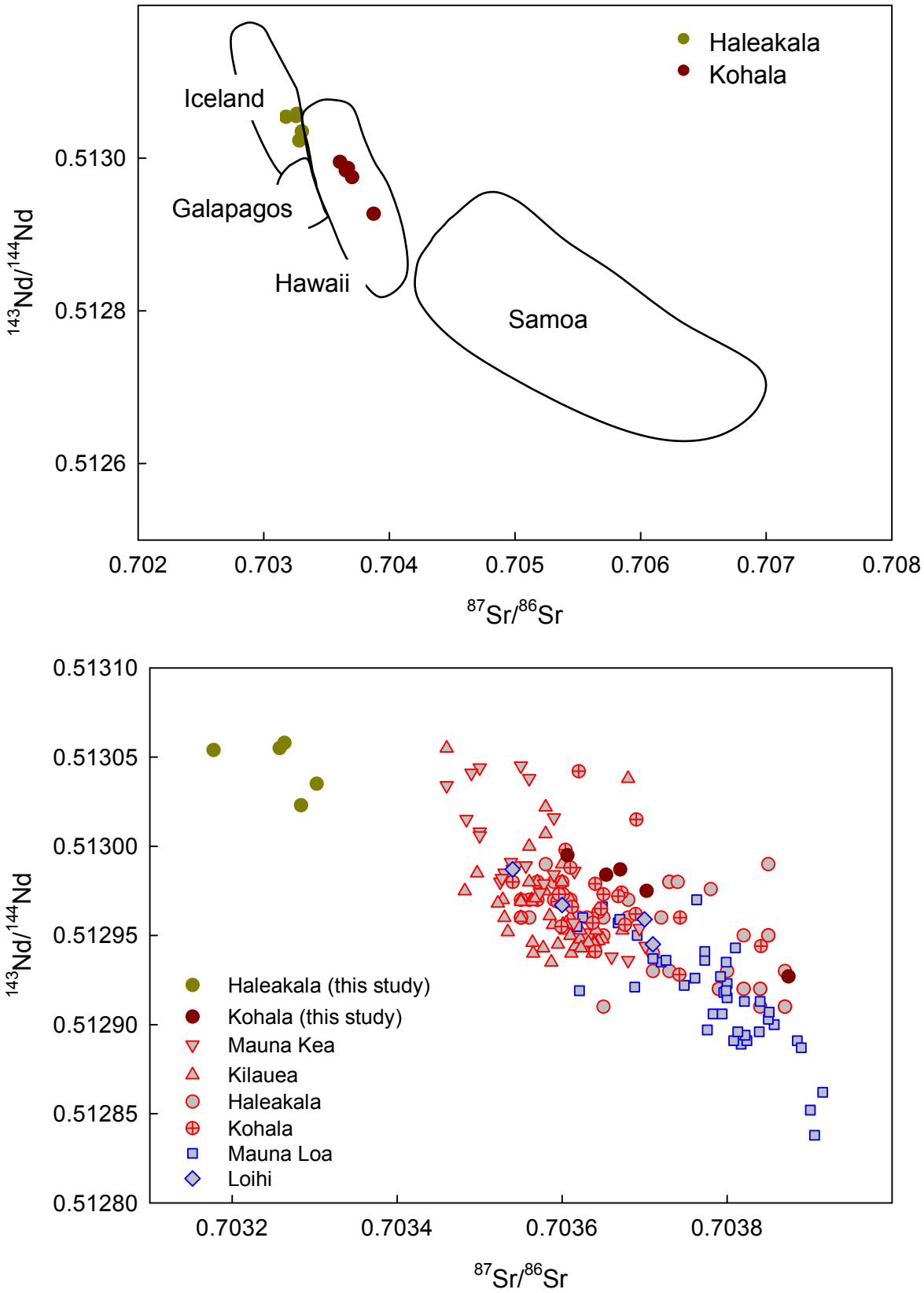

Figure 18: $^{143}Nd/^{144}Nd$ versus $^{87}Sr/^{86}Sr$ diagram for samples from Kohala and Haleakala. The fields encompass paired analyses of the samples (upper panel). Data for several Hawaiian volcanoes that define the Hawaii field are shown separately (lower panel). Blue and red circled symbols reflect Loa and Kea trend volcanoes, respectively. Data and references can be found in the GEOROC geochemical database.

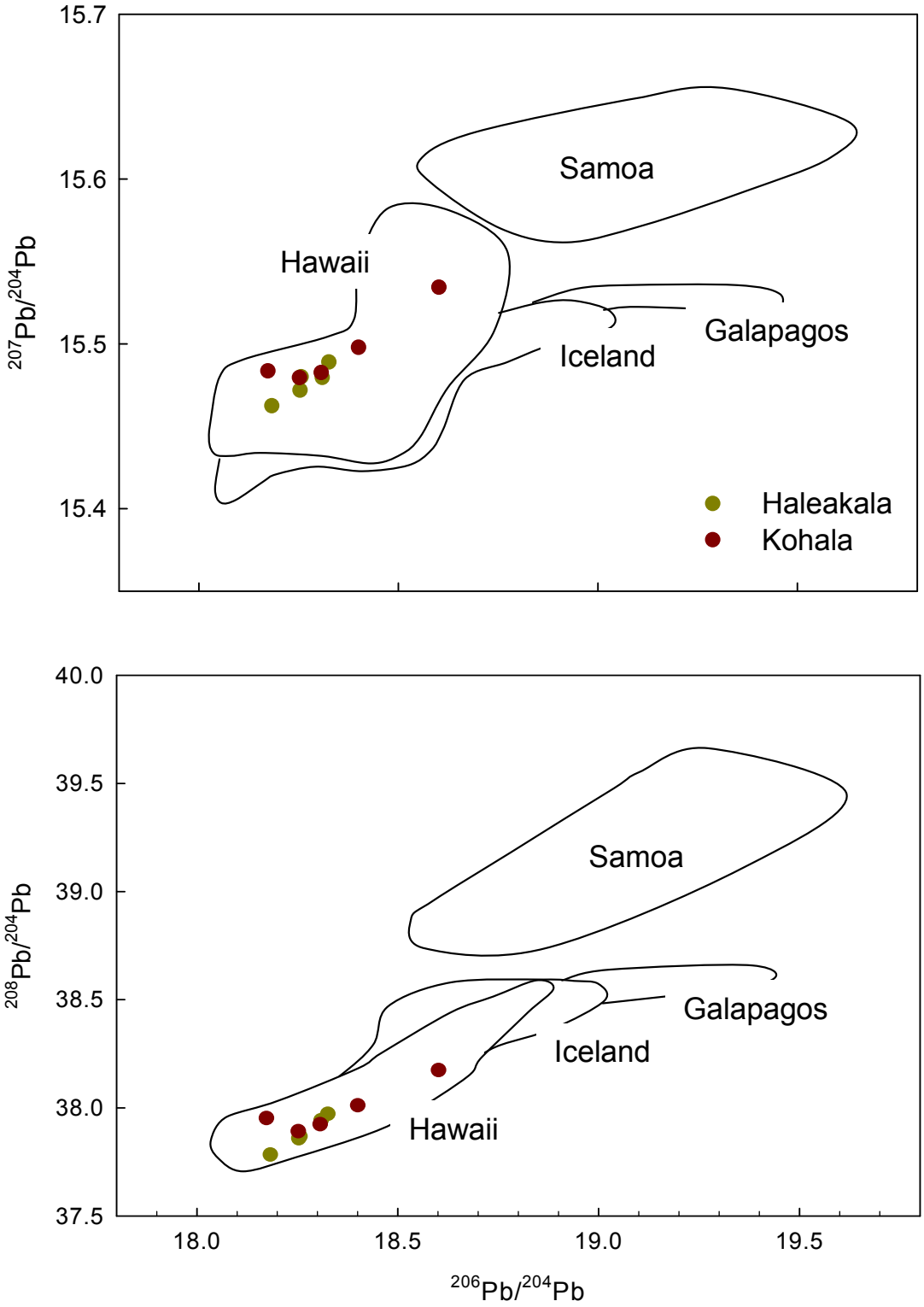

Figure 19: $^{206}Pb/^{204}Pb$ versus $^{207}Pb/^{204}Pb$ (upper panel) and $^{206}Pb/^{204}Pb$ versus $^{208}Pb/^{204}Pb$ (lower panel) diagrams of samples from Kohala and Haleakala. The fields encompass paired analyses of the samples. Data and references can be found in the GEOROC geochemical database.

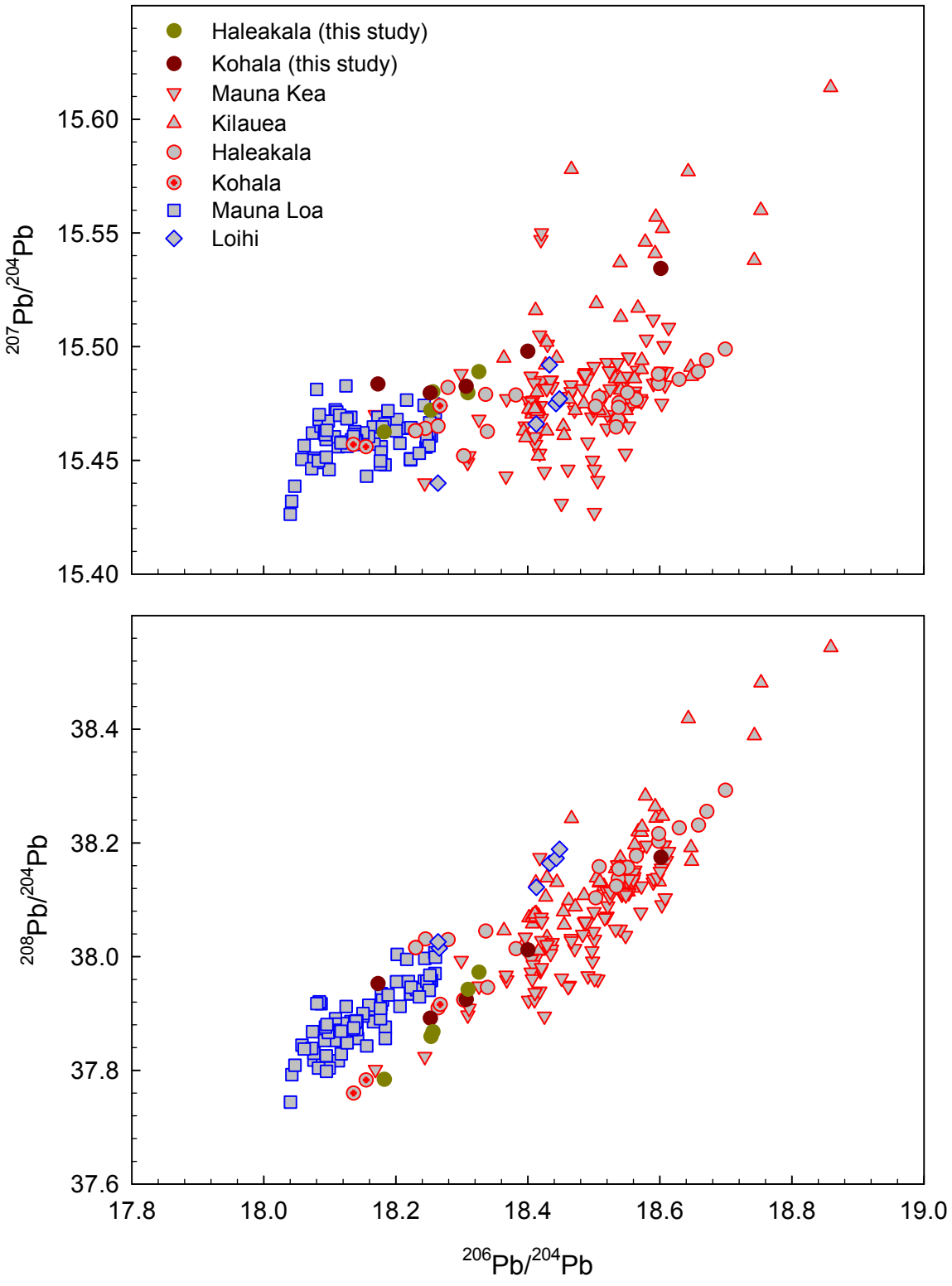

Figure 20: $^{206}Pb/^{204}Pb$ versus $^{207}Pb/^{204}Pb$ (upper panel) and $^{206}Pb/^{204}Pb$ versus $^{208}Pb/^{204}Pb$ (lower panel) diagrams of samples from Kohala and Haleakala. Data from different Hawaiian volcanoes are shown for comparison.). Blue and red circled symbols reflect Loa and Kea trend volcanoes, respectively. Data and references can be found in the GEOROC geochemical database.

4.4 Electron Microprobe Analysis of Olivine Phenocrysts

The major element compositions, including Mg, Si, Al, Ca, Ti, Mn, Fe, Ni and Cr, of olivine phenocrysts from selected samples from Mauna Kea, Kohala, Kilauea, and Haleakala volcanoes have been determined using a Cameca XS 100 Electron Microprobe, and are summarized in Table A3 (Appendix). All measurements were conducted with an electron beam accelerated by an electrical potential of 20 kV. For the analysis, a beam current of 20 nA was used and the electron beam was focussed to a diameter of 1-2 µm. Used standards include the common, natural and synthetic minerals and oxides.

Figure 21 shows the relationship between Ni and forsterite (Fo) contents of olivine phenocrysts from the investigated Hawaiian volcanoes. The Ni concentration generally decreases with decreasing Fo content. Olivines from the shield-stage lavas of Mauna Kea, Kohala, and Kilauea show higher NiO contents compared to olivines from the post-shield lavas of Haleakala volcano. The average NiO contents for Mauna Kea, Kohala and Kilauea are 0.30 wt%, 0.25 wt%, and 0.32 wt%, respectively, the average NiO content for Haleakala olivines is 0.18 wt%.

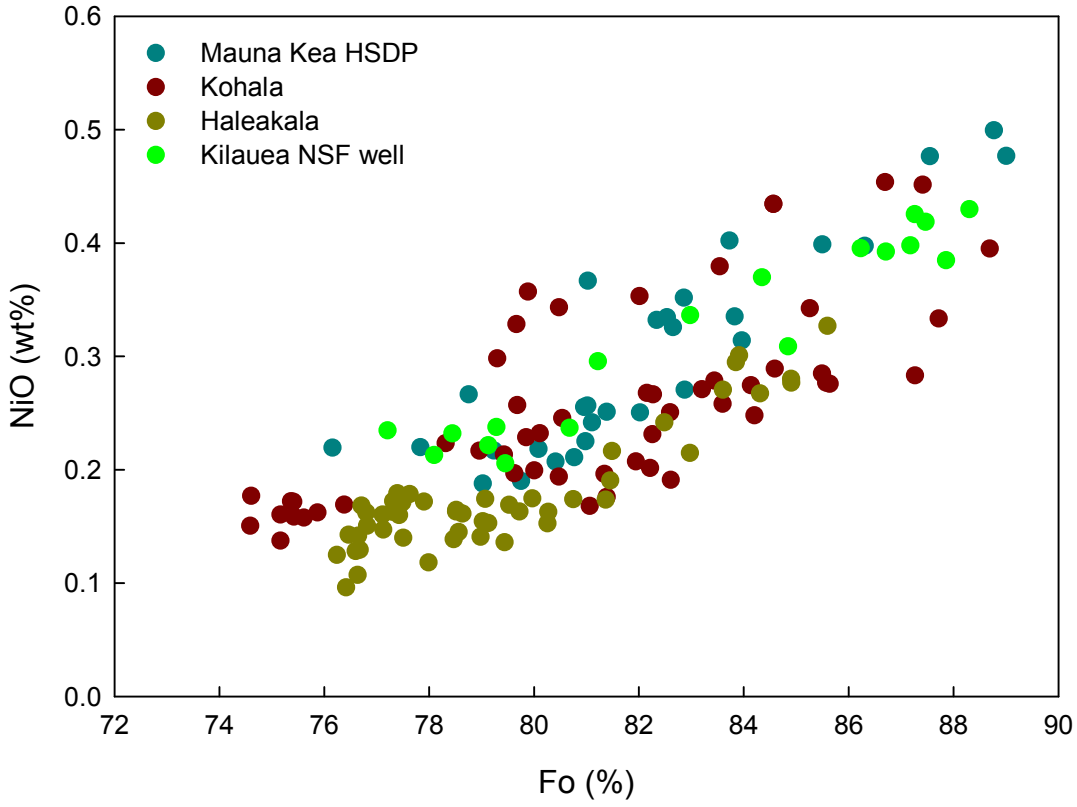

Figure 21: Compositions of olivines from Mauna Kea, Kohala, Kilauea, and Haleakala volcanoes.

4.5 Results of the Noble Gas Measurements

The results of the noble gas analysis of lava samples from Mauna Kea, Kilauea, Kohala and Haleakala volcanoes are compiled in Table A1 (Appendix).

In contrast to the drill core samples from Mauna Kea (HSDP) and Kilauea (NSF well), which have been shielded from cosmic radiation by overlying lava flows, the surface samples from Kohala and Haleakala volcanoes may have been exposed to cosmic rays since eruption. This may have led to an accumulation of cosmogenic ^{3}He and ^{21}Ne, which can alter the original magmatic isotope signals significantly due to the low concentrations of these isotopes in the olivine. Although attention was paid during the sampling campaign that the samples were shielded from cosmic irradiation by at least 1m of overlying rock, it became obvious during the noble gas measurements that several samples have nevertheless been affected by post-depositional irradiation. We therefore started to extract the noble gases not only thermally, but also mechanically by crushing separate aliquots of the sample material, to release only the noble gases from inclusions within the mineral grains, which are not significantly affected by cosmogenic components.

4.5.1 Helium

Total helium amounts in the HSDP samples vary from 0.864 - 5.25 $*10^{-8}$ cm^3 STP/g, with the major amount being released in the highest heating steps. All HSDP samples show $^{3}He/^{4}He$ ratios greater than the atmospheric ratio of $1.39*10^{-6}$, ranging from 11 to 18 R_A. Helium in the lowest temperature step usually shows a lower $^{3}He/^{4}He$ ratio correlated with a lower abundance than in the highest temperature steps. Figure 22 shows the measured $^{3}He/^{4}He$ ratios of the HSDP olivine separates versus the drilling depth. The analysed samples from the submarine section in the core are quite uniform in their total $^{3}He/^{4}He$ ratios, ranging around 12 R_A, with the exception of sample SR0760, showing a total $^{3}He/^{4}He$ ratio of 18 R_A.

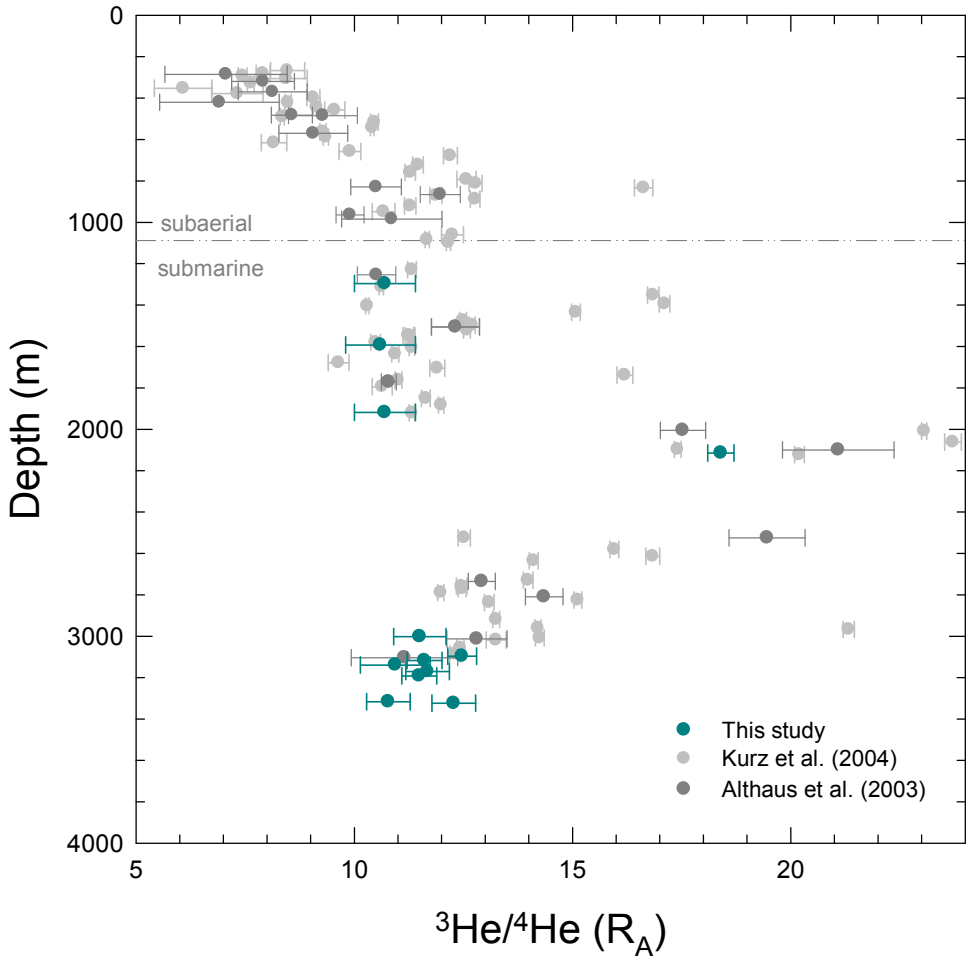

Figure 22: $^{3}He/^{4}He$ ratios versus borehole depth for submarine Mauna Kea (HSDP) samples. Uncertainties are 2σ. Included are data of Althaus et al. (2003) and Kurz et al. (2004) from Mauna Kea (HSDP).

Total helium amounts in the NSF well samples from Kilauea vary from 0.609-1.96*10^{-8} cm^3 STP/g. The gas was extracted from the olivine grains in two temperature steps, 1000°C and 1750°C, the major amount of helium was released at 1750°C. $^{3}He/^{4}He$ ratios of the Kilauea samples range from 13 to 17 R_A.

Contamination with cosmogenic noble gases was a problem in the Kohala samples, as became obvious during the thermal extraction of the noble gases. Aliquots of samples 0310KO1, 0410KO4, and 0510KO14 were therefore measured using the crusher. Total helium concentrations in the Kohala samples vary from 0.0519- 0.455 *10^{-8} cm^3 STP/g in the crushed samples (0310KO1, 0410KO4, 0510KO14), and one stepwise heating sample that showed no contamination (0610KO15) yielded 0.414 *10^{-8} cm^3 STP/g. The investigated samples have a range of $^{3}He/^{4}He$ ratios from 8 to 15 R_A (Figure 23).

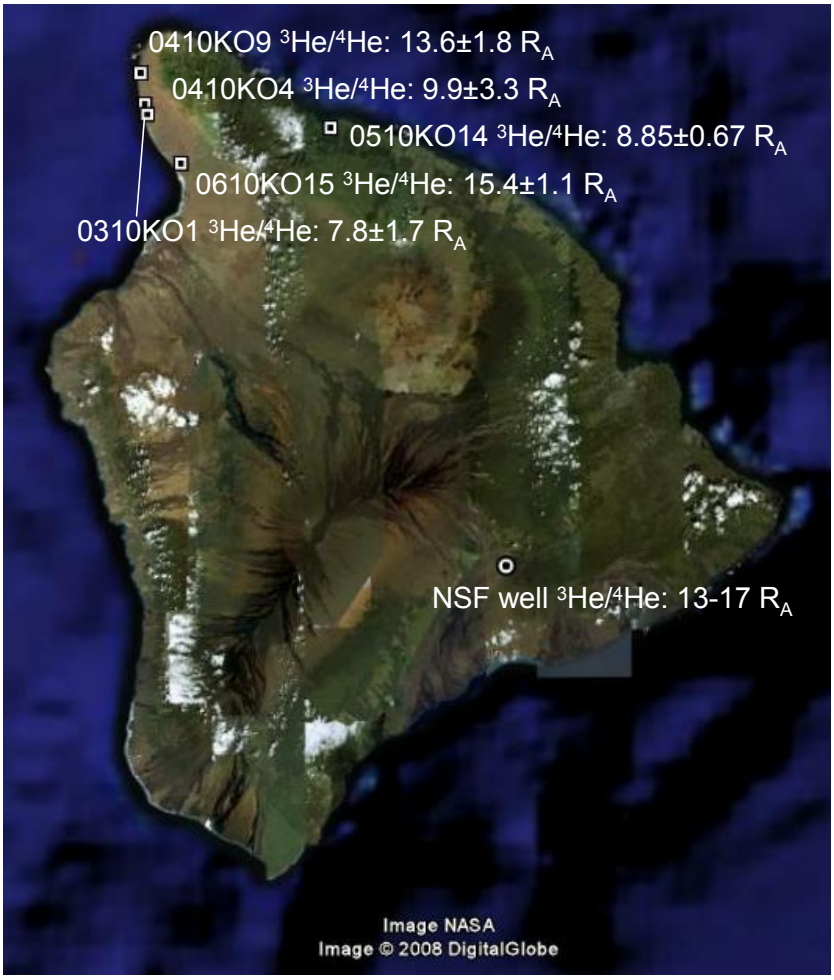

Figure 23: Map showing $^{3}He/^{4}He$ ratios of surface samples from Kohala and drill core samples from Kilauea (NSF well).

Only one sample from Haleakala volcano showed cosmogenic contamination in all temperature steps (1410HA9B). Two samples show however cosmogenic and radiogenic contamination in the lowest temperature step (1410HA13, 1310HA4), but the higher temperature step is unaffected. This conclusion can be drawn from the comparison of the $^{3}He/^{4}He$ ratios from the high temperature step with the results from crushing of another aliquot of the same sample. Total helium concentrations in the stepwise heating samples vary from 0.559-1.518 $*10^{-8}$ cm^3 STP/g, and in the crushed samples from 0.0413-0.677 $*10^{-8}$ cm^3 STP/g. $^{3}He/^{4}He$ ratios are about 8 R_A in all Haleakala lavas (Figure 24).

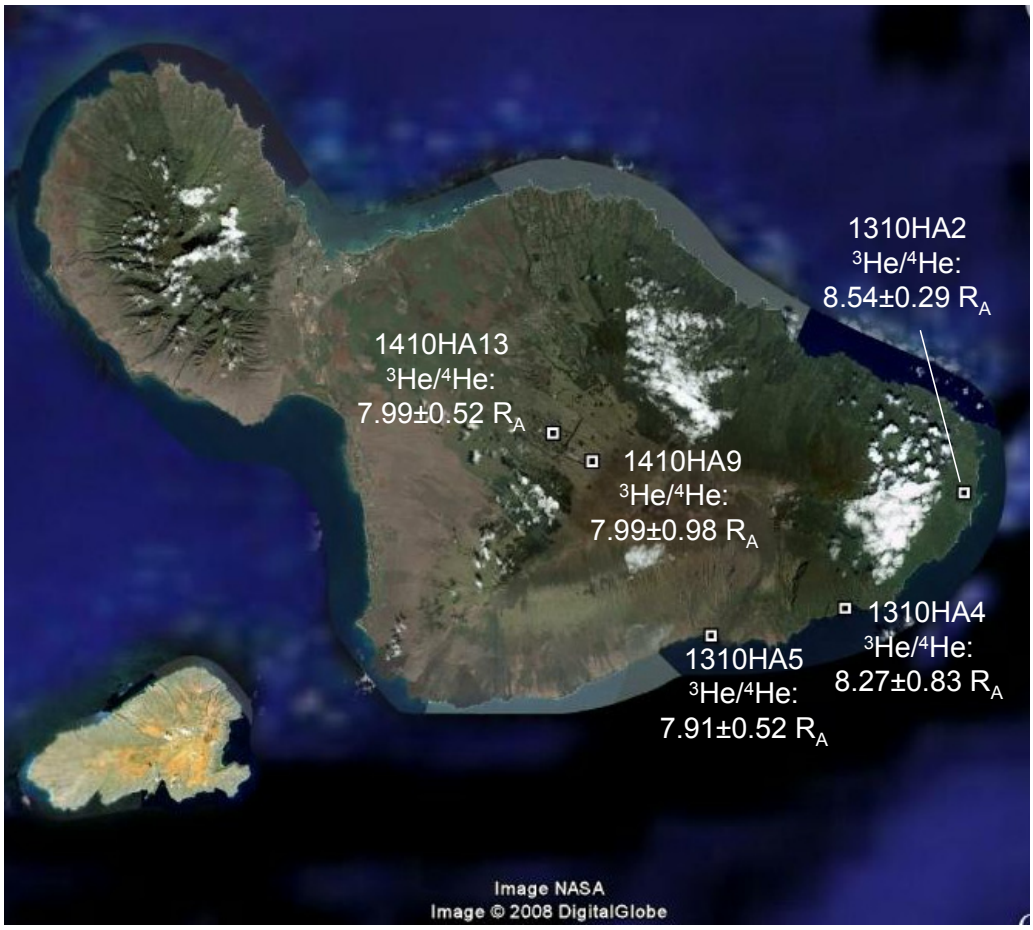

Figure 24: Map showing $^{3}He/^{4}He$ ratios of surface samples from Haleakala.

4.5.2 Neon

Total neon amounts in the HSDP samples vary from 126.8 - 437 $*10^{-12}$ cm^3 STP/g. Large amounts of atmospheric neon are released in the lower temperature steps. Some samples exhibit an excess in $^{20}Ne/^{22}Ne$ and $^{21}Ne/^{22}Ne$ relative to air in the higher temperature steps, others remain indistinguishable from the atmospheric value. Three samples show $^{20}Ne/^{22}Ne$ and $^{21}Ne/^{22}Ne$ different from air for the highest extraction temperature: samples SR 0720, SR 0760, and SR 0979 have $^{20}Ne/^{22}Ne$ and $^{21}Ne/^{22}Ne$ ratios of 10.37±0.14 and 0.0369±0.0039, 10.95±0.30 and 0.0351±0.0023, and 10.47±0.56 and 0.0316±0.0060, respectively.

Total neon amounts in the NSF well samples from Kilauea vary from 33.5-86.9$*10^{-12}$ cm^3 STP/g. The major amount of neon is released at 1000°C, showing $^{20}Ne/^{22}Ne$ and $^{21}Ne/^{22}Ne$ ratios close to the atmospheric values. At the higher extraction temperature, sample CR1-4A shows an excess in $^{20}Ne/^{22}Ne$ and $^{21}Ne/^{22}Ne$ of 10.29±0.40 and 0.0317±0.0040, respectively, while the others remain close to the atmospheric values.

Total neon amounts in the Kohala samples vary from 5.77-17.09 $*10^{-12}$ cm^3 STP/g in the crushed samples, while the stepwise heating sample yields 75.2 $*10^{-12}$ cm^3 STP/g. All but one sample are close to atmospheric $^{20}Ne/^{22}Ne$ and $^{21}Ne/^{22}Ne$ ratios. Sample 0510KO14 however shows $^{20}Ne/^{22}Ne$ and $^{21}Ne/^{22}Ne$ ratios of 10.33±0.22 and 0.0339±0.0025, respectively.
Lavas from Haleakala range in total neon amounts from 8.35 to 76.8 $*10^{-12}$ cm^3 STP/g in the crushed samples, and from 14.24 to 96.9 $*10^{-12}$ cm^3 STP/g in the stepwise heating samples. $^{20}Ne/^{22}Ne$ and $^{21}Ne/^{22}Ne$ ratios are atmospheric throughout all temperature steps of the Haleakala sample suite.

4.5.3 Argon

The results of the argon measurements are shown in Figures 25-27. Total argon concentrations in the HSDP samples vary from 6.68 – 163 $*10^{-8}$ cm^3 STP/g. This large range is due to different amounts of atmospheric contamination of the submarine HSDP samples, as can be seen in the release pattern of argon. The samples from the 2b drilling phase show a higher gas amount released at the lowest extraction temperature, indicating a higher degree of contamination. Both ^{40}Ar and ^{36}Ar are simultaneously released in the lowest heating step, where the weakly fixed atmospheric Ar is extracted from the samples. Some samples reveal a higher $^{40}Ar/^{36}Ar$ ratio at higher extraction temperatures which is, as typical for OIBs, considerably lower than the $^{40}Ar/^{36}Ar$ ratios observed in MORBs. The HSDP samples, all measured in three temperature steps, release the major amounts of ^{36}Ar and ^{40}Ar at 1000°C, with the exception of samples SR 720 and SR 517 that release the major amounts of ^{36}Ar and ^{40}Ar in the highest temperature step. These two samples show $^{40}Ar/^{36}Ar$ ratios very close to the atmospheric value of 295.5 in all temperature steps. Samples SR760 and SR979 show atmospheric isotopic compositions in the lowest temperature step, but elevated $^{40}Ar/^{36}Ar$ ratios at 1400° and 1750°C. Samples R050, R060, R125, and R129 show near atmospheric isotopic compositions at 1000°C. $^{40}Ar/^{36}Ar$ ratios reach up to 960 at medium and high temperatures. Sample R008 shows the highest $^{40}Ar/^{36}Ar$ ratio at 1400°C and sample R021 remains close to the atmospheric value in all temperature steps.

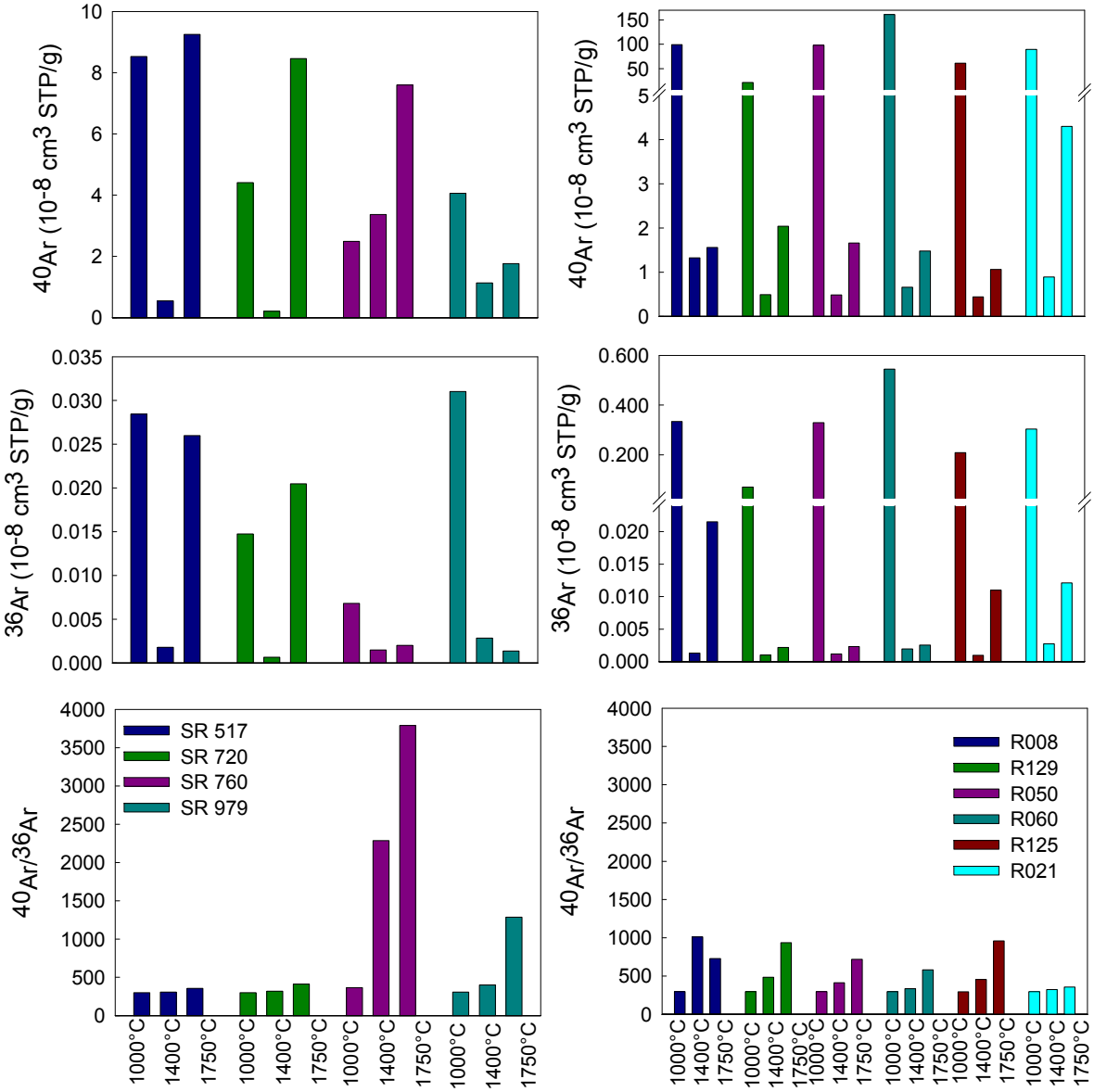

Figure 25: Release patterns of ^{40}Ar and ^{36}Ar and $^{40}Ar/^{36}Ar$ ratios of Mauna Kea drill core samples (HSDP). Note different scales for ^{40}Ar and ^{36}Ar in the left and right panels, respectively.

Total argon concentrations in the NSF well samples from Kilauea vary from 1.98-5.69*10^{-8} cm^3 STP/g. The samples from Kilauea, all measured in two temperature steps at 1000°C and 1750°C, release the major amounts of ^{36}Ar and ^{40}Ar in the higher temperature step, except for sample CR2-2A. All samples show $^{40}Ar/^{36}Ar$ ratios close to atmosphere at 1000°C and $^{40}Ar/^{36}Ar$ ratios between about 375 and 710 at 1750°C.

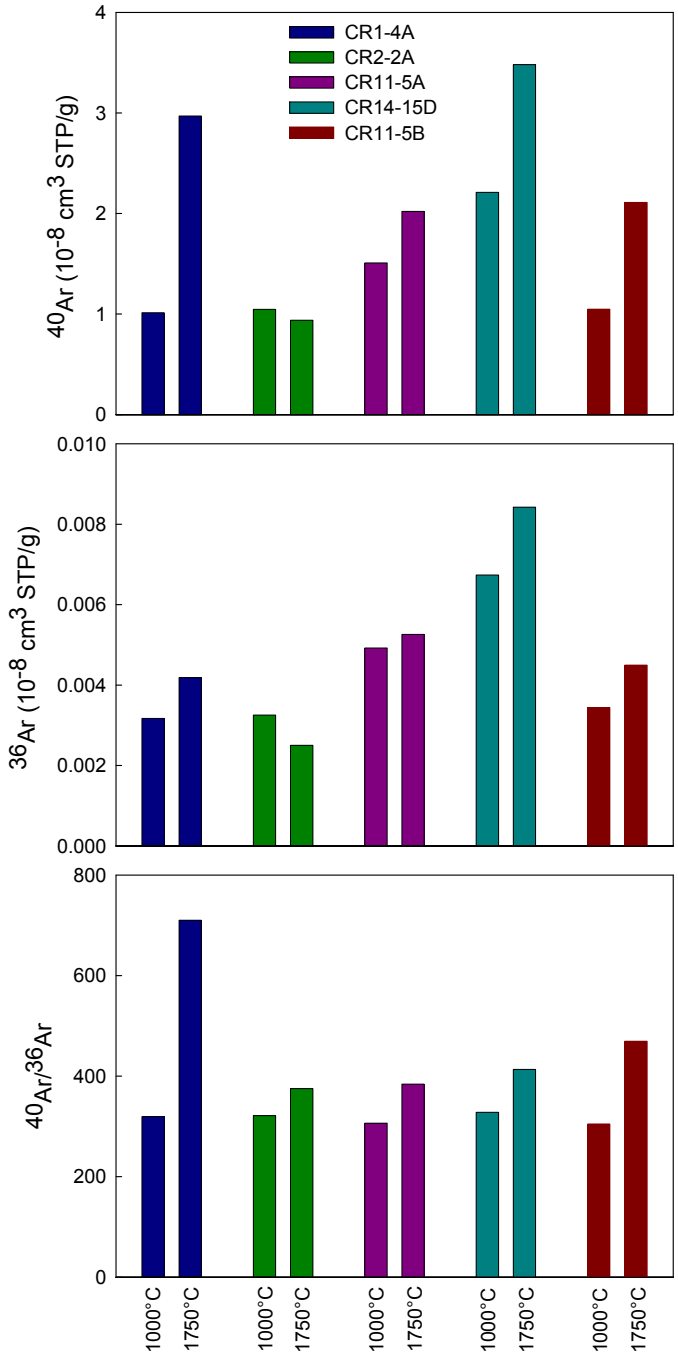

Figure 26: Release patterns of ^{40}Ar and ^{36}Ar and $^{40}Ar/^{36}Ar$ ratios of Kilauea drill core samples (NSF well).

Total argon concentrations of lavas from Kohala vary from 0.521-3.76 $*10^{-8}$ cm^3 STP/g. Samples from Kohala, measured in two or three temperature steps, release the major amount of ^{36}Ar and ^{40}Ar at 1750°C. A few samples have $^{40}Ar/^{36}Ar$ ratios slightly higher than atmospheric. Aliquots of samples 0410KO4, 0310KO1 and 0510KO14 have been measured using the crusher for gas extraction. The $^{40}Ar/^{36}Ar$ ratios of the crushed aliquots of samples

0410KO4 and 0310KO1 are close to the ratios obtained by stepwise heating. Sample 0510KO14 however yields a $^{40}Ar/^{36}Ar$ ratio of 953 ± 14 with the crushing method and 448 ± 4 at 1750°C with the stepwise heating method. This large discrepancy may be due to sample inhomogeneity.

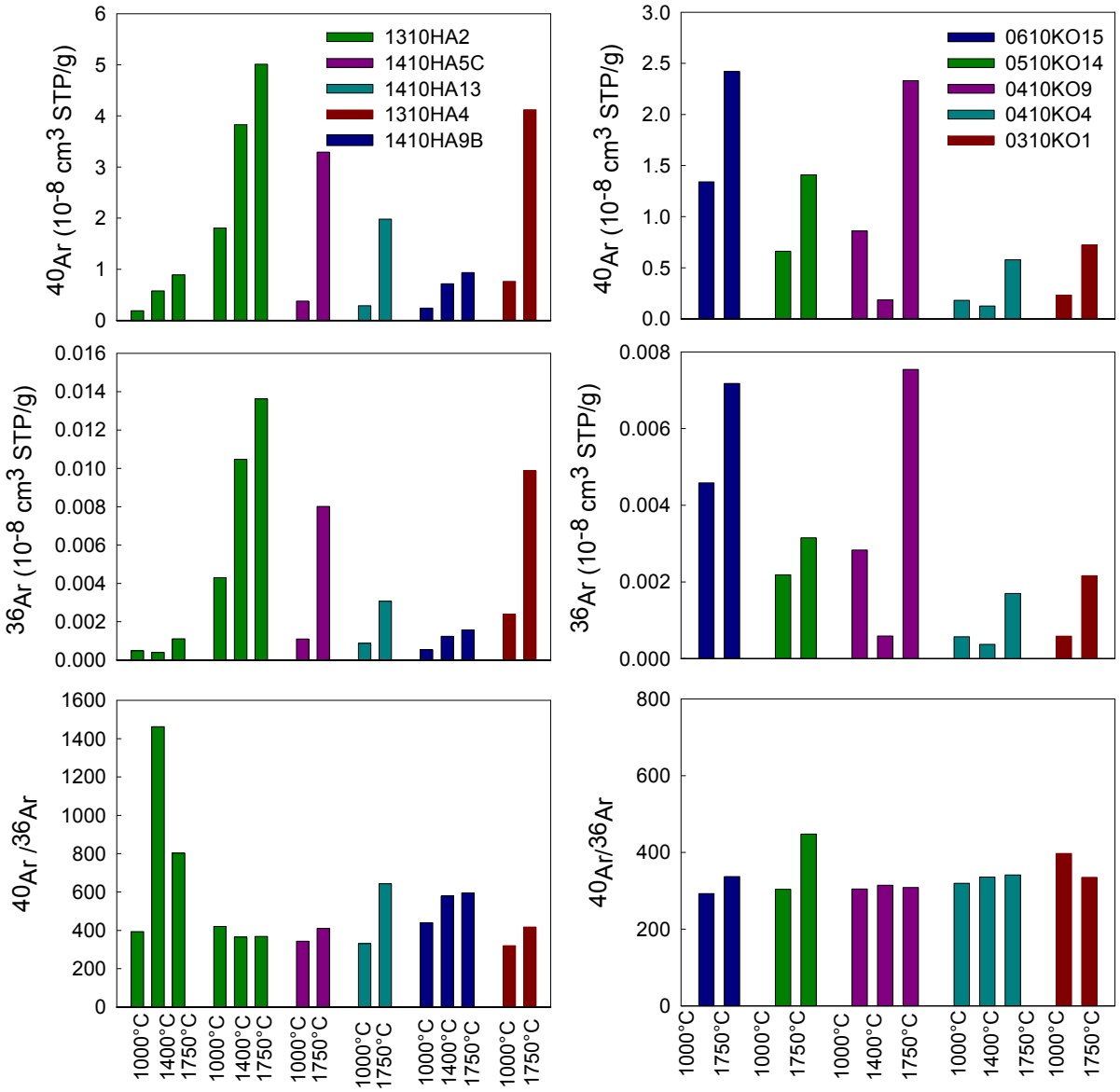

Figure 27: Release patterns of ^{40}Ar and ^{36}Ar and $^{40}Ar/^{36}Ar$ ratios of Kohala and Haleakala surface samples.

Total argon concentrations of lavas from Haleakala vary from 1.14 -10.65 $*10^{-8}$ cm^3 STP/g. Samples from Haleakala were measured in two or three temperature steps. At medium (when measured) and high temperatures the released ^{36}Ar and ^{40}Ar amounts are higher than those released at 1000°C. Two aliquots of samples 1310HA2 have been measured using the thermal

gas extraction. Although both sample aliquots show similar release patterns of ^{36}Ar and ^{40}Ar, the gas amounts are quite different, as well as the $^{40}Ar/^{36}Ar$ ratios. Samples 1410HA5C and 1310HA4 show $^{40}Ar/^{36}Ar$ ratios close to 400 at both temperatures. Samples 1410HA13 and 1410HA9B show maximum $^{40}Ar/^{36}Ar$ ratios of 643 ± 20 and 595 ± 3, respectively. Three samples have also been measured by crushing aliquots of the same samples. The results of the crushed and thermally extracted samples agree quite well for sample 1310HA4. Sample 1410HA9B shows a higher total $^{40}Ar/^{36}Ar$ ratio in the thermal extraction, whereas sample 1410HA13 has a $^{40}Ar/^{36}Ar$ ratio twice as high with the crushing method. Like samples from Kohala, samples from Haleakala show large variations in argon concentrations and isotopic composition.

4.5.4 Krypton and Xenon

Total Krypton and Xenon abundances are compiled in Table 7. Krypton and Xenon isotope ratios do not show an excess relative to the atmospheric values in the entire sample suite.

Table 7: Krypton and xenon elemental abundances of Mauna Kea, Kilauea, Kohala and Haleakala samples.

Volcano	*Total ^{84}Kr abundance [10^{-12} cm^3 STP/g]*	*Total ^{132}Xe abundance [10^{-12} cm^3 STP/g]*
Mauna Kea (HSDP)	10.01 - 239	8.8 - 33.5
Kilauea (NSF well)	2.40 - 5.28	0.36 - 1.38
Kohala	0.229-3.66	0.0496-0.569
Haleakala	0.297-12.09	0.058-10.65

Principle Observations

The Major Element and REE compositions of the analysed lavas lie well within the range typical for Hawaii. Compared to MORB, the analysed lavas are richer in incompatible elements (e.g. K, Rb, and Ba) and light REE, as is typical for OIBs. The radiogenic isotope signatures of the analysed Kohala and Haleakala lavas are within the range previously observed for Hawaii, as are the He and Ne isotopic patterns.

5 Discussion

He-Ne-Ar Systematics

From extensive geochemical studies of material from the Earth's mantle like mid-ocean-ridge basalts (MORB) and ocean island basalts (OIB), it is known that the mantle is heterogeneous in its major element, trace element, and isotopic composition. These heterogeneities exist on all scales; on large scale a number of reservoirs or components have been identified, mainly due to differences in trace element composition and isotope ratios of studied volcanic rocks. These differences are partly intrinsic to the mantle sources and partly due to changes during mixing of the magma with other components and during magma generation processes. It is still a matter of debate how many mantle domains exist and where they are located in the Earth's mantle. Mantle domains used to describe large scale heterogeneities include depleted MORB mantle (DMM), two enriched mantle components (EM 1; EM 2), HIMU (high μ, $\mu=^{238}U/^{204}Pb$), FOZO (Focal Zone), and PHEM (Primitive Helium Mantle) (e.g. FARLEY et al., 1992; STRACKE et al., 2005). A key question in this context is whether a primitive undifferentiated and undegassed reservoir could be preserved in the lower mantle. Radiogenic isotope studies of MORBs and OIBs do not necessarily support the conclusion generally drawn from high $^{3}He/^{4}He$ ratios in oceanic basalts that these high ratios are intrinsic to a relatively undegassed reservoir in the deep mantle. The question is whether high $^{3}He/^{4}He$ ratios can be found in both, primitive reservoirs and also in depleted residues. A key to resolve this problem may be the behavior of helium relative to radiogenic parents of ^{4}He (U, Th). In the standard model, He is assumed to be more incompatible than U and Th, hence, melting events would result in a mantle residue enriched in U and Th relative to He that will have low $^{3}He/^{4}He$ ratios due to radiogenic ingrowth of ^{4}He. If the reservoir is however primitive and has not experienced melting events, gas amounts would be higher and radiogenic ingrowth would not be as effective, resulting in a reservoir with high $^{3}He/^{4}He$ ratios. Recent studies of crystal-melt partitioning of noble gases do however indicate that He might rather be less incompatible than U and Th (PARMAN et al., 2005; HEBER et al., 2007): In this scenario, melting events would result in decreasing (U+Th)/He ratios of the mantle residue and radiogenic ingrowth would be less efficient compared to an unmelted reservoir. The $^{3}He/^{4}He$ ratio of a depleted reservoir would therefore be higher, assuming that He is less incompatible than U and Th, than the $^{3}He/^{4}He$ ratio of the primitive reservoir. Another important difference between these two scenarios is the He concentration. In the

standard model one would assume that the He concentration is highest in the undegassed, high $^{3}He/^{4}He$ reservoir. In the alternative scenario, the depleted reservoir with the highest $^{3}He/^{4}He$ ratios would have low He concentrations (PARMAN et al., 2005). Throughout noble gas studies of MORBs and OIBs it has been recognized that the helium concentrations of MORB glasses are systematically higher compared to OIB glasses ("helium paradox"). It is however unclear if the measured helium concentrations reflect their sources, or if degassing processes during generation and eruption of magmas obscure the source signal. If however the low helium concentrations are intrinsic to the OIB source, the alternative scenario would provide a plausible explanation for the helium isotope and abundance systematics. Assuming that the noble gases behave less incompatible than their radioactive parents during mantle melting (BROOKER et al., 2003; PARMAN et al., 2005; HEBER et al., 2007) (HEBER et al., 2007); partial melting would leave the residual mantle with a weak ingrowth of ^{4}He, ^{21}Ne, and ^{40}Ar due to the preferential extraction of U, Th and K (HEBER et al., 2007). The residual mantle would in this scenario preserve higher $^{3}He/^{4}He$ ratios, lower $^{21}Ne/^{22}Ne$ ratios, and lower $^{40}Ar/^{36}Ar$ ratios, combined with lower noble gas abundances relative to the MORB source. Recycled into the source regions of the OIBs, this residual reservoir could explain the primitive noble gas isotope and abundance characteristics (PARMAN et al., 2005; HEBER et al., 2007). In this scenario, an undegassed mantle reservoir would not be necessary to explain the noble gas characteristics of OIBs, which would be in good agreement with more recent geophysical models demanding whole mantle convection (VAN KEKEN et al., 2002) rather than the classical view of a two-layered mantle with a degassed layer as the source for MORBs (upper mantle) and an undegassed layer (lower mantle) as the source for OIBs.

Noble gas abundances and elemental ratios in mantle-derived materials are affected by multiple processes that superimpose the signals intrinsic to their respective source region in the mantle (HONDA and PATTERSON, 1999). These processes include the degree of partial melting, the crystal-melt partitioning during magma generation and evolution, magma degassing and the contamination with atmospheric gases during transport and eruption to the surface (LUX, 1987; HONDA and PATTERSON, 1999).

Correction for atmospheric contamination is necessary for the heavier noble gases. For helium atmospheric contamination is, due to a very low abundance in the atmosphere and high abundance in the mantle, usually negligible. The low abundance of helium in the atmosphere is caused by the gravitational escape of helium to space and the fact that it is probably not recycled by plate tectonics back into the Earth (GRAHAM, 2002). It is therefore acceptable to

consider all ^{4}He to be of radiogenic origin generated inside the Earth and all ^{3}He to be primordial (HONDA and PATTERSON, 1999). For neon and argon, the nucleogenic and radiogenic components can be calculated using the method described by GRAHAM (2002). For neon, samples that have non-atmospheric $^{20}Ne/^{22}Ne$ and $^{21}Ne/^{22}Ne$ ratios can be corrected for air contamination with this method based on the understanding that Ne in a volcanic rock is a mixture of atmosphere-derived neon and mantle neon, where the latter is composed of a nucleogenic component and a primordial component (HONDA et al., 1991; HONDA et al., 1993a; HONDA et al., 1993b; HONDA and PATTERSON, 1999; GRAHAM, 2002). Whether the primordial component has a composition similar to solar wind ($^{20}Ne/^{22}Ne$= 13.6 (WIELER, 2002)) or is more Neon-B-like (Neon-B describes solar-type Ne in meteorites with $^{20}Ne/^{22}Ne$= 12.5 (TRIELOFF et al., 2000)) is still a matter of debate.

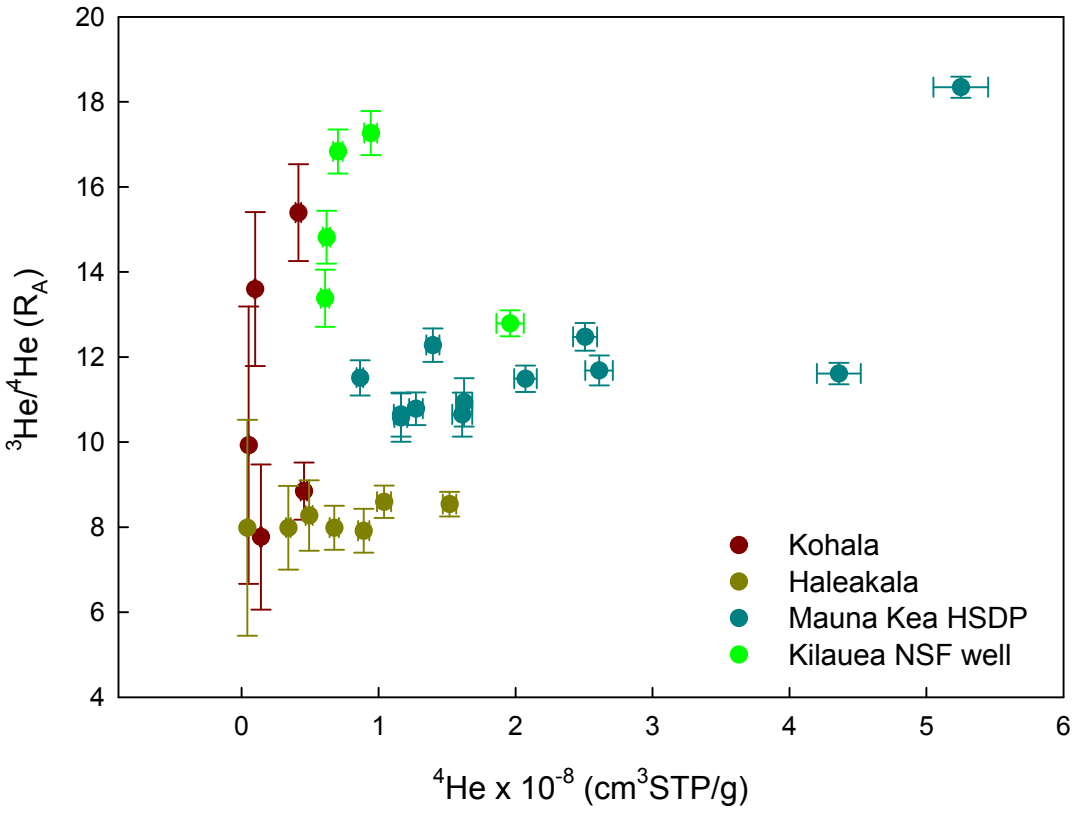

Figure 28: $^{3}He/^{4}He$ ratios plotted against ^{4}He for surface samples from Kohala and Haleakala and drill core samples from Mauna Kea (HSDP) and Kilauea (NSF well).

Samples from this study show $^{3}He/^{4}He$ ratios from MORB-like to moderately high values and, as expected, quite low gas amounts (Figure 28). In Figure 29, samples with excesses in $^{20}Ne/^{22}Ne$ and $^{21}Ne/^{22}Ne$ ratios are shown. The Mauna Kea and Kilauea data agree well with

the Loihi-Kilauea line defined by HONDA et al. (1991). The Kohala sample, in contrast to Mauna Kea and Kilauea samples, plots on the MORB correlation line from SARDA et al. (1988), correlated with MORB-like $^{3}He/^{4}He$ ratio for this sample.

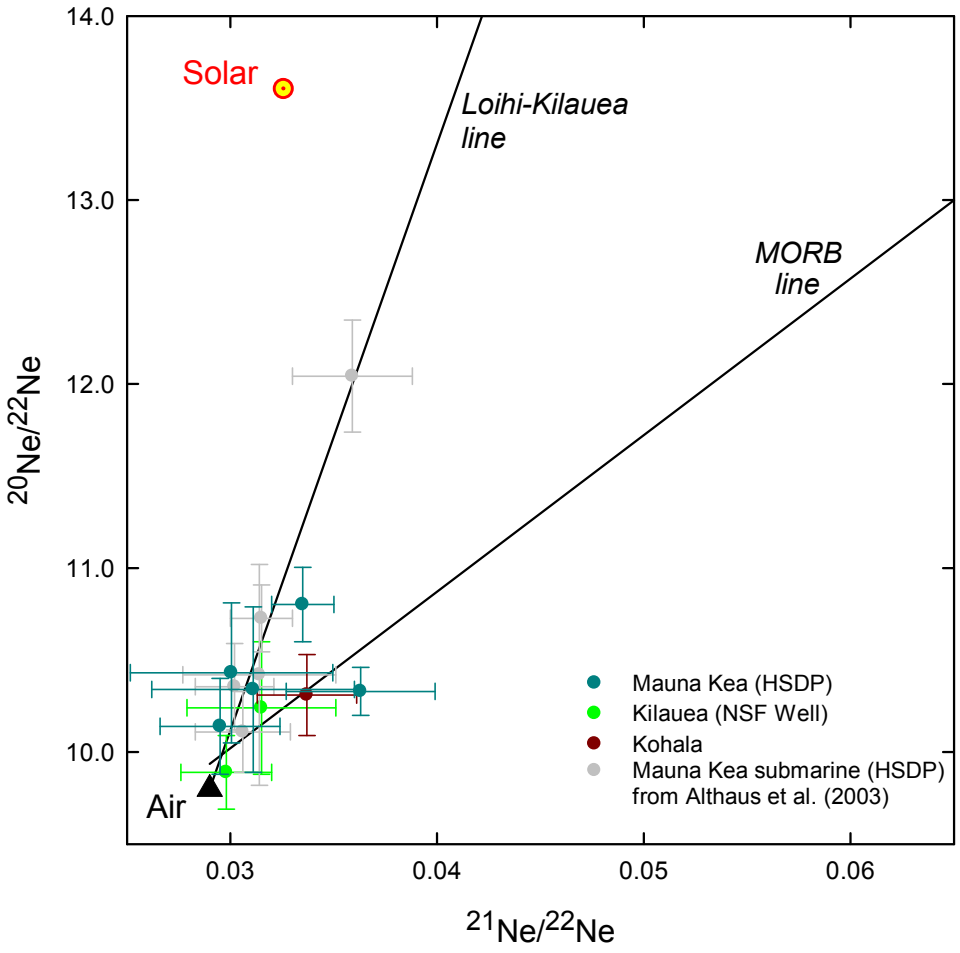

Figure 29: Neon three-isotope plot showing data of HSDP Mauna Kea and NSF well Kilauea samples as well as one data point of Kohala. Neon isotope data represent all temperature steps different from the isotopic neon signature of air on the 2σ level. Unlike Table A1 (Appendix), the data in this plot have not been corrected for analytical blanks. Included are submarine Mauna Kea (HSDP) data of Althaus et al. (2003).

With air-corrected neon and argon values, the mantle-derived elemental ratios of $^{4}He/^{40}Ar^{*}$, $^{4}He/^{21}Ne^{*}$ and $^{3}He/^{22}Ne_{S}$ can be used to infer if the analysed samples were affected by elemental fractionation. The $^{4}He/^{40}Ar^{*}$ ratio is a useful parameter to assess a closed system behavior (OZIMA and IGARASHI, 2000), because in a closed system the $^{4}He/^{40}Ar^{*}$ ratio would be constant. This is because ^{4}He and $^{40}Ar^{*}$ are essentially radiogenic and their ratio in a reservoir is controlled by the relative abundances of U, Th and K and the accumulation time (OZIMA and IGARASHI, 2000). A reservoir that remains a closed system will evolve

towards a constant $^{4}He/^{40}Ar^{*}$ value over a few tens of Ma (OZIMA and PODOSEK, 2002). This constant ratio will be close to the theoretical mantle production ratio. In Figure 30, samples from this study plot below the closed system range, with only a few exceptions, and show a large range in $^{4}He/^{40}Ar^{*}$, indicating a significant fractionation of helium with respect to argon, with a deficiency in ^{4}He.

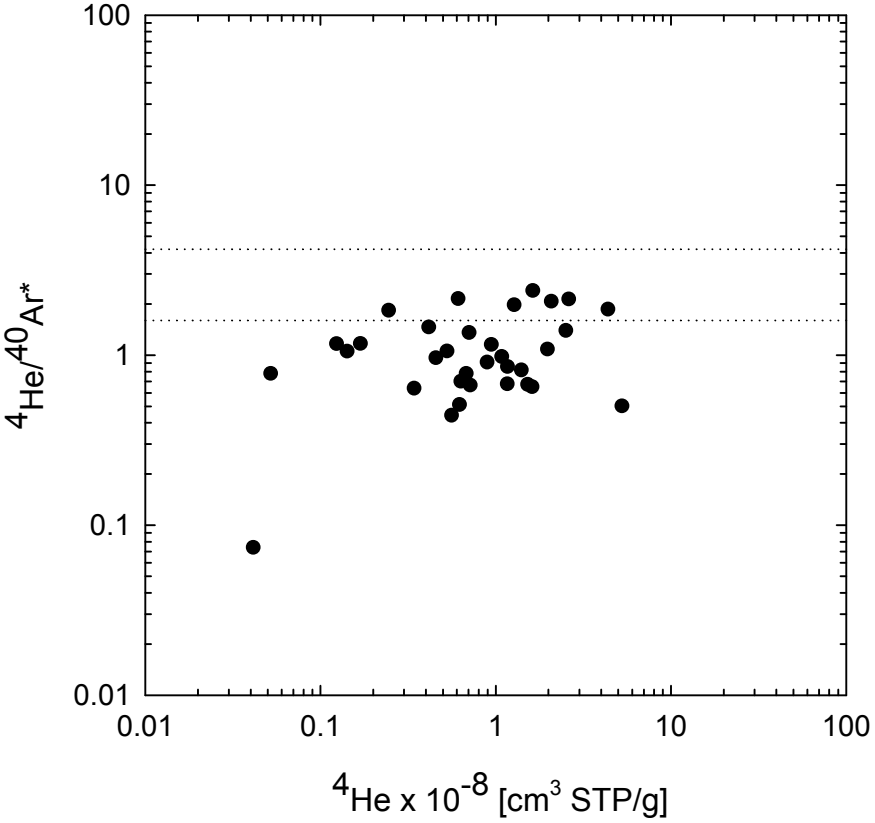

Figure 30: $^{4}He/^{40}Ar^{*}$ is plotted against ^{4}He. T he dashed lines indicate the range for to the $^{4}He/^{40}Ar^{*}$ production ratio (GRAHAM, 2002) and therefore a closed system (see text).

The same can be seen in Figure 31, where the $^{3}He/^{22}Ne_{S}$ ratio is compared to the $^{4}He/^{21}Ne^{*}$ ratio for samples showing excess in $^{20}Ne/^{22}Ne$ and $^{21}Ne/^{22}Ne$. For an unfractionated noble gas signal one would expect the $^{4}He/^{21}Ne^{*}$ ratios to reflect the production ratio estimated for the mantle ($2.2 \pm 0.1 * 10^{7}$ (YATSEVICH and HONDA, 1997)). For the $^{3}He/^{22}Ne_{S}$ ratio, an unfractionated ratio would equal the primordial ratio of the Earth (7.7 ± 2.6 (HONDA and MCDOUGALL, 1998). The range of the data set and the deviation from the primordial and production ratios of $^{3}He/^{22}Ne_{S}$ and $^{4}He/^{21}Ne^{*}$ indicate fractionation of helium with respect to neon (Figure 31). The correlation of the $^{3}He/^{22}Ne_{S}$ and $^{4}He/^{21}Ne^{*}$ ratios suggests that both elemental ratios have equally been affected by fractionation and that the $^{4}He/^{21}Ne^{*}$ ratio has

not evolved back to the production ratio by radiogenic ^{4}He and nucleogenic $^{21}Ne^{*}$ ingrowth after the fractionation event.

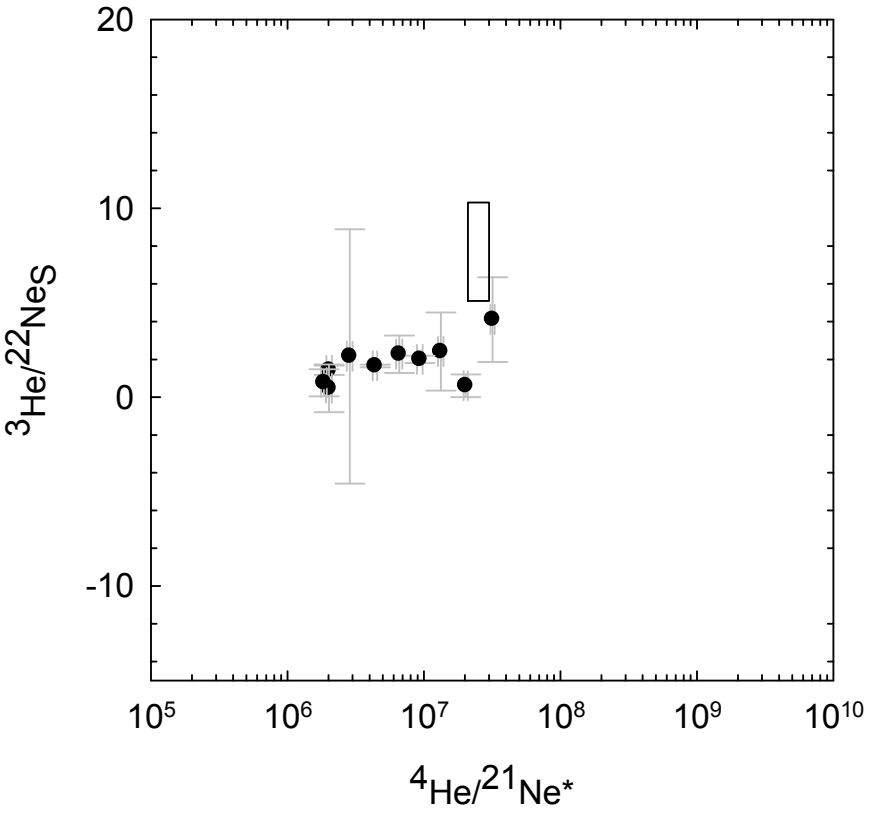

Figure 31: $^{3}He/^{22}Ne_S$ is plotted against $^{4}He/^{21}Ne^{*}$. The box corresponds to the primordial and production ratios of $^{3}He/^{22}Ne_S$ and $^{4}He/^{21}Ne^{*}$, respectively (YATSEVICH and HONDA, 1997; HONDA and MCDOUGALL, 1998).

The apparent He/Ne fractionation over two orders of magnitude relative to the primordial $^{3}He/^{22}Ne$ ratio and the $^{4}He/^{21}Ne^{*}$ production ratio is characterised by a depletion of He with respect to Ne, the same can be concluded for the He/Ar systematics, where He is depleted with respect to Ar (Figure 32). The broad correlation in Figures 31 and 32 and the fact that the data plot consistently below the production and primordial range suggests that both elemental ratios have been equally affected by a depletion of helium.

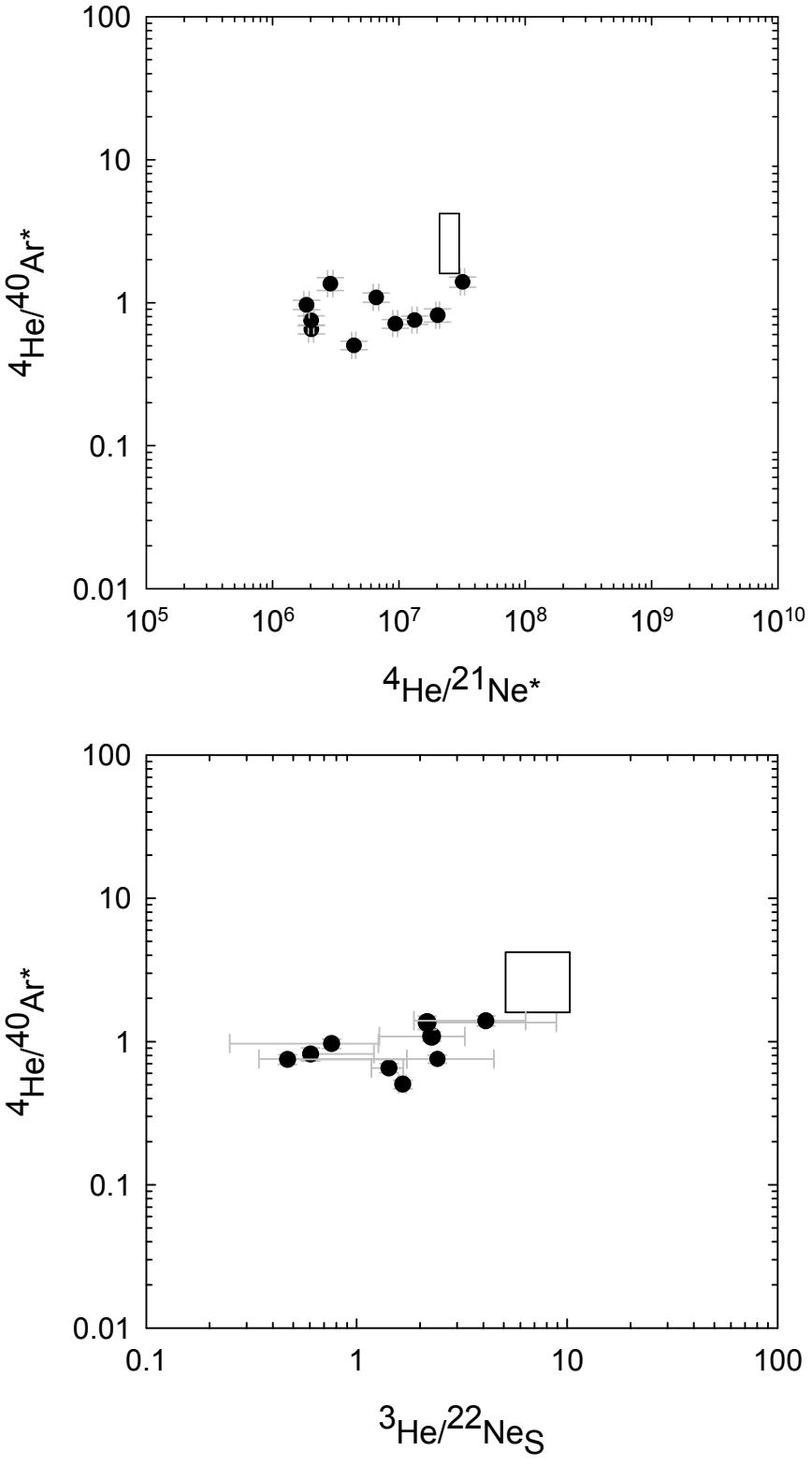

Figure 32: Plot of $^4He/^{40}Ar^*$ versus $^4He/^{21}Ne^*$ (upper panel) and $^4He/^{40}Ar^*$ versus $^3He/^{22}Ne_S$ (lower panel), the boxes represent the production range and primordial ratio range for $^4He/^{40}Ar$ (GRAHAM, 2002), $^4He/^{21}Ne^*$ (YATSEVICH and HONDA, 1997), and $^3He/^{22}Ne_S$ (HONDA and MCDOUGALL, 1998), respectively. The data plot consistently below the production and primordial range, indicating a depletion of He relative to Ar and Ne.

The elemental fractionation in the measured samples is due to a "relatively" recent event, otherwise the $^{4}He/^{40}Ar^{*}$ and $^{4}He/^{21}Ne^{*}$ elemental ratios would have evolved back to the production ratios due to radiogenic and nucleogenic ingrowth (HONDA and PATTERSON, 1999). Elemental fractionation of the He/Ne isotope system is also reflected in the binary mixing model for the measured data (Figure 33), where data from ALTHAUS et al. (2003) from the submarine part of the HSDP drill core have been added. In the mixing model, $^{21}Ne/^{22}Ne_{extrapolated}$ values are plotted versus $^{4}He/^{3}He$ ratios, where $^{21}Ne/^{22}Ne_{extrapolated}$ is the $^{21}Ne/^{22}Ne$ ratio corrected for atmospheric contamination. The straight line in Figure 33 represents mixing between MORB and a primordial or plume end-member with unfractionated $^{3}He/^{22}Ne$ values, represented by a curve parameter r of 1. The curve parameter is defined as $r = (^{3}He/^{22}Ne)_{MORB}/(^{3}He/^{22}Ne)_{PLUME\ or\ PRIMORDIAL}$. The hyperbolic lines represent mixing between the end-members MORB and plume or primordial with r values between 0.1 and 15, reflecting different degrees of fractionation of the $^{3}He/^{22}Ne$ values. The measured data do not lie on a single mixing curve. However, most data are best explained by an r value of about 15. The measured data, which have experienced a relatively recent elemental fractionation in various degrees, reflected by different r values needed to account for the data, can be explained by a binary mixing between MORB and plume or primordial end-members.

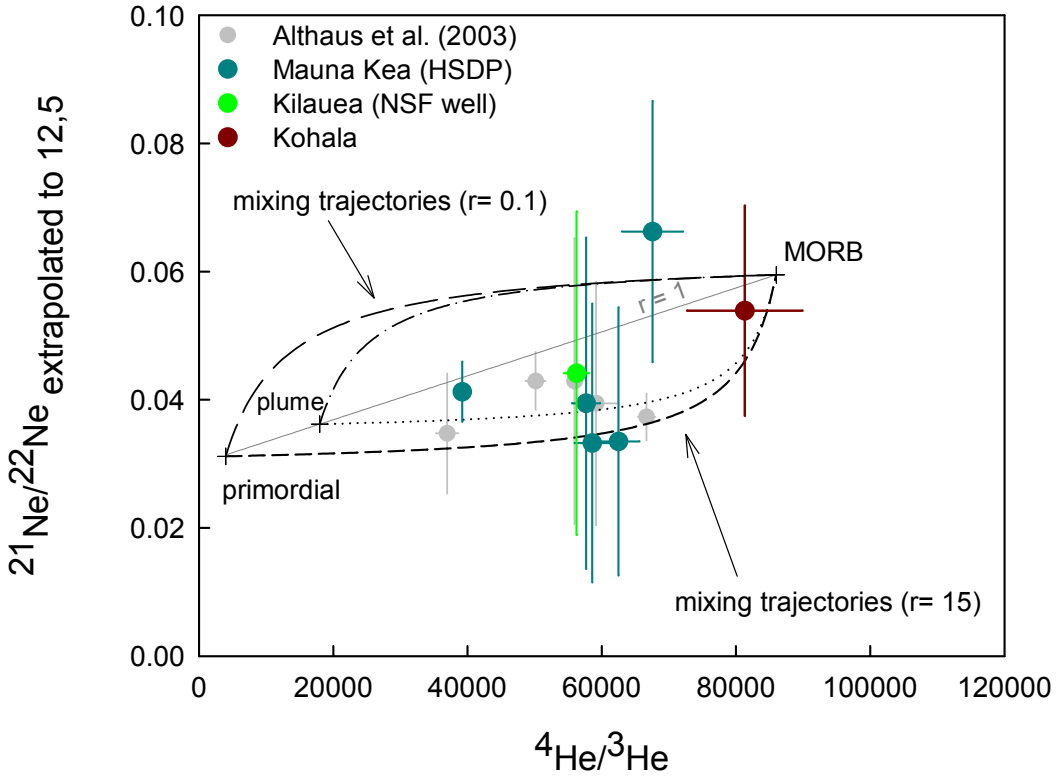

Figure 33: Plot of $^{21}Ne/^{22}Ne_{extrapolated}$ versus $^{4}He/^{3}He$. $^{21}Ne/^{22}Ne_{extrapolated}$ values were determined by extrapolation to a $^{20}Ne/^{22}Ne$ mantle ratio of 12.5 (Ne-B [e.g. (BLACK, 1972)]) in order to correct for atmospheric contamination. Hyperbolic lines represent mixing between MORB ($^{4}He/^{3}He$ = 86,000; $^{21}Ne/^{22}Ne$ = 0.0595) and "plume" ($^{4}He/^{3}He$ = 18,000; $^{21}Ne/^{22}Ne$ = 0.0362) and between MORB and a primordial end-member ($^{4}He/^{3}He$ = 4,000; $^{21}Ne/^{22}Ne$ = 0.03118), respectively. The curve parameter r is defined as r = $(^{3}He/^{22}Ne)_{MORB}/(^{3}He/^{22}Ne)_{PLUME\ or\ PRIMORDIAL}$. The straight line with a curve parameter r=1 requires that both end-members have equal $^{3}He/^{22}Ne$ values. Mixing lines with r values different from 1 represent end-members with different $^{3}He/^{22}Ne$ values. Data from ALTHAUS et al. (2003) are shown for comparison.

Recent elemental fractionation of He relative to Ne and Ar may have been caused by magmatic processes like crystal-melt partitioning during partial melting and fractional crystallisation, solubility controlled partitioning between melt and gas phases during bubble formation and magma outgassing, and diffusion-related differences in the mobility of noble gases in crystal and melt (HONDA and PATTERSON, 1999). Results of a recent study on the crystal-melt partitioning of noble gases from HEBER et al. (2007) showed that all noble gases behave incompatible during melting and crystallisation and that He and Ne have quite similar partition coefficients in the range of 10^{-4} in olivine while Ar yields a partition coefficient of about 10^{-3} in olivine, suggesting that Ar is less incompatible than He and Ne. To understand the depletion of noble gases in the silicate Earth and the relative fractionation of noble gases in different reservoirs within the Earth, knowledge of the partition behavior is vital. The

solubility of noble gases is another critical parameter to consider. Since the solubility of noble gases is generally low, magma ascent will lead to exsolution of noble gases due to decompression. The early exsolved vapour phase will be dominated by CO_2 over H_2O due to the lower solubility of the former. Together with CO_2, the noble gases will be preferentially partitioned into the vapour phase and due to differences in solubility, the noble gas abundances will be fractionated. This process is however ineffective in closed-system degassing. In open system degassing, where the vapour and magma are separated and the fractionation is a function of the amount of gas loss, the noble gas abundances may be highly fractionated (CARROLL and DRAPER, 1994). As illustrated in Figure 30, samples from this study appear to record the open system behavior of their source in the $^{4}He/^{40}Ar^{*}$ values. Hence the observed noble gas fractionation may be partly due to solubility controlled gas loss during magma ascent and the crystal-melt partition behavior during partial melting.

He-Sr-Nd-Pb Isotope Systematics of Kohala and Haleakala

Helium isotopes are plotted against $^{206}Pb/^{204}Pb$, $^{143}Nd/^{144}Nd$, and $^{87}Sr/^{86}Sr$ in Figure 34. Haleakala lavas show a very narrow range in both, $^{3}He/^{4}He$ and $^{206}Pb/^{204}Pb$ ratios. $^{3}He/^{4}He$ and $^{206}Pb/^{204}Pb$ ratios in Kohala lavas are inversely correlated, samples with lower $^{3}He/^{4}He$ ratios are more radiogenic in $^{206}Pb/^{204}Pb$. Kohala samples extend to higher $^{3}He/^{4}He$ ratios and more radiogenic $^{206}Pb/^{204}Pb$ ratios compared to Haleakala lavas. $^{143}Nd/^{144}Nd$ and $^{87}Sr/^{86}Sr$ ratios are anticorrelated for Haleakala and Kohala lavas as would be expected from the relative compatibilities of the parent-daughter pairs (WHITE, 2005). Fields for Hawaii, Samoa, Galapagos and Iceland are shown for comparison (Figure 34). The Sr-Nd-Pb characteristics of Haleakala and Kohala basalts are within the range typical for MORBs, as well as the He characteristics of the analysed Haleakala samples and three of the Kohala samples. However, one Kohala sample shows a higher $^{3}He/^{4}He$ ratio, plotting within the field for Hawaii.

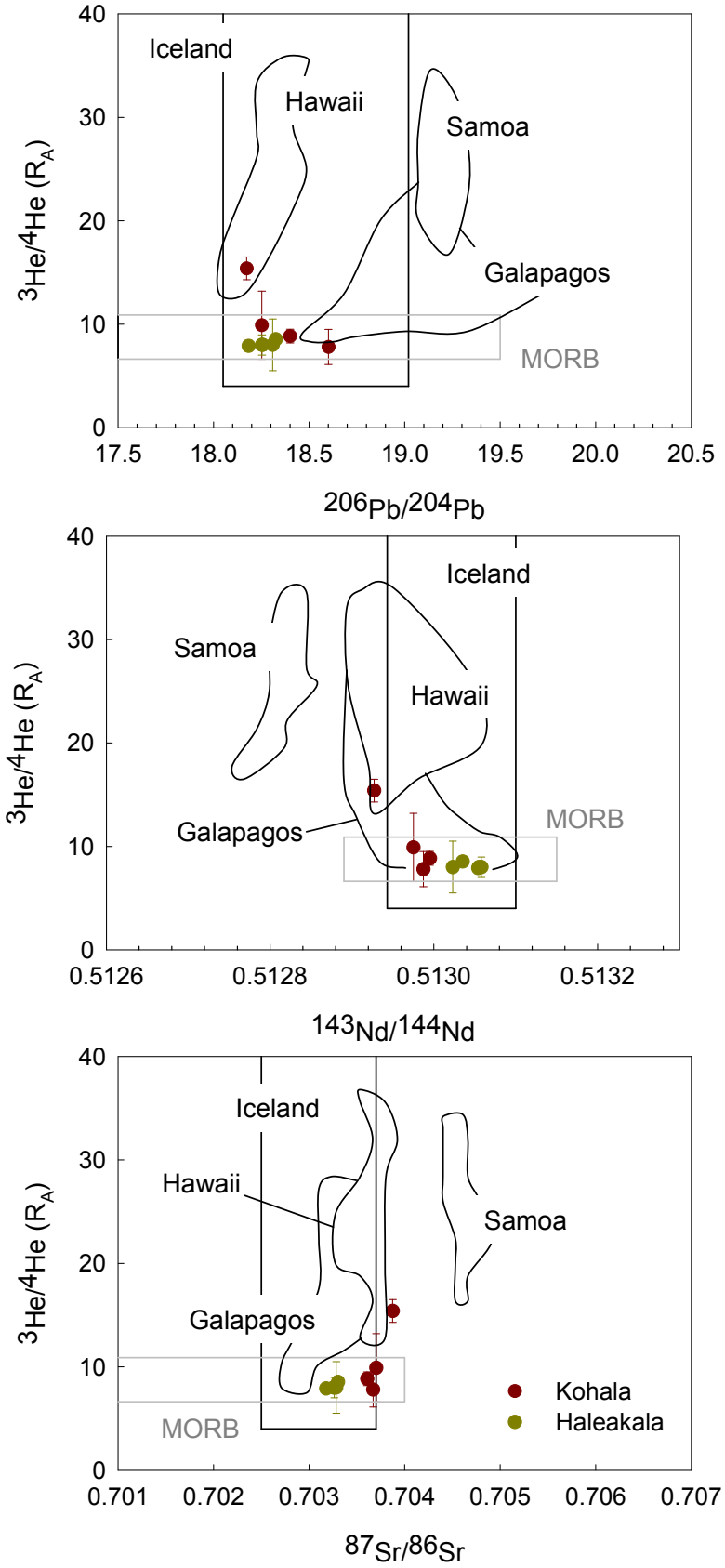

Figure 34: He-Pb, He-Nd, and He-Sr isotope relations for Haleakala and Kohala basalts. The fields encompass paired analyses of the samples. The box encompasses the range of values. Data and references can be found in the GEOROC geochemical database.

Constraints about the Hawaiian Mantle Plume Source

The structure of the Hawaiian plume is a strongly debated topic, which has important implications on large-scale mantle processes and the understanding of mantle dynamics. The main issue in mantle geochemistry is the nature of the mechanisms that lead to the observed heterogeneities in the mantle and the preservation of these heterogeneities during large-scale mixing processes. In addition to whole mantle processes, each mantle plume produces small-scale geochemical variations. Several models have been suggested to explain the geochemical and geophysical characteristics of the Hawaiian hotspot. One model postulated by KURZ et al. (1996; 2004) and refined by DEPAOLO et al. (2001) proposes that the plume is concentrically zoned. This model is based on the assumption that the high $^{3}He/^{4}He$ material, which is derived from an undegassed source, is associated with the centre of the hotspot and the material with lower $^{3}He/^{4}He$ is characteristic for the rim of the hotspot and that the volcanoes sample these different materials as they move over the hotspot. As elaborated on above, a reservoir with high $^{3}He/^{4}He$ is not necessarily confined to the existence of an undegassed reservoir, but can evolve in a reservoir due to melt generation and a more compatible behavior of He with respect to U and Th during silicate melting. Another model proposes that the Hawaiian mantle plume has a bilateral rather than a concentric zoning (ABOUCHAMI et al., 2005). This model is based on the two different Pb isotope arrays of the Hawaiian volcanoes that are due to large-scale heterogeneities in the source layer. According to this model, these heterogeneities are drawn into the plume stem, experience vertical compression, and are stretched and eventually sampled by the Hawaiian volcanism forming the Kea and Loa trend volcanoes. Several studies propose that recycled material was incorporated into the Hawaiian plume (LASSITER and HAURI, 1998; BLICHERT-TOFT et al., 1999; SOBOLEV et al., 2000; SOBOLEV et al., 2005): SOBOLEV et al. (2005) for example propose a model where the rising plume contains eclogite bodies derived from recycled oceanic crust, that react with peridotite to produce pyroxenite. The remaining peridotite and the pyroxenite form melts that eventually mix in conduits and magma chambers. This multi-stage generation process proposed by SOBOLEV et al. (2005) is used to explain the high Ni and Si contents in Hawaiian shield-lavas. WANG and GAETANI (2008) propose an alternative explanation for existence of high Ni-olivines, which is based on the assumption of a higher compatibility of Ni in olivine crystallization from siliceous melts than in the model of SOBOLEV et al. (2005). WANG and GAETANI (2008) claim that Hawaiian lavas are derived from mixtures of eclogite and primitive Hawaiian tholeiitic lavas with

moderate Ni contents. JACKSON and DASGUPTA (2008) propose lherzolite (+MORB-like, silica excess pyroxenite) or harzburgite as a possible source lithology.

The results of this study show that the Hawaiian shield-stage lavas of Mauna Kea, Kilauea, and Kohala show differences with respect to the noble gas isotopic composition. While Kohala samples range from MORB-like values up to 15 R_A , Mauna Kea (HSDP) and Kilauea samples show $^3He/^4He$ ratios uniformly higher than MORB, up to 18 R_A. Samples of Mauna Kea and Kilauea with elevated $^{20}Ne/^{22}Ne$ and $^{21}Ne/^{22}Ne$ ratios plot near the Loihi-Kilauea Line in a neon three isotope plot. This Ne and He isotopic signature could be evidence for primitive material in the source regions of these volcanoes. However, the one tholeiitic sample from Kohala which shows elevated $^{20}Ne/^{22}Ne$ and $^{21}Ne/^{22}Ne$ ratios plots directly on the MORB-line, correlating with a $^3He/^4He$ ratio that equals MORB values. This suggests that the magma source of Kohala contains upper mantle material. This is supported by the radiogenic isotope signatures of Kohala samples which are in the range for typical MORB. The post-shield stage lavas from Haleakala show consistently MORB-like values in their noble gas and radiogenic isotope signatures. The isotopic signatures of the analysed samples reflect the preservation of heterogeneities within the convecting mantle that are sampled in different degrees of the Hawaiian volcanoes. The compositional change within the source of one volcano as it moves off the hotspot and samples the outer parts of the hotspot that are associated with a decreasing amount of melting can be seen in the Zr/Nb ratios of the Kohala samples. The Zr/Nb ratios are higher in the tholeiitic samples and decrease in the transitional and alkalic samples where they show the lowest values (Figure 14). This pattern is however not reflected in the $^3He/^4He$ ratios of the Kohala samples. While the highest $^3He/^4He$ ratio is measured in a tholeiitic Kohala sample, the second highest value is reached by an alkalic Kohala sample. MORB-like $^3He/^4He$ values were measured in remaining tholeiitic, transitional and alkalic Kohala samples. The post-shield lavas from Haleakala show the lowest Zr/Nb ratios from the sample suite, associated with uniformly MORB-like $^3He/^4He$ ratios. The Zr/Nb ratios of the shield-stage samples from Mauna Kea and Kilauea are in the range of the tholeiitic Kohala samples, associated with $^3He/^4He$ values higher than MORB. The change from tholeiitic to alkalic volcanism, associated with a decrease in the extent of melting, suggests that alkalic volcanism samples the cooler outer parts of the plume that are characterized by a higher amount of incorporated material with MORB-like helium and neon isotopic compositions as well as a lower Zr/Nb ratios than in the tholeiitic lavas. The amount of material carrying the primitive helium and neon signals differs in the different Hawaiian volcanoes, Kohala for example exhibits Sr-Nd-Pb isotope systematics that are MORB-like

combined with MORB-like helium and neon isotope systematics, suggesting that Kohala does not sample this material in the late stages of tholeiitic volcanism. Mauna Kea and Kilauea volcanoes do show neon isotope systematics consistent with the Loihi-Kilauea line in a neon three-isotope diagram and elevated $^{3}He/^{4}He$ ratios, both indicative of a source carrying a primitive noble gas signal. Whether this material really is primitive and could have remained (partly) isolated over time or the helium and neon isotope systematics are rather due to their behavior during magmatic processes remains to be established.

6 Conclusions

Shield stage Mauna Kea, Kohala and Kilauea lavas yielded MORB-like to moderately high $^{3}He/^{4}He$ ratios, while post-shield stage Haleakala lavas did not show $^{3}He/^{4}He$ ratios higher than typical MORB values. Mauna Kea and Kilauea data agree well with the Loihi-Kilauea line in a neon-three isotope plot, whereas the one Kohala sample, that is different from air, plots on the MORB correlation line. $^{87}Sr/^{86}Sr$, $^{143}Nd/^{144}Nd$ and $^{206}Pb/^{204}Pb$ data of Haleakala and most Kohala lavas are in the range for typical MORB. It has also been shown that the $^{4}He/^{40}Ar^{*}$ versus ^{4}He variations imply open system fractionation of He from Ar with a ^{4}He deficiency. The $^{4}He/^{40}Ar^{*}$, $^{4}He/^{21}Ne^{*}$, and $^{3}He/^{22}Ne_{S}$ systematics further corroborate a fractionation of helium from the heavier noble gases, where helium is depleted with respect to argon and neon. In a binary mixing model, the helium and neon data are best explained by a mixture of a MORB-like end-member with a plume like or primordial end-member with a fractionation in $^{3}He/^{22}Ne$, represented best by a curve parameter r of 15 ($r=(^{3}He/^{22}Ne)_{MORB}/(^{3}He/^{22}Ne)_{PLUME\ or\ PRIMORDIAL}$). The helium depletion is partly due to solubility controlled gas loss during magma ascent. However, the crystal-melt-partitioning behavior during partial melting is also crucial, indicating that He is more incompatible than Ar and Ne. The fractionation has moreover been assessed to be a “relative” recent event, since the data have not evolved back to the respective production ratios of $^{4}He/^{40}Ar^{*}$ and $^{4}He/^{21}Ne^{*}$. The large geochemical variations in the investigated samples reflect heterogeneities within the Hawaiian plume due to source heterogeneity, incorporation of upper mantle material and magmatic processes. Whether the high $^{3}He/^{4}He$ ratios in Hawaiian lavas are indicating the presence of a primitive component in the plume or are rather a product of the crystal-melt- partitioning behavior remains to be resolved.

7 References

Abouchami W., Galer S. J. G., and Hofmann A. W. (2000) High precision lead isotope systematics of lavas from the Hawaiian Scientific Drilling Project. *Chem. Geol.* 169, 187-209.

Abouchami W., Hofmann A. W., Galer S. J. G., Frey F. A., Eisele J., and Feigenson M. (2005) Lead isotopes reveal bilateral asymmetry and vertical continuity in the Hawaiian mantle plume. *Nature* 434, 851-856.

Anderson D. L. (1998a) The helium paradoxes. *Proceedings of the National Academy of Sciences of the United States of America* 95(9), 4822-4827.

Anderson D. L. (1998b) A model to explain the various paradoxes associated with mantle noble gas geochemistry. *Proceedings of the National Academy of Sciences of the United States of America* 95(16), 9087-9092.

Ballentine C. J. and Burnard P. (2002) Production, Release and Transport of Noble Gases in the Continental Crust. *In Noble Gases in Geochemistry and Cosmochemistry (eds. D. Porcelli, C.J. Ballentine and R. Wieler)* Reviews in Mineralogy and Geochemistry 47. Mineralogical Society of America, 481-529.

Begemann F., Weber H. W., and Hintenberger H. (1976) On the primordial abundance of argon-40. *The Astrophysical Journal* 203, 155-157.

Benkert J.-P., Baur H., Signer P., and Wieler R. (1993) He, Ne, and Ar From the Solar Wind and Solar Energetic Particles in Lunar Ilmenites and Pyroxenes. *Journal of Geophysical Research* 98, 13147-13162.

Black D. C. (1972) On the origins of trapped helium, neon and argon isotopic variations in meteorites--I. Gas-rich meteorites, lunar soil and breccia. *Geochimica et Cosmochimica Acta* 36(3), 347-375.

Blichert-Toft J., Albarede F., and Frey F. (1999) Hf isotopic evidence for pelagic sediments in the source of Hawaiian basalts. *Science* 285, 879-882.

Brooker R. A., Heber V. S., Kelley S. P., and Wood B. J. (2003) Noble gas partition behaviour during mantle melting: a possible explanation for the 'He paradox'? *EOS Trans. AGU, Fall meet. Suppl.* .

Burnard P., Graham D., and Turner G. (1997) Vesicle-Specific Noble Gas Analyses of "Popping Rock": Implications for Primordial Noble Gases in Earth. *Science* 276(5312), 568-571.

Carroll M. R. and Draper S. D. (1994) Noble gases as trace elements in magmatic processes. *Chemical Geology*(117), 37-56.

Chen C.-Y., Frey F., Garcia M. O., and Dalrymple G. B. (1991) The tholeiitic to alkalic basalt transition at Haleakala Volcano, Maui, Hawaii *Contributions to Mineralogy and Petrology* 106, 183-200.

Clague D. A. (1982) Petrology of tholeiitic basalt dredged from Hualalai Volcano, Hawaii. *Eos Trans. AGU* 63, 1138.

Clague D. A. (1987) Hawaiian xenolith populations, magma supply rates, and development of magma chambers. *Bulletin of Volcanology* 49, 577-587.

Clague D. A. and Dalrymple G. B. (1987) The Hawaiian-Emperor volcanic chain. Part I. Geologic Evolution. *US Geological Survey Professional Paper 1350*, 5-54.

Clague D. A. and Moore J. G. (1991) Geology and petrology of Mahukona Volcano, Hawaii. *Bulletin of Volcanology* 53(3), 159-172.

Cottrell J. S. and Greathead R. J. (1986) Extending the mass range of a sector mass spectrometer. *Mass Spectrometry Reviews* 5(3), 215-247.

Courtillot V., Dacaille A., Besse J., and Stock J. (2003) Three distinct types of hotspots in the Earth's mantle. *Earth and Planetary Science Letters* 205, 295-308.

Cousens B. L., Clague D. A., and Sharp W. A. (2003) Chronology, chemistry, and origin of trachytes from Hualalai Volcano, Hawaii. *Geochemistry Geophysics Geosystems* 4(9), doi:10.1029/2003GC000560.

DePaolo D. J., Bryce J. G., Dodson A., Shuster D. L., and Kennedy B. M. (2001) Isotopic evolution of Mauna Loa and the chemical structure of the Hawaiian plume. *Geochemistry Geophysics Geosystems* 2(7), doi:10.1029/2000GC000139.

Dickin A. P. (1997) *Radiogenic isotope geology*. Camebridge University Press.

Dixon E. T. (2003) Interpretation of helium and neon isotopic heterogeneity in Icelandic basalts. *Earth and Planetary Science Letters* 206(1-2), 83-99.

Dixon E. T., Honda M., McDougall I., Campbell I. H., and Sigurdsson I. (2000) Preservation of near-solar neon isotopic ratios in Icelandic basalts. *Earth and Planetary Science Letters* 180(3-4), 309-324.

Farley K. A. and Craig H. (1994) Atmospheric argon contamination of ocean island basalt olivine phenocrysts. *Geochimica et Cosmochimica Acta* 58(11), 2509-2517.

Farley K. A., Natland J. H., and Craig H. (1992) Binary mixing of enriched and undegassed (primitive?) mantle components (He, Sr, Nd, Pb) in Samoan lavas. *Earth and Planetary Science Letters* 111(1), 183-199.

Farley K. A. and Neroda E. (1998) Noble Gases in the Earth´s Mantle. *Annual Reviews of Earth and Planetary Sciences Letters* 26, 189-218.

Fisher D. E. (1985) Noble gases from oceanic island basalts do not require an undepleted mantle source. *Nature* 316(6030), 716-718.

Fisher D. E. (1989) Evaluation of rare gas data in relation to oceanic magmas. *Geological Society, London, Special Publications* 42(1), 301-311.

Frey F. A., Garcia M. O., and Roden M. F. (1994) Geochemical characteristics of Koolau Volcano: Implications of intershield geochemical differences among Hawaiian volcanoes. *Geochimica et Cosmochimica Acta* 58(5), 1441-1462.

Frey F. A. and Rhodes J. M. (1993) Intershield geochemical differences among Hawaiian volcanoes: Implications for source compositions, melting processes, and magma ascent paths. *Philos. Trans. R. Soc. London* 342, 121-136.

GEOROC database M. P. I., Mainz, Germany. (http://georoc.mpch-mainz.gwdg.de/georoc/).

Graham D. W. (2002) Noble Gas Isotope Geochemistry of Mid-Ocean Ridge and Ocean Island Basalts: Characterization of Mantle Source Reservoirs. *In Noble Gases in Geochemistry and Cosmochemistry (eds. D. Porcelli, C.J. Ballentine and R. Wieler)* Reviews in Mineralogy and Geochemistry 47. Mineralogical Society of America, 247-318.

Hammer J. E., Coombs M. L., Shamberger P. J., and Kimura J.-I. (2006) Submarine silver in North Kona: A window into the early magmatic and growth history of Hualalai Volcano, Hawaii. *Journal of Volcanology and Geothermal Research* 151, 157-188.

Haskins E. and Garcia M. (2004) Scientific drilling reveals geochemical heterogeneity within the Koolau shield, Hawaii. *Contributions to Mineralogy and Petrology* 147(2), 162-188.

Hauri E., Lassiter J. C., and DePaolo D. J. (1996) Osmium isotope systematics of drilled lavas from Mauna Loa, Hawaii. *J. Geophys. Res.* 101, 11793-11806.

Heber V. S., Brooker R. A., Kelley S. P., and Wood B. J. (2007) Crystal-melt partitioning of noble gases (helium, neon, argon, krypton, and xenon) for olivine and clinopyroxene. *Geochimica et Cosmochimica Acta* 71(4), 1041-1061.

Hilton D. R. and Porcelli D. (2003) Noble Gases as Mantle Tracers Treatise on Geochemistry (ed. H. D. Holland and K. K. Turekian), pp. 277-318. Pergamon.

Honda M. and McDougall I. (1998) Primordial helium and neon in the Earth - a speculation on early degassing. *Geophysical Research Letters* 25, 1951-1954.

Honda M., McDougall I., and Patterson D. (1993a) Solar noble gases in the Earth; the systematics of helium-neon isotopes in mantle derived samples. *Lithos* 30(3-4), 257-265.

Honda M., McDougall I., Patterson D. B., Doulgeris A., and Clague D. A. (1991) Possible solar noble-gas component in Hawaiian basalts. *Nature* 349(6305), 149-151.

Honda M., McDougall I., Patterson D. B., Doulgeris A., and Clague D. A. (1993b) Noble gases in submarine pillow basalt glasses from Loihi and Kilauea, Hawaii; a solar component in the Earth. *Geochimica et Cosmochimica Acta* 57(4), 859-874.

Honda M. and Patterson D. B. (1999) Systematic elemental fractionation of mantle-derived helium, neon, and argon in mid-oceanic ridge glasses. *Geochimica et Cosmochimica Acta* 63(18), 2863-2874.

Hopp J. and Trieloff M. (2008) Helium deficit in high-3He/4He parent magmas: Predegassing fractionation, not a ‘‘helium paradox’’. *Geochemistry Geophysics Geosystems* 9(3), Q03009, doi:10.1029/2007GC001833.

Huang S. and Frey A. F. (2003) Trace element abundances of Mauna Kea basalt from phase 2 of the Hawaii Scientific Drilling Project: Petrogenetic implications of correlations with major element content and isotopic ratios. *Geochemistry Geophysics Geosystems* 4(6), 8711, doi:10.1029/2002GC000322.

Jackson E. D., Silver E. A., and Dalrymple G. B. (1972) Hawaiian-Emperor chain and its relation to Cenozoic circumpacific tectonics. *Geological Society of America Bulletin* 83, 601-617.

Jackson M. G. and Dasgupta R. (2008) Compositions of HIMU, EM1, and EM2 from global trends between radiogenic isotopes and major elements in ocean island basalts. *Earth and Planetary Science Letters* 276(1-2), 175-186.

Keller G. V., Grose L. T., Murray J. C., and Skokan C. K. (1979) Results of an experimental drill hole at the summit of Kilauea Volcano, Hawaii. *Journal of Volcanology and Geothermal Research* 5, 345-385.

Kennedy B. M., Hiyagon H., and Reynolds J. H. (1990) Crustal neon: a striking uniformity. *Earth and Planetary Science Letters* 98(3-4), 277-286.

Kurz M. D., Curtice J., Lott III D. E., and Solow A. (2004) Rapid helium isotopic variability in Mauna Kea shield lavas from the Hawaiian Scientific Drilling Project. *Geochemistry Geophysics Geosystems* 5(4), Q04G14, doi:10.1029/2002GC000439.

Kurz M. D., Kenna T. C., Lassiter J. C., and DePaolo D. J. (1996) Helium isotopic evolution of Mauna Kea Volcano; first results from the 1-km drill core. *Journal of Geophysical Research, B, Solid Earth and Planets* 101(5), 11,781-11,791.

Kurz M. D., le Roex A. P., and Dick H. J. B. (1998) Isotope Geochemistry of the Oceanic Mantle Near the Bouvet Triple Junction. *Geochimica et Cosmochimica Acta* 62(5), 841-852.

Kurz M. D., Moreira M., Curtice J., Lott III D. E., Mahoney J. J., and Sinton J. M. (2005) Correlated helium, neon, and melt production on the super fast spreading East Pacific Rise near 17°S. *Earth and Planetary Science Letters* 232, 125-142.

Lal D. (1991) Cosmic ray labeling of erosion surfaces: in situ nuclide production rates and erosion models. *Earth and Planetary Science Letters* 104, 424-439.

Langenheim V. A. M. and Clague D. A. (1987) The Hawaiian-Emperor volcanic chain. Part II. Stratigraphic framework of volcanic rocks in the Hawaiian Islands. *US Geological Survey Professional Paper 1350*, 55-84.

Lanphere M. A. and Frey A. F. (1987) Geochemical evolution of Kohala Volcano, Hawaii. *Contributions to Mineralogy and Petrology* 95, 100-113.

Lassiter J. C., DePaolo D. J., and Tatsumoto M. (1996) Isotopic evolution of Mauna Kea volcano: Results from the initial phase of the Hawaiian Scientific Drilling Project. *Journal of Geophysical Research* 101, 11769-11780.

Lassiter J. C. and Hauri E. H. (1998) Osmium-isotope variations in Hawaiian lavas. Evidence for recycled oceanic lithosphere in the Hawaiian plume. *Earth and Planetary Science Letters* 164, 83-96.

Le Bas M. J., Le Maitre R. W., Streckeisen A., and Zanettin B. A. (1986) Chemical classification of volcanic rocks based in the total alkali-silica diagram. *Journal of Petrology* 27, 745-750.

Lux G. (1987) The behavior of noble gases in silicate liquids: Solution, diffusion, bubbles and surface effects, with applications to natural samples. *Geochimica et Cosmochimica Acta* 51(6), 1549-1560.

Macdonald G. A., Abbott A. T., and Peterson F. L. (1983) *Volcanoes in the Sea, 2nd ed.* University of Hawaii Press.

Macdonald G. A. and Katsura T. (1964) Chemical composition of Hawaiian lavas. *Journal of Petrology* 5, 82-133.

McBirney A. R. (1993) *Igneous Petrology*. Jones and Barlett Publishers.

McDonough W. F. and Sun S.-S. (1995) The composition of the Earth. *Chem. Geol.* 120, 223-254.

Montelli R., Nolet G., Dahlen F. A., Masters G., Engdahl E. R., and Hung S. H. (2004) Finite-frequency tomography reveals a variety of plumes in the mantle. *Science* 303(5656), 338-43.

Moore J. G. and Clague D. A. (1992) Volcano growth and evolution of the island of Hawaii. *Geological Society of America Bulletin* 104(11), 1471-1484.

Morgan W. J. (1971) Convection Plumes in the Lower Mantle. *Nature* 230(5288), 42-43.

Niedermann S., Bach W., and Erzinger J. (1997) Noble gas evidence for a lower mantle component in MORBs from the southern East Pacific Rise: Decoupling of helium and neon isotope systematics. *Geochimica et Cosmochimica Acta* 61, 2697-2715.

Ozima M. and Igarashi G. (2000) The primordial noble gases in the Earth; a key constraint on Earth evolution models. *Earth and Planetary Science Letters* 176(2), 219-232.

Ozima M. and Podosek F. A. (1999) Formation age of Earth from 129I/127I and 244Pu/238U systematics and the missing Xe. *Journal of Geophysical Research* 104, 25493-25499.

Ozima M. and Podosek F. A. (2002) Noble Gas Geochemistry- 2nd ed. *Cambridge University Press*.

Ozima M., Wieler R., Marty B., and Podosek F. A. (1998) Comparative Studies of Solar, Q-Gases and Terrestrial Noble Gases, and Implications on the Evolution of the Solar Nebula. *Geochimica et Cosmochimica Acta* 62(2), 301-314.

Parman S. W., Kurz M. D., Hart S. R., and Grove T. L. (2005) Helium solubility in olivine and implications for high 3He/4He in ocean island basalts. *Nature* 437, 1140-1143.

Patzer A. and Schultz L. (2002) Noble gases in enstatite chondrites II: The trapped component. *Meteoritics and Planetary Science* 37, 601-612.

Pepin R. O. (1991) On the origin and early evolution of terrestrial planet atmospheres and meteoritic volatiles. *Icarus* 92(1), 2-79.

Ren Z.-Y., Takahashi E., Orihashi Y., and Johnson K. T. M. (2004) Petrogenesis of Tholeiitic Lavas from the Submarine Hana Ridge, Haleakala Volcano, Hawaii 10.1093/petrology/egh076. *J. Petrology* 45(10), 2067-2099.

Rhodes M. J. (1996) Geochemical stratigraphy of lava flows sampled by the Hawaii Scientific Drilling Project. *Journal of Geophysical Research* 101, 11729-11746.

Rhodes M. J. and Vollinger a. M. J. (2004) Composition of basaltic lavas sampled by phase-2 of the Hawaii Scientific Drilling Project: Geochemical stratigraphy and magma types. *Geochemistry Geophysics Geosystems* 5(3), Q03G13, doi:10.1029/2002GC000434.

Romer R. L., Heinrich W., Schröder-Smeibidl B., Meixner A., Fischer C. O., and Schulz C. (2005) Elemental dispersion and stable isotope fractionation during reactive fluid-flow and fluid immiscibility in the Bufa del Diente aureole, NE-Mexico: evidence from radiographies and Li, B, Sr, Nd, and Pb isotope systematics. *Contributions to Mineralogy and Petrology* 149, 400-429.

Sharp W. A. and Renne P. R. (2005) 40Ar/39Ar dating of core recovered by the Hawaii Scientific Drilling Project (phase 2), Hilo, Hawaii. *Geochemistry Geophysics Geosystems*.

Shaw A. M., Hilton D. R., Macpherson C. G., and Sinton J. M. (2001) Nucleogenic neon in high 3He/4He lavas from the Manus back-arc basin: a new perspective on He-Ne decoupling. *Earth and Planetary Science Letters* 194(1-2), 53-66.

Sherrod D. R., Nishimitsu Y., and Tagami T. (2003) New K-Ar ages and the geologic evidence against rejuvenated-stage volcanism of the Hawaiian island chain *Geological Society of America Bulletin* 115, 683-694.

Sherrod D. R., Sinton J. M., Watkins S. E., and Brunt K. M. (2007) Geologic Map of the State of Hawaii. *U.S. Geological Survey Open-File Report 2007-1089, 83p., 8 plates, scales 1:100,000 and 1:250,000, with GIS database*

Sleep N. H. (1990) Hotspots and Mantle Plumes: Some Phenomenology. *Journal of Geophysical Research* 95, 6715-6736.

Sobolev A. V., Hofmann A. W., and Nikogosian I. K. (2000) Recycled oceanic crust observed in "ghost plagioclase" within the source of Mauna Loa lavas. *Nature* 404, 986-990.

Sobolev A. V., Hofmann A. W., Sobolev S. V., and Nikogosian I. K. (2005) An olivine-free mantle source of Hawaiian shield basalts. *Nature* 434, 590-597.

Staudacher T. and Allègre C. J. (1982) Terrestrial xenology. *Earth and Planetary Science Letters* 60(3), 389-406.

Staudacher T. and Allègre C. J. (1989) Noble gases in glass samples from Tahiti: Teahitia, Rocard and Mehetia. *Earth and Planetary Science Letters* 93(2), 210-222.

Stracke S., Hofmann A., and Hart S. (2005) FOZO, HIMU, and the rest of the mantle zoo. *Geochemistry Geophysics Geosystems* 6 (5), Q05007, doi:10.1029/2004GC000824.

Stroncik N. A., Niedermann S., and Haase K. M. (2008) Plume-ridge interaction revisited: Evidence for melt mixing from He, Ne and Ar isotope and abundance systematics. *Earth and Planetary Science Letters* 268(3-4), 424-432.

Tatsumoto M. (1978) Isotopic composition of lead in oceanic basalt and its implication to mantle evolution. *Earth and Planetary Science Letters* 38, 63-87.

Trieloff M., Kunz J., Clague D. A., Harrison D., and Allègre C. J. (2000) The Nature of Pristine Noble Gases in Mantle Plumes. *Science* 288, 1036-1038.

USGS. (1998) Evolution of Hawaiian Volcanoes. Retrieved on 2008-10-11. http://hvo.wr.usgs.gov/volcanowatch/1995/95_09_08.html.

van Keken P. E., Hauri E. H., and Ballentine C. J. (2002) Mantle mixing: the generation, preservation, and destruction of chemical heterogeneity. *Annual Reviews of Earth and Planetary Sciences Letters* 30, 493-525.

Verchovsky A. B., Sephton M. A., Wright I. P., and Pillinger C. T. (2002) Separation of planetary noble gas carrier from bulk carbon in enstatite chondrites during stepped combustion. *Earth and Planetary Science Letters* 199(3-4), 243-255.

Wang Z. and Gaetani G. A. (2008) Partitioning of Ni between olivine and siliceous eclogite partial melt: experimental constraints on the mantle source of Hawaiian basalts. *Contributions to Mineralogy and Petrology* 156, 661-678.

West H. B. and Leeman W. P. (1987) Isotopic evolution of lavas from Haleakala Crater, Hawaii. *Earth and Planetary Science Letters* 84, 211-225.

West H. B. and Leeman W. P. (1994) The open-system geochemical evolution of alkalic cap lavas from Haleakala Crater, Hawaii, USA. *Geochimica et Cosmochimica Acta* 58(2), 773-796.

White W. M. (2005) Geochemistry. *On-Line Textbook* 2005.

Wieler R. (2002) Cosmic-Ray-Produced Noble Gases in Meteorites. *In Noble Gases in Geochemistry and Cosmochemistry (eds. D. Porcelli, C.J. Ballentine and R. Wieler)* Reviews in Mineralogy and Geochemistry 47. Mineralogical Society of America, 125-163.

Wiersberg T. (2002) Edelgase als Tracer für Wechselwirkungen von Krusten- und Mantelfluiden mit diamantführenden Gesteinen des östlichen Baltischen Schildes. Dissertation,GFZ Potsdam, Scientific Technical Report, 02/11.

Wilson J. T. (1963) A possible origin of the Hawaiian Isands. *Canadian Journal of Physics* 41, 863-870.

Wolfe E. W. and Morris J. (1996) Geologic Map of the Island of Hawaii. *U.S. Geological Survey Miscellaneous Investigations Series I-2524-A, scale 1:100,000*.

Wright T. L. and Fiske R. S. (1971) Origin of the Differentiated and Hybrid Lavas of Kilauea Volcano, Hawaii 10.1093/petrology/12.1.1. *J. Petrology* 12(1), 1-65.

Yatsevich I. and Honda M. (1997) Production of nucleogenic neon in the Earth from natural radioactive decay. *Journal of Geophysical Research* 102, 10291-10298.

8 Appendix

Appendix A1: Results of the noble gas analyses of olivine separates from Mauna Kea HSDP drill core samples, one Mauna Kea surface sample, one Kilauea surface sample, Kilauea NSF well drill core samples, Hualalai and Mauna Loa surface samples, and Kohala and Haleakala surface samples.

Appendix A2: Major element composition of lavas from Mauna Kea, Kilauea, and surface samples of Kohala and Haleakala.

Appendix A3: Major element composition and Fo content of olivines from Mauna Kea HSDP samples, Kilauea NSF well samples, and surface samples of Kohala and Haleakala.

Appendix A4: REE composition of lavas from Mauna Kea, Kilauea, and surface samples of Kohala and Haleakala.

Appendix

Table A1: Results of the noble gas analyses of olivine separates from Mauna Kea HSDP drill core samples, one Mauna Kea surface sample, one Kilauea surface sample, Kilauea NSF well drill core samples, Hualalai and Mauna Loa surface samples, and Kohala and Haleakala surface samples.

Sample	T. °C	^{4}He	^{20}Ne	^{40}Ar	^{84}Kr	^{132}Xe	^{3}He/^{4}He.	^{20}Ne/^{22}Ne	^{21}Ne/^{22}Ne	^{40}Ar/^{36}Ar	^{38}Ar/^{36}Ar
		10^{-8} cm^3/g	*10^{-12} cm^3/g*	*10^{-8}cm^3/g*	*10^{-12} cm^3 STP/g*	*10^{-12} cm^3 STP/g*	*$10^{-6.}$*				
SR0517-8.5 Olivine	1000	0.0496	114.8	8.53	32.1	18.21	11.3	9.817	0.0292	300.0	0.1877
(HSDP. Mauna Kea)		±0,0078	±6.0	±0.43	±1.6	±0.92	±3.8	±0.073	±0.0015	±2.2	±0.0011
0.49045 g	1400	0.0987	2.12	0.548	0.933	1.361	15.6	9.5	0.0284	307.5	0.1857
Depth 1296 m		±0.0055	±0.39	±0.031	±0.093	±0.081	±3,6	±1,0	±0,0052	±4,7	±0,0036
	1750	1.015	9.92	9.25	1.352	2.21	14.9	9.96	0.0310	355.7	0.1880
		±0.051	±0.72	±0.54	±0.093	±0.12	±1,1	±0,24	±0,0025	±3,3	±0,0013
	Total	1.163	126.8	18.33	34.4	21.78	14.8	9.823	0.0293	326.0	0.1878
		±0.052	±6.1	±0.69	±1.6	±0.93	±1.0	±0.071	±0.0014	±2,2	±0.0008
SR0626-5.7 Olivine	<1000	0.0188	79.6	2.27	9.18	8.49	11.6	9.946	0.029	296.2	0.187
(HSDP. Mauna Kea)		±0.0028	±4.2	±0.12	±0.48	±0.44	±5.5	±0.065	±0.0013	±2.4	±0.0014
1.00983 g	<1400	0.0139	20.8	1.073	1.064	0.165	13	9.83	0.0291	303.5	0.1882
Depth 1593 m		±0.0013	±1.1	±0.056	±0.064	±0.014	±5.2	±0.13	±0.0031	±2.6	±0.0019
	<1750	0.0224	6.03	0.11	0.608	0.647	14	9.74	0.0277	460	0.186
		±0.0016	±0.41	±0.10	±0.045	±0.040	±4.0	±0.48	±0.0036	$^{+\infty}_{-110}$	±0.026
	1000	0.0111	13.7	1.207	1.005	0.28	14.3	9.72	0.0281	294.4	0.1871
		±0.0015	±1.3	±0.062	±0.085	$^{+0.30}_{-0.28}$	±6.6	±0.42	±0.0037	±5.2	±0.0014
	1400	0.199	1.5	0.302	0.357	1.15	15.4	11.1	0.03	330.3	0.1871
		±0.010	±1.0	±0.019	±0.058	±0.43	±1.6	±1.4	±0.018	±6.5	±0.0028
	1750	0.898	13.7	1.722	0.627	<0.41	14.7	9.88	0.0304	1099	0.1865
		±0.046	±1.4	±0.091	±0.067		±1.4	±0.17	±0.0032	±41	±0.0030
		1.163	135.3	6.68	12.84	10.73	14.7	9.9	0.029	370.9	0.1872
		±0.047	±4.9	±0.20	±0.50	$^{+0.80}_{-0.68}$	±1.1	±0.069	±0.0011	$^{+6.8}_{-5.8}$	±0.0009

Table A1: continued

Sample	T. °C	^{4}He	^{20}Ne	^{40}Ar	^{84}Kr	^{132}Xe	$^{3}He/^{4}He.$	$^{20}Ne/^{22}Ne$	$^{21}Ne/^{22}Ne$	$^{40}Ar/^{36}Ar$	$^{38}Ar/^{36}Ar$
		10^{-8} cm^3/g	10^{-12} cm^3/g	$10^{-8}cm^3/g$	10^{-12} cm^3 STP/g	10^{-12} cm^3 STP/g	$10^{-6.}$				
SR0720-17.0 Olivine	1000	0.0385	282	4.41	34.2	23.4	10.6	9.912	0.02883	298.7	0.1879
(HSDP. Mauna Kea)		±0.0029	±15	±0.22	±1.8	±1.2	±4.7	±0.048	±0.00066	±2.3	±0.0012
0.58722 g	1400	0.11	3.93	0.207	1.041	4.21	15.7	9.7	0.0285	319.3	0.1843
Depth 1919 m		±0.0063	±0.37	±0.014	±0.083	±0.27	±1.7	±0.30	±0.0053	±6.9	±0.0056
	1750	1.461	11.05	8.46	1.89	5.91	14.8	10.37	0.0369	412.8	0.18726
		±0.073	±0.72	±0.49	±0.12	±0.30	±1.1	±0.14	±0.0039	±4.9	±0.00097
	Total	1.61	297	13.08	37.1	33.5	14.8	9.925	0.02911	364.2	0.18747
		±0.073	±15	±0.54	±1.8	±1.3	±1.0	±0.046	±0.00065	±3.6	±0.00075
SR0760-12.8 Olivine	1000	0.1505	111.1	2.49	8.82	5.4	22.8	9.901	0.0292	365.8	0.1885
(HSDP. Mauna Kea)		±0.0077	±5.8	±0.13	±0.46	±0.43	±2.8	±0.063	±0.0014	±6.1	±0.0012
1.06638 g	1400	1.327	6.59	3.37	0.693	2.31	26.1	11.3	0.0328	2286	0.188
Depth 2115 m		±0.066	±0.65	±0.17	±0.065	±0.42	±1.0	±0.42	±0.0022	±58	±0.0025
	1750	3.77	21.7	7.6	0.5	<0.20	25.39	10.95	0.0351	3790	0.1874
		±0.19	±1.6	±0.39	±0.11		±0.56	±0.30	±0.0023	±180	±0.0041
	Total	5.25	139.4	13.46	10.01	7.71	25.5	10.111	0.0302	1309	0.1882
		±0.20	±6.1	±0.44	±0.48	$^{+0.63}_{-0.60}$	±0.48	±0.071	±0.0012	±55	±0.0012

Table A1: continued

Sample	T. °C	^{4}He	^{20}Ne	^{40}Ar	^{84}Kr	^{132}Xe	$^{3}He/^{4}He.$	$^{20}Ne/^{22}Ne$	$^{21}Ne/^{22}Ne$	$^{40}Ar/^{36}Ar$	$^{38}Ar/^{36}Ar$
		10^{-8} cm^3/g	10^{-12} cm^3/g	$10^{-8}cm^3/g$	10^{-12} cm^3 STP/g	10^{-12} cm^3 STP/g	$10^{-6.}$				
SR0952-1.9 Olivine	1000	0.0641	142.5	4.8	12.74	11.63	10.6	9.971	0.02880	301.1	0.18816
(HSDP. Mauna Kea)		±0.0033	±7.3	±0.24	±0.66	±0.59	±3.4	±0.068	±0.00064	±2.2	±0.00095
0.77380 g	1400	0.0462	6.9	0.946	0.733	0.774	17.1	9.770	0.0290	320.8	0.1855
Depth 3002 m		±0.0026	±0.49	±0.051	±0.073	±0.060	±2.2	±0,42	±0.0042	±6.3	±0.0072
	~1600	0.409	1.92	0.202	0.25	2.08	16.3	11.11	0.031	1190	0.184
		±0.021	±0.68	±0.068	±0.019	±0.13	±1.1	±0.94	±0.010	$^{+\infty}_{-540}$	±0.013
	~1650	0.1395	<0.78	0.54	0.029	<0.0062	16.3	>9.4	<0.038	610	0.1903
		±0.0072		±0.10	$^{+0.039}_{-0.029}$		±2,1			±110	±0.0039
	~1700	0.1910	0.31	0.69	0.171	0.026	16.9	14	0.06	1080	0.1881
		±0.0098	$^{+0.92-0.31}$	±0,14	±0.041	±0.012	±1,5	$^{+16}_{-14}$	$^{+0.12-0.06}$	±550	±0.0057
	~1750	0.0142	1.20	1.13	0.369	0.067	13.7	10.2	0.026	326.2	0.1877
		±0.0017	±0.93	±0.27	±0.058	±0.014	±7.4	±1.4	±0.013	±8.7	±0.0016
	Total	0.864	152.9	8.31	14.29	14.58	16.0	9.982	0.02886	345	0.1878
		±0.025	±7.5	±0.41	±0.67	±0.61	±0.8	±0.074	±0.00068	±17	±0.0011
	1750	1.529	3.95	1.763	0.5	0.113	16.9	10.47	0.0316	1286	0.1872
		±0.077	±0.40	±0.093	±0.040	±0.026	±0.85	±0.56	±0.0060	±53	±0.0025
	Total	2.507	426	6.96	11.29	2.54	17.34	9.769	0.02896	398.3	0.1884
		±0.088	±23	±0.24	±0.49	±0.12	±0.63	±0.054	±0.00082	±7.4	±0.0011

Table A1: continued

Sample	T. °C	^{4}He 10^{-8} cm^3/g	^{20}Ne 10^{-12} cm^3/g	^{40}Ar $10^{-8}cm^3/g$	^{84}Kr 10^{-12} cm^3 STP/g	^{132}Xe 10^{-12} cm^3 STP/g	$^{3}He/^{4}He.$ $10^{-6.}$	$^{20}Ne/^{22}Ne$	$^{21}Ne/^{22}Ne$	$^{40}Ar/^{36}Ar$	$^{38}Ar/^{36}Ar$
SR 979-1.9 Olivine	1000	0.1234	410	4.06	9.44	2	10.8	9.764	0.02892	306.2	0.189
(HSDP. Mauna Kea)		±0.0062	±23	±0.21	±0.48	±0.11	±1.7	±0.055	±0.00084	±4.1	±0.0013
1.05530 g	1400	0.855	11.94	1.133	1.345	0.422	19.06	9.71	0.0295	399.7	0.1864
		±0.043	±0.74	±0.062	±0.073	±0.032	±0.99	±0.31	±0.0049	±7.7	±0.0027
	1750	1.529	3.95	1.763	0.5	0.113	16.9	10.47	0.0316	1286	0.1872
		±0.077	±0.40	±0.093	±0.040	±0.026	±0.85	±0.56	±0.0060	±53	±0.0025
	Total	2.507	426	6.96	11.29	2.54	17.34	9.769	0.02896	398.3	0.1884
		±0.088	±23	±0.24	±0.49	±0.12	±0.63	±0.054	±0.00082	±7.4	±0.0011
SR 008 Olivine	1000	0.1225	387	99.2	242	19.6	6.4	9.831	0.02855	296.9	0.1881
(HSDP. Mauna Kea)		±0.0063	±20	±6.8	±12	±1.7	±1.7	±0.083	±0.00058	±1.7	±0.0011
0.77174 g	1400	2.13	34.7	1.324	8.04	3.82	16.56	9.8	0.0297	1012	0.188
Depth 3117 m		±0.11	±2.0	±0.087	±0.90	±0.22	±0.74	±0.28	±0.0016	±59	±0.0043
	1750	2.11	14.9	1.56	1.29	0.37	16.28	9.95	0.029	728	0.1876
		±0.11	±1.1	±0.11	±0.27	±0.11	±0.69	±0.38	±0.0055	±39	±0.0035
	Total	4.36	437	102.1	251	23.8	16.14	9.833	0.02866	302.4	0.1881
		±0.16	±20	±6.8	±12	±1.7	±0.49	±0.078	±0.00056	±1.8	±0.0011
SR 021 Olivine	1000	0.1061	339	89.6	175.2	14.7	8.4	9.788	0.02874	295.1	0.1879
(HSDP. Mauna Kea)		±0.0056	±20	±6.1	±9.0	±2.4	±2.5	±0.053	±0.00069	±3.0	±0.0011
0.44877 g	1400	0.495	14.9	0.892	7.75	2.93	16.2	9.93	0.0295	324.4	0.1878
Depth 3139 m		±0.025	±1.1	±0.066	±0.43	±0.20	±1.9	±0.36	±0.0047	±6.8	±0.0028
	1750	1.024	16.1	4.3	1.67	0.43	15.5	9.89	0.0293	355.3	0.187
		±0.053	±1.3	±0.24	±0.12	±0.10	±1.4	±0.28	±0.0034	±6.2	±0.0014
	Total	1.625	370	94.8	184.6	18.1	15.2	9.798	0.02879	297.6	0.1879
		±0.059	±20	±6.1	±9.0	±2.4	±1.1	±0.052	±0.00068	±2.9	±0.0011

Table A1: continued

Sample	T. °C	^{4}He 10^{-8} cm^3/g	^{20}Ne 10^{-12} cm^3/g	^{40}Ar $10^{-8}cm^3/g$	^{84}Kr 10^{-12} cm^3 STP/g	^{132}Xe 10^{-12} cm^3 STP/g	$^{3}He/^{4}He.$ $10^{-6.}$	$^{20}Ne/^{22}Ne$	$^{21}Ne/^{22}Ne$	$^{40}Ar/^{36}Ar$	$^{38}Ar/^{36}Ar$
SR 050 Olivine	1000	0.0933	273	98	230	22.3	4.8	9.815	0.0289	295.8	0.1882
(HSDP. Mauna Kea)		±0.0048	±14	±6.6	±12	±1.8	±1.4	±0.071	±0.0012	±1.9	±0.0011
0.77987 g	1400	0.617	34.8	0.484	6.89	4.6	17.5	9.72	0.0283	413	0.1873
Depth 3171 m		±0.031	±2.0	±0.038	±0.37	±0.36	±1.0	±0.16	±0.0018	±13	±0.0028
	1750	1.896	16.5	1.66	2.07	0.94	16.39	9.81	0.0301	719	0.1871
		±0.096	±1.3	±0.13	±0.32	±0.18	±0.87	±0.31	±0.0036	±44	±0.0034
	Total	2.61	324	100.1	239	27.8	16.24	9.804	0.0289	299.1	0.1882
		±0.10	±14	±6.6	±12	±1.8	±0.68	±0.064	±0.0010	±1.9	±0.0011
SR 060 Olivine	1000	0.1329	148.2	161	372	30.7	5.2	9.79	0.0285	295.8	0.18807
(HSDP. Mauna Kea)		±0.0068	±7.7	±11	±19	±2.0	±2.0	±0.14	±0.0022	±1.8	±0.00088
0.87572 g	1400	0.36	82.1	0.66	14.35	8.15	16.9	9.75	0.0289	336	0.1892
Depth 3192 m		±0.018	±4.3	±0.10	±0.83	±0.52	±1.8	±0.14	±0.0012	±17	±0.0027
	1750	1.579	10.78	1.48	1.99	0.74	16.66	9.77	0.0306	583	0.1869
		±0.080	±0.98	±0.11	±0.42	±0.21	±0.64	±0.41	±0.0028	±21	±0.0028
	Total	2.072	241.1	163	167.2	39.6	15.97	9.78	0.0287	297.3	0.18807
		±0.082	±8.9	±11	±7.6	±2.1	±0.60	±0.10	±0.0014	±1.8	±0.00087
SR 125 Olivine	1000	0.0865	302	61.5	121.3	7.8	5.4	9.854	0.02913	294.3	0.1883
(HSDP. Mauna Kea)		±0.0045	±16	±4.2	±6.3	±2.0	±2.1	±0.069	±0.00027	±3.4	±0.0013
0.52943 g	1400	0.266	24	0.439	5.79	2.3	15.2	9.66	0.029	454	0.1882
Depth 3317 m		±0.013	±1.5	±0.046	±0.35	±0.17	±2.2	±0.23	±0.0032	±23	±0.0033
	1750	0.92	7.5	1.06	0.58	0.14	15.83	9.86	0.0292	960	0.1869
		±0.048	±1.3	±0.10	±0.10	$^{+0.42}_{-0.14}$	±0.77	±0.61	±0.0072	±160	±0.0043
	Total	1.273	334	63	127.7	10.2	14.99	9.84	0.02912	298.5	0.1883
		±0.050	±16	±4.2	±6.3	±2.0	±0.74	±0.066	±0.00038	±3.5	±0.0013

Table A1: continued

Sample	T. °C	^{4}He 10^{-8} cm^3/g	^{20}Ne 10^{-12} cm^3/g	^{40}Ar $10^{-8}cm^3/g$	^{84}Kr 10^{-12} cm^3 STP/g	^{132}Xe 10^{-12} cm^3 STP/g	$^{3}He/^{4}He.$ $10^{-6.}$	$^{20}Ne/^{22}Ne$	$^{21}Ne/^{22}Ne$	$^{40}Ar/^{36}Ar$	$^{38}Ar/^{36}Ar$
SR 129 Olivine	1000	0.078	182.1	21.7	43.8	7.1	7.2	9.799	0.0286	297.1	0.18794
(HSDP. Mauna Kea)		±0.0040	±9.4	±1.1	±2.4	±1.1	±1.6	±0.089	±0.0012	±1.4	±0.00087
1.00126 g	1400	0.583	28.1	0.492	2.76	1.358	18.22	9.82	0.0289	483	0.1873
Depth 3324 m		±0.029	±1.5	±0.033	±0.18	±0.093	±0.98	±0.21	±0.0031	±15	±0.0044
	1750	0.735	23.7	2.04	1.05	0.335	17.2	10.16	0.0296	935	0.1871
		±0.038	±1.4	±0.12	±0.12	±0.057	±1.2	±0.26	±0.0029	±43	±0.0023
	Total	1.396	233.9	24.2	47.6	8.8	17.07	9.837	0.0287	317.8	0.18791
		±0.048	±9.6	±1.1	±2.4	±1.1	±0.76	±0.078	±0.0010	±2.3	±0.00084
MKEA 3 Olivine	1000	0.0275	5.19	0.29	0.764	0.341	7.4	10.2	0.0282	307.9	0.188
(Mauna Kea)		±0.0015	±0.45	±0.043	±0.044	±0.025	±4.8	±0.42	±0.0047	±6.0	±0.0045
1.03580 g	1750	0.301	22.7	1.327	1.382	0.356	10.7	9.92	0.0298	435.4	0.1874
		±0.016	±1.4	±0.092	±0.072	±0.024	±1.5	±0.097	±0.0024	±9.8	±0.0027
	Total	0.329	27.9	1.62	2.146	0.697	10.4	9.97	0.0295	405.3	0.1875
		±0.016	±1.5	±0.10	±0.084	±0.035	±1.4	±0.11	±0.0021	±8.5	±0.0023
KIL 1 Olivine	1000	0.1311	86.6	0.408	0.688	0.341	16.2	9.891	0.029	543	0.187
(Kilauea)		±0.0066	±4.5	±0.047	±0.039	±0.021	±2.8	±0.081	±0.0012	±46	±0.0033
1.00494 g	1750	1.231	9.3	2.44	1.537	0.479	17.96	10.2	0.0304	880	0.1878
		±0.062	±0.80	±0.14	±0.080	±0.030	±0.89	±0.42	±0.0049	±38	±0.0025
	Total	1.362	95.9	2.85	2.225	0.82	17.79	9.92	0.0291	808	0.1876
		±0.062	±4.6	±0.15	±0.089	±0.037	±0.85	±0.083	±0.0012	±32	±0.0021

Table A1: continued

Sample	T. °C	^{4}He 10^{-8} cm^3/g	^{20}Ne 10^{-12} cm^3/g	^{40}Ar $10^{-8}cm^3/g$	^{84}Kr 10^{-12} cm^3 STP/g	^{132}Xe 10^{-12} cm^3 STP/g	$^{3}He/^{4}He.$ $10^{-6.}$	$^{20}Ne/^{22}Ne$	$^{21}Ne/^{22}Ne$	$^{40}Ar/^{36}Ar$	$^{38}Ar/^{36}Ar$
CR1-4A Olivine	1000	0.0926	43.3	1.012	1.45	0.398	1.45	9.93	0.0294	319.4	0.1872
(NSF well. Kilauea)		±0.0052	±2.6	±0.071	±0.10	±0.034	±0.53	±0.13	±0.0023	±6.1	±0.0023
0.94492 g	1750	1.87	12.99	2.97	2.01	0.448	18.59	10.29	0.0317	710	0.1875
Depth 10.7-14.0 m		±0.10	±0.87	±0.15	±0.12	±0.036	±0.62	±0.40	±0.0040	±13	±0.0017
	Total	1.96	56.3	3.98	3.46	0.846	17.78	10.01	0.0299	542	0.1874
		±0.10	±2.7	±0.17	±0.16	±0.050	±0.59	±0.14	±0.0020	±11	±0.0014
CR2-2A Olivine	1000	0.0124	26.2	1.046	1.92	0.447	13.6	9.87	0.0296	321.4	0.1883
(NSF well Kilauea)		±0.0025	±1.7	±0.076	±0.13	±0.037	±8.0	±0.18	±0.0025	±6.4	±0.0016
0.83544 g	1750*	0.597	7.26	0.938	1.042	0.213	18.7	9.88	0.0283	375.1	0.1875
Depth 26.2-32.2 m		±0.031	±0.69	±0.056	±0.087	±0.030	±1.3	±0.31	±0.0045	±7.6	±0.0020
	Total*	0.609	33.5	1.984	2.96	0.66	18.6	9.87	0.0293	344.7	0.188
		±0.031	±1.8	±0.094	±0.16	±0.048	±1.3	±0.16	±0.0022	±5.1	±0.0013
CR11-5A Olivine	1000	0.0222	57.3	1.507	1.59	0.305	15.6	9.81	0.0293	306.4	0.1873
(NSF well Kilauea)		±0.0013	±3.3	±0.091	±0.10	±0.029	±4.4	±0.14	±0.0012	±5.5	±0.0017
1.00238 g	1750	0.681	29.6	2.02	2.75	1.07	23.7	9.9	0.0299	383.8	0.188
Depth 154.9-157.4 m		±0.034	±1.9	±0.16	±0.15	±0.23	±1.0	±0.21	±0.0023	±8.4	±0.0025
	Total	0.703	86.9	3.53	4.34	1.38	23.4	9.84	0.0295	346.4	0.1877
		±0.034	±3.8	±0.18	±0.18	±0.23	±1.0	±0.12	±0.0011	±5.4	±0.0015
CR11-5B Olivine	1000	0.00478	59.8	1.048	0.879	0.127	24	9.94	0.0293	305	0.1871
(NSF well Kilauea)		±0.00068	±3.5	±0.069	±0.053	±0.024	±17	±0.17	±0.0019	±5.8	±0.0024
1.06464 g	1750	0.938	26.4	2.11	1.516	0.228	24	10	0.0291	469.4	0.1875
Depth 154.9-157.4 m		±0.047	±1.6	±0.11	±0.084	±0.027	±1.0	±0.16	±0.0020	±8.4	±0.0019
	Total	0.943	86.2	3.16	2.395	0.355	24	9.96	0.0292	398.2	0.1873
		±0.047	±3.8	±0.13	±0.099	±0.036	±1.0	±0.13	±0.0015	±6.4	±0.0015

Table A1: continued

Sample	T. °C	^{4}He	^{20}Ne	^{40}Ar	^{84}Kr	^{132}Xe	$^{3}He/^{4}He.$	$^{20}Ne/^{22}Ne$	$^{21}Ne/^{22}Ne$	$^{40}Ar/^{36}Ar$	$^{38}Ar/^{36}Ar$
		10^{-8} cm^3/g	*10^{-12} cm^3/g*	*$10^{-8}cm^3/g$*	*10^{-12} cm^3 STP/g*	*10^{-12} cm^3 STP/g*	*$10^{-6.}$*				
CR14-15D Olivine	1000	0.0918	36.7	2.21	3.02	0.477	20.3	9.87	0.029	328	0.1882
(NSF well Kilauea)		±0.0047	±2.2	±0.12	±0.17	±0.035	±3.6	±0.18	±0.0033	±5.7	±0.0015
0.99468 g	1750	0.528	18.9	3.48	2.26	0.69	20.6	9.87	0.0298	413.2	0.1879
Depth 324.2-327.3m		±0.027	±1.3	±0.21	±0.21	±0.16	±1.3	±0.22	±0.0030	±6.5	±0.0013
	Total	0.62	55.6	5.69	5.28	1.17	20.6	9.87	0.0293	375.3	0.188
		±0.027	±2.6	±0.24	±0.27	±0.16	±1.2	±0.14	±0.0024	±4.7	±0.0010
HUA 1B Olivine	600	0.00148	10.5	0.092	0.554	0.288	35	9.83	0.0281	306.7	0.1873
(Hualalai)		±0.00099	±0.64	±0.019	±0.035	±0.020	±15	±0.37	±0.0037	±6.6	±0.0088
1.13250 g	900	0.00537	54.9	0.13	0.411	0.224	14.3	9.908	0.02922	328	0.1884
		±0.00058	±2.9	±0.037	±0.025	±0.013	±8.6	±0.090	±0.00094	±13	±0.0098
	1750	0.183	14.19	1.66	2.01	0.694	11.3	9.78	0.0292	494	0.1875
		±0.011	±0.97	±0.12	±0.10	±0.037	±1.3	±0.28	±0.0046	±16	±0.0024
	Total	0.19	79.6	1.88	2.98	1.206	11.6	9.875	0.0291	464	0.1876
		±0.011	±3.1	±0.13	±0.11	±0.044	±1.3	±0.094	±0.0012	±14	±0.0023
MLO4	1000	0.241	58	0.465	0.554	0.103	12.5	9.89	0.0295	543	0.1864
(Mauna Loa)		±0.012	±3.4	±0.049	±0.038	±0.023	±1.5	±0.14	±0.0015	±41	±0.0032
1.01524 g	1750	3.81	7.43	6.33	1.212	0.229	11.72	11.14	0.0365	2184	0.1881
		±0.19	±0.59	±0.32	±0.071	±0.033	±0.39	±0.49	±0.0062	±59	±0.0019
	Total	4.05	65.4	6.8	1.766	0.332	11.77	10.02	0.0302	1810	0.1877
		±0.19	±3.5	±0.32	±0.081	±0.040	±0.38	±0.14	±0.0015	±57	±0.0016

Table A1: continued

Sample	T. °C	^{4}He 10^{-8} cm^3/g	^{20}Ne 10^{-12} cm^3/g	^{40}Ar $10^{-8}cm^3/g$	^{84}Kr 10^{-12} cm^3 STP/g	^{132}Xe 10^{-12} cm^3 STP/g	$^{3}He/^{4}He.$ $10^{-6.}$	$^{20}Ne/^{22}Ne$	$^{21}Ne/^{22}Ne$	$^{40}Ar/^{36}Ar$	$^{38}Ar/^{36}Ar$
0610KO15 Olivine	1000	0.0208	29	1.341	1.38	0.217	25	9.85	0.0287	292.4	0.187
(Kohala)		±0.0014	±1.7	±0.082	±0.10	±0.036	±11	±0.19	±0.0011	±5.2	±0.0021
1.00136 g	1750	0.393	46.2	2.42	2.28	0.285	21.2	9.845	0.0299	336.9	0.1877
		±0.020	±2.6	±0.13	±0.13	±0.031	±2.2	±0.073	±0.0018	±5.4	±0.0017
	Total	0.414	75.2	3.76	3.66	0.502	21.4	9.847	0.0294	319.6	0.1874
		±0.020	±3.1	±0.15	±0.16	±0.048	±2.2	±0.086	±0.0012	±4.0	±0.0013
0510KO14 Olivine	Cr.	0.455	5.77	0.682	0.229	0.0496	12.3	10.33	0.0339	953	0.1879
(Kohala)		±0.023	±0.32	±0.034	±0.015	±0.0073	±1.3	±0.22	±0.0025	±14	±0.0040
1.24262 g											
0410KO4 Olivine	Cr.	0.0519	10.43	0.712	0.688	0.1002	13.8	9.69	0.0285	325.9	0.1888
(Kohala)		±0.0027	±0.59	±0.036	±0.038	±0.0096	±6.3	±0.26	±0.0051	±4.7	±0.0022
0.84186 g											
0310KO1 Olivine	Cr.	0.1417	17.09	0.521	0.449	0.0788	10.8	9.82	0.0289	397.9	0.1891
(Kohala)		±0.0071	±0.89	±0.026	±0.026	±0.0091	±3.3	±0.21	±0.0022	±5.1	±0.0026
1.12472 g											
1310HA2 Olivine	1000	0.22	22.5	1.81	1.94	0.429	13.5	9.94	0.0299	420.4	0.1883
(Haleakala. Maui)		±0.011	±1.4	±0.10	±0.12	±0.045	±2.0	±0.20	±0.0018	±6.1	±0.0023
1.07030 g	1400	0.73	21.8	3.83	4.65	0.796	11.82	9.79	0.0303	365.2	0.1881
		±0.037	±1.2	±0.20	±0.24	±0.051	±0.83	±0.26	±0.0024	±3.9	±0.0011
	1750	0.568	52.6	5.01	5.5	0.963	11.31	9.809	0.0298	367.9	0.1886
		±0.030	±2.8	±0.27	±0.31	±0.064	±0.68	±0.067	±0.0021	±3.6	±0.0012
	Total	1.518	96.9	10.65	12.09	2.188	11.87	9.835	0.0299	374.9	0.1884
		±0.049	±3.4	±0.35	±0.41	±0.094	±0.56	±0.083	±0.0013	±2.5	±0.0008

Table A1: continued

Sample	T. °C	^{4}He	^{20}Ne	^{40}Ar	^{84}Kr	^{132}Xe	$^{3}He/^{4}He.$	$^{20}Ne/^{22}Ne$	$^{21}Ne/^{22}Ne$	$^{40}Ar/^{36}Ar$	$^{38}Ar/^{36}Ar$
		10^{-8} cm^3/g	10^{-12} cm^3/g	$10^{-8}cm^3/g$	10^{-12} cm^3 STP/g	10^{-12} cm^3 STP/g	$10^{-6.}$				
1310HA2 Olivine	1000	0.061	2.53	0.189	0.345	0.0856	10.7	9.7	0.0284	393	0.1883
(Haleakala. Maui)		±0.0031	±0.25	±0.022	±0.034	±0.0097	±3.3	±0.22	±0.0053	±15	±0.0051
1.64404 g	1400	0.347	1.34	0.578	0.141	0.0426	11.7	9.87	0.035	1462	0.1876
		±0.017	±0.16	±0.029	±0.011	±0.0049	±1.0	±0.48	±0.011	±40	±0.0033
	1750	0.307	10.37	0.893	0.375	0.0466	10.5	9.82	0.0313	802	0.1882
		±0.016	±0.89	±0.069	±0.030	±0.0086	±1.2	±0.21	±0.0019	±76	±0.0028
	Total	0.715	14.24	1.66	0.861	0.175	11.1	9.8	0.0311	834	0.1881
		±0.024	±0.94	±0.078	±0.047	±0.014	±0.8	±0.16	±0.0020	±46	±0.0021
1310HA5c Olivine	1000	0.0866	9.51	0.377	0.911	0.183	7.5	9.73	0.0297	343.9	0.1889
(Haleakala. Maui)		±0.0044	±0.80	±0.044	±0.080	±0.034	±1.5	±0.24	±0.0032	±7.9	±0.0047
1.10196 g	1750	0.804	57.7	3.29	2.53	0.225	11.4	9.85	0.0295	410.8	0.1892
		±0.041	±3.0	±0.18	±0.16	±0.036	±1.1	±0.12	±0.0015	±5.2	±0.0015
	Total	0.891	67.2	3.67	3.44	0.408	11	9.83	0.0295	402.7	0.1892
		±0.041	±3.1	±0.19	±0.18	±0.050	±1.0	±0.11	±0.0014	±4.8	±0.0014
1410HA13 Olivine	1000	0.0399	6.01	0.29	0.501	0.163	40.8	9.75	0.0302	330.9	0.1865
(Haleakala. Maui)		±0.0021	±0.39	±0.025	±0.041	±0.012	±7.1	±0.43	±0.0034	±5.1	±0.0025
1.63464 g	1750	1.04	19.9	1.98	0.739	0.102	11.95	9.822	0.0358	643	0.1888
		±0.052	±1.3	±0.11	±0.055	±0.015	±0.74	±0.092	±0.0017	±20	±0.0019
	Total	1.08	25.9	2.27	1.24	0.265	13.02	9.81	0.0345	574	0.1883
		±0.052	±1.4	±0.11	±0.069	±0.019	±0.76	±0.12	±0.0015	±17	±0.0016

Table A1: continued

Sample	T. °C	^{4}He 10^{-8} cm^3/g	^{20}Ne 10^{-12} cm^3/g	^{40}Ar $10^{-8}cm^3/g$	^{84}Kr 10^{-12} cm^3 STP/g	^{132}Xe 10^{-12} cm^3 STP/g	$^{3}He/^{4}He.$ $10^{-6.}$	$^{20}Ne/^{22}Ne$	$^{21}Ne/^{22}Ne$	$^{40}Ar/^{36}Ar$	$^{38}Ar/^{36}Ar$
1310HA4 Olivine	1000	0.0664	13.64	0.765	0.639	0.1089	6.9	9.75	0.0286	320.2	0.1872
(Haleakala. Maui)		±0.0034	±0.75	±0.045	±0.045	±0.0099	±1.8	±0.19	±0.0034	±3.6	±0.0021
1.65106 g	1750	0.493	65.5	4.12	2.1	0.171	11.5	9.84	0.02925	417.3	0.1876
		±0.025	±3.5	±0.22	±0.11	±0.013	±1.6	±0.12	±0.00094	±3.6	±0.0016
	Total	0.559	79.1	4.89	2.74	0.28	11	9.82	0.02914	398.4	0.1875
		±0.025	±3.6	±0.22	±0.12	±0.016	±1.4	±0.10	±0.00098	±3.2	±0.0014
1410HA13 Olivine	Cr.	0.677	8.35	1.14	0.297	0.058	11.1	9.81	0.0302	1232	0.1875
(Haleakala. Maui)		±0.034	±0.46	±0.11	±0.019	±0.010	±1.0	±0.20	±0.0026	±17	±0.0050
1.09326 g											
1310HA4 Olivine	Cr.	0.0413	28	1.944	1.252	0.1094	11.1	9.83	0.0291	339.5	0.1877
(Haleakala. Maui)		±0.0021	±1.4	±0.098	±0.065	±0.0089	±4.9	±0.14	±0.0014	±3.5	±0.0018
1.30272 g											
1410HA9B Olivine	Cr.	0.341	76.8	4.85	2.97	0.228	11.1	9.818	0.0293	332	0.1876
(Haleakala. Maui)		±0.017	±3.9	±0.24	±0.15	±0.015	±1.9	±0.086	±0.0012	±2.9	±0.0012
0.98944 g											

Table A2: Major element composition of lavas from Mauna Kea, Kilauea, and surface samples of Kohala and Haleakala.

Sample	SiO_2 [wt%]	TiO_2 [wt%]	Al_2O_3 [wt%]	Fe_2O_3 [wt%]	MnO [wt%]	MgO [wt%]	CaO [wt%]	Na_2O [wt%]	K_2O [wt%]	P_2O_5 [wt%]	H_2O [wt%]	CO_2 [wt%]	Sum [wt%]
R 8	49.64	2.60	12.95	12.50	0.17	7.50	10.57	1.97	0.36	0.25	1.15	0.10	99.76
R 21	49.67	2.61	13.05	12.48	0.17	7.34	10.63	2.00	0.35	0.25	1.12	0.12	99.80
R 50	49.50	2.59	13.08	12.45	0.17	7.44	10.51	1.99	0.40	0.25	1.24	0.13	99.75
R 60	44.99	1.72	8.98	12.13	0.16	17.85	11.06	1.11	0.19	0.18	1.15	0.12	99.63
R 125	49.67	2.60	13.20	12.36	0.17	7.12	10.73	2.04	0.32	0.25	1.17	0.10	99.73
R 129	48.70	2.10	11.52	11.80	0.16	12.29	9.71	1.66	0.25	0.19	1.18	0.14	99.70
CR1-4A	49.76	2.39	13.04	11.95	0.17	8.75	10.41	2.09	0.42	0.24	0.45	0.07	99.74
CR2-2A	50.12	2.47	13.49	11.76	0.16	7.50	10.70	2.19	0.47	0.25	0.59	0.08	99.78
CR11-5A	48.40	2.03	11.17	12.76	0.18	13.00	9.35	1.75	0.32	0.18	0.46	0.09	99.68
CR11-5B	48.78	2.04	11.61	12.18	0.17	12.28	9.56	1.96	0.33	0.19	0.46	0.08	99.64
KIL 1	46.90	1.82	9.51	12.57	0.16	18.31	8.09	1.29	0.31	0.18	0.40	0.09	99.64
0410KO6	47.49	3.54	13.59	14.64	0.20	5.33	10.00	2.86	0.84	0.49	0.63	0.05	99.65
0410KO7	48.73	2.83	16.01	12.47	0.17	5.09	10.68	2.63	0.73	0.38	0.90	0.05	100.67
0410KO9	47.48	3.54	14.67	13.37	0.19	4.87	9.48	3.58	1.24	0.63	0.47	0.10	99.61
0410KO10	47.58	3.53	14.71	13.36	0.19	4.83	9.38	3.60	1.25	0.63	0.56	0.04	99.66
0510KO13	49.86	2.20	13.75	12.16	0.17	7.39	10.64	2.03	0.17	0.21	1.14	0.04	99.76
0510KO14	44.79	2.35	11.58	12.98	0.18	13.93	9.86	1.51	0.51	0.26	1.66	0.04	99.65
0610KO15	46.86	1.92	11.69	13.18	0.18	13.65	8.86	1.66	0.09	0.19	1.28	0.16	99.71
0610KO16	49.58	2.33	13.91	11.84	0.17	7.32	11.23	2.15	0.30	0.24	0.65	0.05	99.76
0610KO18B	49.99	3.16	13.30	13.49	0.18	5.92	9.35	2.64	0.66	0.40	0.61	0.05	99.74
0710KO20	46.52	3.11	15.22	12.81	0.17	6.19	11.05	2.73	0.80	0.43	0.70	0.04	99.76
0710KO22	48.78	2.98	14.07	12.73	0.18	5.75	10.49	2.75	0.76	0.39	0.75	0.06	99.69
1310HA2	42.64	2.89	12.86	15.17	0.19	10.25	11.32	2.52	0.81	0.35	0.57	0.06	99.63
1310HA4	42.63	3.69	14.32	15.63	0.21	6.91	11.07	2.67	0.88	0.44	1.14	0.04	99.62
1310HA5C	41.05	3.40	10.93	15.63	0.19	11.84	12.24	2.62	0.44	0.37	0.80	0.04	99.55
1310HA6	41.85	3.47	13.09	15.53	0.19	8.50	12.01	2.55	0.96	0.40	0.92	0.05	99.52
1310HA7	43.67	3.29	14.77	14.62	0.20	6.97	10.46	3.24	1.19	0.48	0.61	0.09	99.58
1310HA8	42.19	3.01	12.33	15.09	0.19	10.85	11.59	2.48	0.86	0.38	0.55	0.09	99.61

Table A2: continued

Sample	SiO_2 [wt%]	TiO_2 [wt%]	Al_2O_3 [wt%]	Fe_2O_3 [wt%]	MnO [wt%]	MgO [wt%]	CaO [wt%]	Na_2O [wt%]	K_2O [wt%]	P_2O_5 [wt%]	H_2O [wt%]	CO_2 [wt%]	Sum [wt%]
1410HA9B	42.61	2.43	10.46	14.27	0.19	13.78	12.01	2.02	0.71	0.32	0.71	0.07	99.57
1410HA10	41.37	2.49	10.71	15.09	0.19	14.31	11.27	1.49	0.60	0.33	1.61	0.15	99.62
1410HA12	42.42	2.45	10.53	14.46	0.18	13.83	11.85	1.87	0.63	0.32	1.02	0.04	99.60
1410HA13	42.86	2.44	10.41	14.02	0.18	13.61	12.40	2.13	0.59	0.31	0.61	0.07	99.63
HUA 1B	46.66	1.66	11.28	12.42	0.17	12.44	11.57	1.73	0.54	0.19	0.54	0.47	99.67
MLO-4	48.59	1.72	11.29	11.83	0.16	14.23	8.77	1.91	0.33	0.20	0.59	0.07	99.70

Table A3: Major element composition and Fo content of olivines from Mauna Kea HSDP samples, Kilauea NSF well samples, and surface samples of Kohala and Haleakala.

Sample	MgO [wt%]	Al_2O_3 [wt%]	SiO_2 [wt%]	CaO [wt%]	TiO_2 [wt%]	Cr_2O_3 [wt%]	MnO [wt%]	FeO [wt%]	NiO [wt%]	Sum [wt%]	Fo [%]
R129-1	44.34	0.03	39.21	0.29	0.02	0.07	0.21	16.37	0.33	100.85	83
R129-2	47.93	0.06	40.26	0.22	0.02	0.09	0.17	11.96	0.48	101.19	88
R129-3	48.73	0.05	40.32	0.22	0.02	0.08	0.15	10.83	0.50	100.89	89
R129-4	45.23	0.06	39.35	0.23	0.01	0.08	0.20	15.47	0.40	101.03	84
R129-5	44.39	0.04	39.53	0.26	0.03	0.06	0.22	16.16	0.35	101.04	83
R129-6	44.09	0.05	39.32	0.26	0.02	0.07	0.22	16.64	0.33	100.99	82
R129-7	46.85	0.05	40.06	0.23	0.01	0.10	0.16	13.06	0.40	100.91	86
R125-1	45.02	0.03	39.17	0.26	0.02	0.05	0.22	15.25	0.34	100.33	84
R125-7	44.99	0.05	39.53	0.23	0.01	0.07	0.19	15.10	0.31	100.49	84
R050-1	49.02	0.05	40.62	0.22	0.01	0.11	0.16	10.64	0.48	101.31	89
R050-2	43.19	0.03	39.15	0.25	0.01	0.02	0.25	18.08	0.21	101.20	81
R050-3	43.32	0.03	39.37	0.24	0.01	0.04	0.26	17.83	0.37	101.47	81
R008-1	43.47	0.04	39.04	0.24	0.02	0.04	0.23	17.49	0.25	100.81	81
R008-2	42.35	0.03	38.94	0.24	0.02	0.02	0.25	18.53	0.22	100.61	80
R008-3	46.25	0.04	39.94	0.26	0.02	0.07	0.17	13.78	0.40	100.93	85
R008-4	41.55	0.02	38.77	0.22	0.02	0.04	0.25	19.74	0.27	100.87	79
R008-5	44.04	0.03	39.50	0.25	0.01	0.02	0.22	16.38	0.33	100.79	83
R008-6	39.74	0.03	38.29	0.24	0.02	0.02	0.30	21.86	0.22	100.71	76
R008-7	42.90	0.04	38.95	0.25	0.02	0.03	0.23	17.74	0.23	100.38	81
R021-1	42.86	0.05	39.32	0.25	0.02	0.05	0.24	17.72	0.26	100.78	81
R021-3	43.52	0.02	39.24	0.26	0.02	0.04	0.23	16.77	0.25	100.36	82
R021-4	41.72	0.03	38.83	0.25	0.01	0.02	0.27	19.23	0.22	100.57	79
R021-5	42.03	0.03	39.01	0.25	0.02	0.03	0.25	18.77	0.19	100.59	80
R060-1	43.15	0.03	39.49	0.25	0.02	0.03	0.25	17.67	0.24	101.13	81
R060-3	42.75	0.05	39.22	0.25	0.02	0.04	0.23	17.62	0.26	100.43	81
R060-5	44.05	0.03	39.54	0.26	0.01	0.04	0.22	16.01	0.27	100.45	83
R060-7	42.26	0.03	39.03	0.24	0.02	0.03	0.26	18.08	0.21	100.16	80
R060-8	40.74	0.03	38.81	0.23	0.02	0.02	0.28	20.41	0.22	100.76	78
R060-9	41.57	0.03	38.88	0.24	0.02	0.01	0.24	19.43	0.19	100.61	79
CR11-1	46.15	0.05	39.85	0.21	0.01	0.10	0.18	12.95	0.40	99.90	86
CR11-2	44.87	0.05	39.43	0.22	0.01	0.08	0.19	14.63	0.37	99.86	84
CR11-3	42.70	0.05	38.93	0.24	0.02	0.06	0.22	17.38	0.30	99.89	81
CR02-1	40.93	0.03	38.72	0.29	0.02	0.04	0.26	20.21	0.21	100.71	78
CR02-2	41.05	0.03	38.77	0.30	0.01	0.05	0.27	19.84	0.24	100.57	78
CR02-3	41.08	0.03	38.73	0.29	0.02	0.03	0.26	19.87	0.23	100.53	78
CR02-5	44.18	0.04	39.44	0.26	0.02	0.06	0.20	15.87	0.34	100.41	83
CR01-1	46.97	0.05	39.79	0.24	0.02	0.08	0.16	12.15	0.40	99.86	87
CR01-2	46.84	0.04	39.98	0.23	0.01	0.08	0.15	11.80	0.42	99.56	87
CR01-3	47.71	0.06	40.14	0.23	0.02	0.09	0.16	11.11	0.43	99.93	88
CR01-4	47.29	0.05	40.06	0.23	0.02	0.11	0.15	11.49	0.38	99.79	88
CR14-1	47.23	0.05	40.01	0.23	0.02	0.09	0.17	12.12	0.43	100.34	87
CR14-2	46.72	0.05	40.12	0.23	0.02	0.09	0.17	12.58	0.39	100.36	87
CR14-3	40.30	0.03	38.45	0.29	0.02	0.05	0.26	20.93	0.23	100.57	77
CR14-4	41.94	0.04	38.97	0.24	0.02	0.05	0.25	18.77	0.31	100.60	85
CR04-1	41.39	0.02	38.72	0.28	0.02	0.05	0.26	19.03	0.24	100.02	79
CR04-2	41.52	0.03	38.80	0.29	0.02	0.05	0.26	18.89	0.21	100.06	79
CR04-3	41.15	0.03	38.70	0.29	0.02	0.05	0.25	19.10	0.22	99.80	79
KO15-1	45.48	0.06	40.37	0.19	0.01	0.08	0.19	14.59	0.43	101.40	85
KO1-2	38.64	0.03	38.61	0.30	0.02	0.02	0.32	22.14	0.17	100.24	75

Table A3: continued

Sample	MgO [wt%]	Al_2O_3 [wt%]	SiO_2 [wt%]	CaO [wt%]	TiO_2 [wt%]	Cr_2O_3 [wt%]	MnO [wt%]	FeO [wt%]	NiO [wt%]	Sum [wt%]	Fo [%]
KO1-3	39.39	0.03	38.83	0.29	0.03	0.01	0.33	21.38	0.17	100.48	76
KO1-4	38.55	0.03	38.62	0.28	0.03	0.02	0.34	22.35	0.14	100.36	75
KO1-5	38.69	0.04	38.75	0.31	0.03	0.01	0.32	22.16	0.16	100.46	75
KO1-6	38.69	0.03	38.62	0.28	0.04	0.02	0.33	22.20	0.17	100.38	75
KO1-7	38.61	0.03	38.71	0.29	0.03	0.02	0.32	22.41	0.16	100.57	75
KO1-8	38.15	0.03	38.39	0.29	0.04	0.02	0.36	22.80	0.15	100.22	75
KO1-9	38.04	0.03	38.25	0.29	0.04	0.01	0.31	22.75	0.18	99.90	75
KO1-10	38.74	0.03	38.56	0.29	0.02	0.02	0.32	21.94	0.16	100.07	76
KO1-11	39.04	0.03	38.77	0.29	0.04	0.02	0.32	21.81	0.16	100.47	76
KO22-1	43.17	0.03	39.69	0.31	0.01	0.02	0.21	16.43	0.20	100.06	82
KO22-2	42.74	0.03	39.86	0.29	0.01	0.02	0.26	17.17	0.18	100.58	81
KO22-4	43.21	0.03	39.47	0.30	0.02	0.03	0.23	16.73	0.21	100.23	82
KO22-5	41.33	0.03	39.34	0.27	0.01	0.02	0.28	18.73	0.21	100.22	79
KO22-6	42.34	0.04	39.50	0.30	0.01	0.03	0.27	17.38	0.17	100.05	81
KO4-1	41.56	0.03	39.14	0.29	0.02	0.02	0.26	18.11	0.23	99.68	80
KO4-3	43.33	0.04	39.36	0.28	0.02	0.03	0.20	16.44	0.27	99.99	82
KO4-4	43.21	0.04	39.37	0.27	0.03	0.04	0.23	16.50	0.27	99.97	82
KO4-5	40.36	0.04	38.32	0.28	0.03	0.03	0.30	19.63	0.22	99.21	78
KO4-7	40.81	0.03	38.38	0.26	0.03	0.02	0.29	19.09	0.22	99.13	79
KO4-8	42.02	0.05	39.15	0.31	0.01	0.02	0.21	17.96	0.19	99.90	80
KO4-9	41.56	0.04	39.12	0.27	0.02	0.02	0.26	18.36	0.23	99.88	80
KO4-10	43.30	0.04	39.31	0.30	0.02	0.03	0.23	16.04	0.25	99.52	83
KO4-11	42.63	0.03	39.23	0.31	0.02	0.03	0.24	17.19	0.20	99.88	81
KO4-12	43.17	0.04	39.38	0.30	0.03	0.01	0.23	16.37	0.23	99.77	82
KO4-13	41.10	0.03	38.61	0.29	0.03	0.02	0.24	17.45	0.25	98.02	81
KO4-14	41.31	0.04	38.71	0.31	0.02	0.03	0.26	18.14	0.20	99.04	80
KO22-1	43.49	0.04	39.59	0.31	0.02	0.03	0.22	16.10	0.19	99.97	83
KO18B-1	44.84	0.03	40.19	0.24	0.01	0.06	0.20	13.61	0.34	99.51	85
KO18B-3	43.72	0.04	39.98	0.30	0.03	0.05	0.21	15.25	0.28	99.85	83
KO18B-4	41.14	0.03	39.36	0.26	0.01	0.04	0.27	18.43	0.26	99.78	80
KO18B-8	42.47	0.05	39.83	0.27	0.03	0.05	0.24	16.06	0.35	99.36	82
KO18B-12	41.20	0.03	39.42	0.25	0.02	0.08	0.24	18.51	0.33	100.07	80
KO9-2	41.06	0.03	39.29	0.31	0.02	0.02	0.27	18.46	0.20	99.67	80
KO15-1	45.48	0.06	40.37	0.19	0.01	0.08	0.19	14.59	0.43	101.40	85
KO15-2	44.53	0.19	40.06	0.20	0.02	0.06	0.19	15.43	0.38	101.07	84
KO15-3	40.96	0.34	39.39	0.69	0.08	0.08	0.20	14.46	0.36	96.55	80
KO15-4	41.88	0.05	39.24	0.22	0.02	0.07	0.25	19.23	0.30	101.26	79
KO15-5	42.74	0.06	39.46	0.19	0.01	0.07	0.23	18.25	0.34	101.34	80
KO15-6	47.35	0.06	40.66	0.20	0.02	0.09	0.17	12.75	0.45	101.74	87
KO15-7	47.80	0.05	40.67	0.19	0.02	0.08	0.16	12.08	0.45	101.50	87
KO14-1	48.73	0.05	41.02	0.25	0.02	0.08	0.16	10.90	0.40	101.60	89
KO14-2	45.43	0.09	40.04	0.30	0.01	0.04	0.21	14.53	0.29	100.94	85
KO14-3	44.23	1.82	40.77	0.40	0.02	0.05	0.19	12.48	0.28	100.24	85
KO14-4	44.58	0.17	40.23	0.41	0.04	0.03	0.22	14.68	0.25	100.60	84
KO14-5	44.87	0.04	39.99	0.30	0.02	0.04	0.24	15.46	0.26	101.21	84
KO14-6	44.55	0.04	40.05	0.33	0.01	0.04	0.24	15.74	0.27	101.27	83
KO14-7	47.14	0.13	40.62	0.31	0.02	0.07	0.17	12.09	0.28	100.84	87
KO14-8	45.78	0.13	40.39	0.37	0.02	0.06	0.19	13.54	0.28	100.76	86
KO14-9	45.16	0.03	40.13	0.35	0.02	0.04	0.21	14.97	0.27	101.18	84
KO14-10	47.70	0.05	40.86	0.32	0.02	0.07	0.17	11.73	0.33	101.24	88
KO14-12	46.38	0.04	40.38	0.37	0.01	0.05	0.21	13.65	0.28	101.37	86

Table A3: continued

Sample	MgO [wt%]	Al_2O_3 [wt%]	SiO_2 [wt%]	CaO [wt%]	TiO_2 [wt%]	Cr_2O_3 [wt%]	MnO [wt%]	FeO [wt%]	NiO [wt%]	Sum [wt%]	Fo [%]
HA5C-5	41.85	0.05	39.69	0.34	0.03	0.03	0.24	18.11	0.15	100.49	80
HA5C-6	41.47	0.05	39.60	0.37	0.03	0.02	0.25	18.27	0.17	100.22	80
HA5C-7	40.53	0.07	39.25	0.35	0.03	0.01	0.26	19.35	0.16	100.01	79
HA5C-8	43.55	0.05	40.10	0.33	0.02	0.05	0.22	15.71	0.21	100.25	83
HA5C-9	41.10	0.05	39.30	0.33	0.03	0.02	0.26	19.17	0.15	100.41	79
HA2-1	41.12	0.06	39.28	0.27	0.03	0.01	0.27	19.23	0.14	100.42	79
HA2-2	40.27	0.04	38.81	0.28	0.02	0.01	0.25	20.59	0.14	100.41	78
HA2-3	42.10	0.06	39.56	0.29	0.02	0.02	0.24	18.20	0.16	100.65	80
HA2-4	39.42	0.04	38.69	0.29	0.03	0.01	0.30	21.36	0.10	100.24	76
HA2-5	39.27	0.04	38.57	0.27	0.03	0.01	0.33	21.49	0.12	100.13	76
HA10-1	40.59	0.04	39.08	0.28	0.03	0.01	0.26	19.52	0.16	99.98	79
HA10-2	39.39	0.05	38.98	0.23	0.03	0.01	0.29	21.10	0.14	100.23	77
HA10-3	39.44	0.04	38.86	0.24	0.02	0.01	0.30	21.08	0.13	100.12	77
HA10-4	39.61	0.05	38.93	0.29	0.03	0.01	0.32	21.21	0.11	100.56	77
HA10-5	39.79	0.05	38.96	0.25	0.04	0.00	0.31	21.11	0.15	100.66	77
HA10-6	40.19	0.05	39.28	0.25	0.03	0.02	0.29	20.71	0.17	100.98	77
HA10-7	40.10	0.05	38.84	0.26	0.03	0.01	0.29	20.59	0.18	100.35	77
HA10-9	39.41	0.05	38.93	0.27	0.03	0.01	0.31	21.31	0.14	100.46	76
HA10-10	39.93	0.04	39.00	0.26	0.03	0.02	0.27	20.62	0.16	100.34	77
HA10-11	40.22	0.06	39.13	0.27	0.04	0.01	0.28	20.55	0.17	100.72	77
HA10-12	39.86	0.04	39.02	0.25	0.03	0.01	0.27	20.79	0.15	100.43	77
HA4-1	45.69	0.05	40.30	0.27	0.01	0.07	0.17	13.50	0.33	100.40	86
HA4-2	45.10	0.06	40.18	0.31	0.02	0.06	0.17	14.11	0.28	100.29	85
HA4-3	42.48	0.06	39.51	0.32	0.02	0.01	0.22	17.03	0.19	99.83	81
HA8-2	40.92	0.05	38.96	0.27	0.01	0.01	0.26	18.62	0.14	99.23	79
HA8-4	44.71	0.06	39.75	0.29	0.02	0.06	0.19	14.63	0.27	99.97	84
HA4-2	44.46	0.08	40.41	0.61	0.02	0.05	0.19	13.69	0.28	99.79	85
HA4-3	42.54	0.06	39.17	0.33	0.02	0.01	0.22	17.15	0.17	99.66	81
HA6-1	42.77	0.05	39.73	0.30	0.02	0.02	0.23	17.09	0.22	100.43	81
HA6-2	41.53	0.05	39.23	0.35	0.03	0.02	0.25	18.57	0.16	100.20	80
HA6-3	40.80	0.04	39.15	0.29	0.02	0.01	0.25	19.65	0.16	100.39	79
HA6-4	44.35	0.05	39.96	0.26	0.02	0.04	0.21	14.93	0.30	100.12	84
HA6-5	41.23	0.09	39.40	0.34	0.03	0.02	0.26	18.62	0.17	100.16	80
HA6-7	42.05	0.05	39.39	0.31	0.02	0.02	0.25	17.62	0.17	99.87	81
HA9B-1	39.17	0.05	38.83	0.26	0.03	0.01	0.28	21.05	0.13	99.80	77
HA9B-2	39.23	0.05	38.92	0.25	0.02	0.01	0.27	20.96	0.17	99.89	77
HA9B-3	39.85	0.05	38.99	0.30	0.03	0.01	0.31	19.83	0.17	99.55	78
HA9B-4	38.88	0.39	39.01	0.27	0.02	0.02	0.27	20.26	0.16	99.29	77
HA9B-5	39.88	0.05	38.99	0.27	0.03	0.01	0.28	20.20	0.18	99.89	78
HA9B-6	43.62	0.05	40.01	0.32	0.02	0.06	0.23	14.99	0.27	99.57	84
HA9B-7	40.74	0.05	39.29	0.26	0.03	0.02	0.25	18.98	0.17	99.79	79
HA9B-8	37.81	0.33	37.87	0.34	0.04	0.01	0.27	19.53	0.16	96.34	77
HA9B-9	43.81	0.13	39.99	0.25	0.02	0.05	0.20	14.82	0.29	99.57	84
HA5C-1	39.44	0.58	39.36	0.39	0.05	0.01	0.27	18.73	0.16	98.99	77
HA5C-2	41.56	0.05	39.24	0.31	0.03	0.01	0.28	20.05	0.14	101.67	78
HA5C-3	40.09	0.21	39.80	0.42	0.05	0.02	0.26	18.45	0.15	99.44	79
HA5C-4	38.75	2.94	38.10	0.34	0.03	0.04	0.16	12.51	0.24	93.10	82
HA5C-11	41.66	0.05	39.24	0.32	0.03	0.01	0.28	19.98	0.15	101.72	79
HA5C-10	41.15	0.05	39.19	0.32	0.02	0.01	0.27	20.43	0.12	101.54	78

Table A4: REE composition of lavas from Mauna Kea, Kilauea, and surface samples of Kohala and Haleakala.

Sample	La (ppm)	Ce (ppm)	Pr (ppm)	Nd (ppm)	Sm (ppm)	Eu (ppm)	Gd (ppm)	Tb (ppm)	Dy (ppm)	Ho (ppm)	Er (ppm)	Tm (ppm)	Yb (ppm)	Lu (ppm)
R 8a	13	33	4.9	22	5.7	2	6.3	0.98	5.8	1	2.9	0.39	2.3	0.34
R 21	13	34	4.8	23	5.9	2.1	6.4	1	6	1.1	2.9	0.4	2.4	0.34
R 50	13	34	4.8	23	5.8	2.1	6.4	0.99	5.9	1	2.9	0.4	2.4	0.34
R 60	13	34	4.8	23	5.8	2.1	6.5	1	6	1	3	0.39	2.4	0.34
R 125	13	33	4.8	23	5.8	2.1	6.3	0.97	5.9	1	2.9	0.4	2.3	0.34
R 129	9.2	24	3.6	17	4.5	1.6	5	0.78	4.7	0.83	2.3	0.31	1.9	0.27
MKEA 3	11	27	3.7	17	4	1.4	4.1	0.63	3.6	0.59	1.6	0.23	1.3	0.18
CR1-4A	12	31	4.2	20	5.4	1.8	5.8	0.98	5.1	0.89	2.5	0.34	2.1	0.28
CR2-2A	13	32	4.5	21	5.6	1.9	6.1	1	5.3	0.93	2.6	0.35	2.2	0.29
CR11-5A	9.5	24	3.3	16	4.4	1.5	4.8	0.84	4.4	0.77	2.2	0.3	1.9	0.25
CR11-15B	9.7	25	3.4	16	4.4	1.5	4.9	0.82	4.4	0.79	2.2	0.29	1.9	0.25
CR14-5D	13	33	4.4	20	5.1	1.7	5.5	0.89	4.7	0.83	2.3	0.32	1.9	0.25
KIL 1	8.7	22	3.3	15	3.9	1.4	4.3	0.66	3.9	0.66	1.9	0.26	1.5	0.22
0310KO1	29	68	8.8	39	8.6	2.9	8.2	1.4	6.6	1.1	3	0.43	2.4	0.35
0410KO2	15	48	5.2	24	5.7	2.1	5.8	0.99	5	0.82	2.3	0.31	1.8	0.25
0410KO4	17	42	5.7	26	6.3	2.1	6.2	1.1	5.3	0.92	2.5	0.35	2	0.29
0410KO5	25	59	7.6	34	7.7	2.6	7.6	1.3	6.4	1.1	3.1	0.43	2.5	0.36
0410KO6	25	61	8	36	8.4	2.8	8.5	1.4	7.1	1.2	3.4	0.48	2.7	0.39
0410KO7	23	49	6.9	31	7	2.4	7.1	1.1	6	1	2.9	0.41	2.3	0.33
0410KO9	33	79	9.7	44	9.4	3.2	9.2	1.5	7.5	1.3	3.6	0.51	2.9	0.42
0410KO10	32	75	9.6	43	9.3	3	9	1.5	7.3	1.3	3.5	0.49	2.8	0.41
0510KO13	8.7	23	3.3	17	4.5	1.7	5.1	0.89	4.8	0.87	2.5	0.34	2.1	0.3
0510KO14	19	41	5.5	25	5.5	1.9	5.4	0.88	4.4	0.72	2	0.28	1.6	0.22
0610KO15	7.8	21	2.9	14	3.9	1.4	4.3	0.76	4	0.7	2	0.26	1.7	0.25
0610KO16	11	28	3.8	19	5.1	1.8	5.6	0.99	5.1	0.89	2.6	0.35	2.1	0.3
0610KO18B	19	47	6.2	30	7.2	2.5	7.6	1.3	6.7	1.2	3.4	0.48	2.8	0.41
0710KO20	21	51	6.8	31	7.1	2.4	7	1.2	5.9	1	2.8	0.38	2.2	0.32
0710KO22	22	53	6.7	31	7.1	2.4	7.2	1.2	6.1	1.1	3	0.41	2.4	0.35
1310HA2	25	54	6.5	28	6.2	2.1	6.1	0.99	4.8	0.78	2.1	0.3	1.7	0.24
1310HA4	26	59	7.2	32	6.9	2.4	6.6	1.1	5.1	0.82	2.2	0.31	1.7	0.24
1310HA5C	26	57	6.9	31	6.7	2.3	6.5	1	4.7	0.69	1.8	0.22	1.3	0.17
1310HA6	27	59	7.1	31	7	2.4	6.8	1.1	5.3	0.83	2.2	0.3	1.7	0.24

Table A4: continued

Sample	La (ppm)	Ce (ppm)	Pr (ppm)	Nd (ppm)	Sm (ppm)	Eu (ppm)	Gd (ppm)	Tb (ppm)	Dy (ppm)	Ho (ppm)	Er (ppm)	Tm (ppm)	Yb (ppm)	Lu (ppm)
1410HA9B	21	46	5.5	24	5.4	1.9	5.4	0.86	4.2	0.66	1.8	0.23	1.3	0.18
1410HA10	22	47	5.6	25	5.4	1.9	5.3	0.87	4.1	0.64	1.7	0.24	1.3	0.18
1410HA12	21	46	5.5	25	5.5	1.9	5.4	0.89	4.2	0.65	1.8	0.24	1.3	0.19
1410HA13	21	45	5.4	24	5.3	1.8	5.3	0.84	4.1	0.64	1.7	0.23	1.3	0.18
MLO-4	8.8	22	3.1	15	4	1.4	4.5	0.75	4.1	0.74	2.1	0.28	1.8	0.24
HUA 1B	13	29	4	16	3.7	1.3	3.9	0.64	3.7	0.64	1.9	0.25	1.6	0.22

Acknowledgements

Ich möchte mich bei den folgenden Personen bedanken, die maßgeblich zur Entsehung dieser Doktorarbeit beigetragen haben:

Prof. Dr. Jörg Erzinger gilt mein Dank für die Ermöglichung dieser Doktorarbeit sowie für die fortwährende Unterstützung.

Dr. Samuel Niedermann danke ich für freundliche und gute Betreuung während der letzten Jahre.

Bei Dr. Nicole Stroncik möchte ich mich für unterstützende Begleitung bedanken.

Besonderer Dank gilt Enzio Schnabel für die gute Zusammenarbeit bei den Edelgasmessungen.

Dr. Rolf Romer danke ich sehr für die Betreuung und Unterstützung während der Sr- Nd- und Pb-Isotopenanalytik.

Ich möchte mich zudem bei Marina Ospald und Hartmut Lieb für die hervorragende Gesteinsaufbereitung bedanken. Dr. Dieter Rhede und Oona Appelt danke ich für die Unterstützung bei den Mikrosondenmessungen. Gerhard Berger danke ich für die Herstellung der Mikrosondendünnschliffe. Dr. Knut Hahne, Rudolf Naumann, Heike Roth, Andrea Gottsche, Sabine Schumann und Sabine Tonn danke ich sehr für die Unterstützung bei den Gesamtgesteinsanalysen.

Ich möchte mich bei allen Kollegen für die Hilfsbereitschaft und die freundliche Arbeitsatmosphäre bedanken. Dies gilt besonders für meine Zimmerkollegen Dr. Thomas Wiersberg und Dr. Peter Pilz.

Dr. Shaul Hurwitz danke ich für die Bereitstellung der Kilauea Bohrkernproben.

Der größte und herzlichste Dank gebührt meinen Freunden und meiner Familie für die moralische Unterstützung während dieser Doktorarbeit, ganz besonders Reiner Mailer.

Eidesstattliche Erklärung

Hiermit versichere ich, die vorliegende Dissertation selbstständig und ohne unerlaubte Hilfsmittel angefertigt zu haben.

Bei der Verfassung der Dissertation wurden keine anderen als die im Text aufgeführten Hilfsmittel verwendet.

Ein Promotionsverfahren zu einem früheren Zeitpunkt an einer anderen Hochschule oder bei einem anderen Fachbereich wurde nicht beantragt.

Tina Mailer, geb. Krüsmann, Berlin Juni 2009